1-8-2015 12:00 AM

Resting-state Functional Network Disruptions in a Rodent Model of Mesial Temporal Lobe Epilepsy (TLE)

Ravnoor Singh Gill
The University of Western Ontario

Supervisor
Stan Leung
The University of Western Ontario Joint Supervisor
Seyed Mirsattari
The University of Western Ontario

Graduate Program in Neuroscience
A thesis submitted in partial fulfillment of the requirements for the degree in Master of Science

RESTING-STATE FUNCTIONAL NETWORK DISRUPTIONS IN A RODENT MODEL OF MESIAL TEMPORAL LOBE EPILEPSY (TLE)

(Thesis format: Monograph)

by

Ravnoor S. Gill

Graduate Program in Neuroscience

A thesis submitted in partial fulfillment
of the requirements for the degree of
Master of Science

The School of Graduate and Postdoctoral Studies
The University of Western Ontario
London, Ontario, Canada

Abstract

Mesial temporal lobe epilepsy (TLE) is the most common form of drug-refractory epilepsy. The clinical application of non-invasively mapped networks using resting-state functional magnetic resonance imaging (rsfMRI) in humans has been rather limited due to heterogeneous (varying etiology, drugs, onset, latent period, etc.) patient groups. We employed a pharmacological (kainic acid) rodent model of TLE to measure the extent of functional network disruptions using rsfMRI, and study selected behaviors and olfactory to hippocampus transmission. Graph theoretical network modelling and analysis revealed significant increase in functional connectivity connectivity to the temporal lobe (hippocampus) in epileptic-rats compared to controls in the limbic (nucleus accumbens, medial dorsal thalamus), and "default mode" network (retrosplenial, sensorimotor, auditory and posterior parietal cortices). Loss in righting reflex that occurred in response to a lower isoflurane concentration in kainate-treated rats compared to controls was also revealed. These results suggest extensive disruptions in brain networks affected by TLE.

Keywords: Temporal lobe epilepsy, hippocampus, resting-state networks, kainic acid, rsfMRI, electrophysiology

Acknowledgements

I would like to express my gratitude towards people who have been supportive during various phases of my graduate education. I am indebted to Dr. Stan Leung and Dr. Seyed Mirsattari for providing me the opportunity to switch to the interdisciplinary field of neuroscience and study the epilepsy disorder.

Dr. Leung has been highly supportive and patient during all facets of the project, including the writing and finalizing this manuscript. I would like to express my utmost gratitude to Dr. Leung and Dr. Mirsattari for their guidance throughout the project, and for their support not only related to scientific research.

Matt Hutchison's expertise in the field of functional connectivity and invaluable feedback on the thesis manuscript are highly appreciated. His comments and suggestions for further development of the thesis project have been invaluable.

My gratitude goes out to Min-Ching Kuo for being my early mentor in teaching me the basics of practical electrophysiology and surgery. I would also like to thank Dr. Jingyi Ma for her unrelenting support and assistance in running experiments, and animal care; and Liangwei Chu for his help with various surgery sessions.

I would also like to extend my appreciation to the the Robarts 9.4T technical staff – Alex Li, Ashley Kirley, and Miranda Bellyou for ensuring compliance with the animal protocol, and essential support during the fMRI scanning sessions.

Finally, I would like to acknowledge the indispensable suggestions, and advice lent by the advisory committee members – Dr. Michael Poulter, Dr. Nagalingam Rajakumar, and Dr. Ravi Menon; and Dr. Paul Gribble for lending me the wisdom to emerge a better statistician.

Contents

Abstract i

Acknowledgements ii

List of Figures vi

List of Tables x

List of Abbreviations xi

1 Introduction 1
- 1.1 Mesial Temporal Lobe Epilepsy (TLE) . . . 1
  - 1.1.1 Neuropathology in TLE . . . 2
  - 1.1.2 Mossy fiber sprouting . . . 3
  - 1.1.3 Pathological oscillations in TLE . . . 4
- 1.2 Competing theories of epileptogenesis . . . 6
- 1.3 Kainate model of TLE . . . 8
  - 1.3.1 Kainic Acid Receptors (KARs) . . . 9
  - 1.3.2 Neuropathological changes . . . 13
  - 1.3.3 Epileptogenesis . . . 14
- 1.4 TLE in a graph theoretical framework . . . 18
  - 1.4.1 Resting State Networks and Multimodal Strategies . . . 22
  - 1.4.2 RSN Pathologies in TLE . . . 25
- 1.5 Effect of Anaesthesia . . . 26
- 1.6 Olfactory System and TLE . . . 27
- 1.7 Current Study . . . 29

2 Materials & Methods 32
- 2.1 Animals . . . 32
- 2.2 Sequence of Experiments . . . 32
- 2.3 Induction of Spontaneous Seizures using Kainic Acid . . . 33
- 2.4 Functional Magnetic Resonance Imaging Procedures . . . 36
  - 2.4.1 Animal Usage and Preparation . . . 36
  - 2.4.2 Image Acquisition . . . 37
  - 2.4.3 Image Preprocessing and Analysis . . . 38
- 2.5 Behavioural Test Procedures & Analysis . . . 41
  - 2.5.1 Open Field Test . . . 41

2.5.2 Pre-Pulse Inhibition . . . 41
2.5.3 Loss of Righting Reflex under Isoflurane . . . 42
2.6 Local Field Potentials (LFPs) Procedures . . . 43
2.6.1 Surgery & Electrode Implantation . . . 43
2.6.2 Local Field Potential (LFP) Recordings . . . 44
2.6.3 Perfusion & Histology . . . 45
2.6.4 Data Analysis & Statistics . . . 46
2.7 Seizure Observation & Inclusion Criteria . . . 47

3 Results **49**
3.1 Functional connectivity of kainate and control rats . . . 49
3.1.1 Differences in connectivity . . . 51
3.1.2 Global parameters of the rat brain functional networks . . . 51
3.1.3 Regional parameters of the rat brain functional networks . . . 53
3.1.4 Small-worldness of networks in TLE . . . 55
3.2 Kainate-induced lesion enhanced anesthetic sensitivity to Isoflurane . . . 56
3.3 Kainate did not affect sensorimotor gating . . . 58
3.4 No behavioural hyperactivity was observed . . . 58
3.5 Effect of Kainate treatment on LFP coherence of olfactory bulb with the limbic system 59
3.6 Effect of Kainate treatment on LFP power of olfactory bulb . . . 60

4 Discussion **61**
4.1 Differences in Functional Connectivity . . . 62
4.1.1 Increased Connectivity within the Limbic Networks . . . 62
4.1.2 Increased Activity within the DMN . . . 63
4.1.3 Changes in the Dopaminergic Mesolimbic System . . . 66
4.1.4 Change in Graph Metrics . . . 67
4.2 Behavioural Alterations in KA Model of TLE . . . 69
4.2.1 Increased Isoflurane Sensitivity in Epileptic Rats . . . 69
4.2.2 PPI Deficits and Hyperlocomotion are not observed in Epileptic Rats . . . 70
4.3 Electrographic Characterization of the KA Model of TLE . . . 71
4.3.1 No Significant Change in Olfactory Bulb Power . . . 71
4.4 Disparity with Human Literature . . . 72
4.5 Study Limitations . . . 72
4.6 Conclusion . . . 73

References **75**

Appendix A Graph Theory Analysis **91**
A.1 Mathematical Notation . . . 91
A.2 Fisher's r-to-Z Normalized Map . . . 93

Appendix B Node Definitions **94**
B.1 Resting-state fMRI . . . 94
B.2 Electrophysiology . . . 95

Appendix C Supplementary Data **97**
C.1 EPI & Anatomical Images 97
C.2 EPI Spectrum 98

Appendix D Documentation of Ethics Approval **99**

Curriculum Vitæ **99**

List of Figures

1.1 Competing hypotheses in epileptogenesis. 7

1.2 **Overview of hippocampal formation connectivity with other limbic structures.** Bold arrows depict well defined afferents and efferents of the hippocampal formation, and the entorhinal cortex. Light grey arrows/boxes represent connectivity of the amygdaloid complex. NST: nucleus of the solitary tract; PAG: periaqueductal grey; PBN: parabrachial nucleus; SNc: substantia nigra pars compacta; VTA: ventral tegmental area. Reproduced from Kandratavicius et al. (2012). 10

1.3 **Myriads of functional changes affected by KARs**. Any alteration in the regulation of these activities, including circuit maturation during development, may provoke sufficient disequilibrium as to lead to a disease state. Reproduced from Lerma and Marques (2013) 11

1.4 **Metabotropic action of KARs**. Presynaptic KARs can bidirectionally modulate neurotransmitter release at glutamatergic and GABAergic synapses. The inhibitory but not the facilitatory activity of KARs is most likely linked to GPCR coupled mechanisms. The inhibition of voltage-gated Ca^{2+}-channels by KARs, independent of ion flux, may contribute to the inhibitory action of KARs on neurotransmitter release. Regulation of synaptic activity is made possible via the presynaptic modulation of neurotransmitter release, and network activity control by regulating neuronal excitability. In addition, postsynaptic KARs can regulate neuronal excitability by inhibition of slow afterhyperpolarization (sAHP). Reproduced from Rodrigues and Lerma (2012) 12

1.5 **(A)** EEG depth recordings in rat depicting a seizure recorded simultaneously in the amygdala, hippocampus and neocortex ~2 h following intra-peritoneal (systemic) administration of KA (6 mg/kg). Gamma oscillations (30–80 Hz) (white bordered rectangles) occurs in the CA1 and CA3 region. **(B)** Seizure-onset is depicted on an expanded time scale. Note: Arrow indicates the seizure start timepoint in the CA3 region. Reproduced from Lévesque and Avoli (2013). 17

1.6 **Random rewiring in network configurations** A random rewiring procedure is dependent on the variable p, the probability of rewiring ($0 < p < 1$). This rewiring commences with a regular ring lattice with edges connecting node with probability p. As p increases, the graph becomes increasingly disordered until for p = 1, all edges are rewired randomly. For intermediate values of p, the graph is a small world network: highly clustered like a regular graph, yet with small characteristic path length, like a random graph. Three realizations of the process (for three different p values) are depicted. Reproduced from Watts and Strogatz (1998, with $n = 20$ vertices an average degree of $k = 4$ edges per vertex). 21

1.7 The characteristic path length $L(p)$ and clustering coefficient $C(p)$ for the family of randomly rewired graphs described in Figure 1.6 (averaged and normalized over 20 realizations). A logarithmic horizontal scale has been used to resolve the rapid drop in $L(p)$, corresponding to the onset of the small-world phenomenon. During this drop, $C(p)$ remains almost constant at its value for the regular lattice, indicating that the transition to a small world is almost undetectable at the local level.Reproduced from Watts and Strogatz (1998, n = 1,000 vertices and an average degree of k = 10 edges per vertex). 22
1.8 Comparison of the homologous Default Mode Network (DMN) in rat, monkey, and human. 24
1.9 The axons of mitral and tufted relay neurons of the OB project through the lateral olfactory tract to the olfactory cortex. The olfactory cortex consists of a number of distinct areas, the largest of which is the PC. From these areas olfactory information is transmitted directly to other brain areas as well as indirectly via the thalamus. Targets include frontal and orbitofrontal areas of the neocortex, which are thought to be important for odor discrimination, and the amygdala and hypothalamus, which may be involved in emotional and physiological responses to odors. Mitral cells in the accessory olfactory bulb project to specific areas of the amygdala that transmit signals to the hypothalamus. Reproduced from Kandel, Schwartz, and Jessell (2012, p. 712). 28

2.1 The following figure, in essence, depicts one complete cycle for the project with the timepoints chosen carefully to tentatively reflect any change/activity that can be attributed to the difference in the experimental variable, i.e. kainic acid treatment v. controls. 33
2.2 **A flowchart to determine subsequent dose administration for each kainate-treated rat.** Following the first full dose (5 mg/kg i.p.), seizure-like behaviour (see Table 2.1) is monitored and recorded for 1 hour. This recorded seizure activity along with the seizure assessment flowchart serves to establish the next course of action (full dose, half dose (2.5 mg/kg), or no dose). Two finite state loops (an hourly assessment loop—left side of figure, thin lines and a 30 minute assessment loop—right side of figure, thick lines) determine the process (rectangles) for each possible decision (diamonds). The start box represents the first hour after the initial kainate injection and all remaining hours until each rat experiences > 3 hours of convulsive SE. SE = status epilepticus; WDS = wet dog shakes. Modified from Dudek and Edward (2005). 35

2.3 **Workflow/pipeline for graph theoretical network modelling and analysis of rsfMRI data.** Nodes correspond to *a priori* chosen ROIs or brain regions. The connections/links reflect the functional connectivity between the the nodes, calculated using the temporal correlation between the signals (preprocessed data: temporally filtered and spatially smoothed); this information is stored in a correlation matrix which is further thresholded (to constitute only the significant links in the brain graph) to obtain binary/sparse connectivity matrices. The brain graph topology is computed by several graph metrics to detect global integration and local segregation. Statistical analysis of the graph metrics reveals significant differences between the 2 groups. Reproduced from De Vico Fallani, Richiardi, Chavez, and Achard (2014). 39

3.1 **Top: Correlation Matrix** The heatmap figure represents the significant intra-group connections in the kainate (left, $P = 0.002$, $n_{kainate} = 6$) and the control (left, $P = 0.014$, $n_{saline} = 7$) group as Pearson's r correlation coefficients ($-1 < r < 1$) in an NBS framework. See Figure A.1 for a Fisher's r-to-Z normalized version of the matrix. **Bottom: Connectivity Matrix** The binary heatmap represents the significant networks as connected and disconnected nodes . See Table 3.1 and Appendix B.1 for edge/node abbreviations. 50

3.2 **Connectivity Graph (KA > Controls)** – The filled rectangles (overlaid with labels) represent the brain regions and the lines represent a significant supra-threshold connection between the two nodes (brain regions or seeds/ROIs). The colour scheme represent nodes with different degrees (K_i). This sub-network was thresholded at $t \geq 3.00$, with $P < 0.05$. Suffices (-r and -l) indicate right and left hemisphere. See Table 3.1 and Appendix B.1 for edge/node abbreviations. 52

3.3 Z-correlation scores of edges (undirected connections) that are signficantly altered between the kainate groups compared to controls are illustrated as mean $\pm$ SEM. Labels corresponding to each edges (pair of 2 nodes) is mentioned along the x-axis. See Table 3.1 for edge/node abbreviations. '*' signifies $P < 0.02$. 54

3.4 **Global Parameters**: Statistical comparison of the global parameters (C_w , L_w , E_{glob} , E_{loc}) of the functional networks between the kainate-treated group and saline-treated controls. Results are expressed as mean $\pm$ SEM. '*' signifies $P < 0.02$, and NS – not statistically significant. 55

3.5 **Isoflurane concentration (% volume) of loss of righting reflex**. Kainate-treated rats have a significantly higher isolflurane sensitivity than saline-treated rats. Results are expressed as mean $\pm$ SEM. '*' signifies $P < 0.001$. 57

3.6 **Prepulse Inhibition at Week 3**. PPI did not significantly differ between the kainate-treated and saline-treated control rats, or across time (Week 3 v. Week 7). Results are expressed as mean $\pm$ SEM. NS signifies not statistically significant. 59

3.7 **Behavioural hyperactivity**. Locomotor activity indicated by counts of interrupted infrared beams in a horizontal plane within 40 minutes in a chamber did not significantly differ between the kainate-treated and saline-treated control rats ($n_{kainate} = 6$, $n_{saline} = 6$), or across time (Week 3 v. Week 7). Results are expressed as mean $\pm$ SEM. NS signifies not statistically significant. 60

A.1 **Correlation Matrix** The heatmap figure represents the significant intra-group connections in the kainate (left, $P = 0.002$, $n_{kainate} = 6$) and the control (left, $P = 0.014$, $n_{saline} = 7$) group as Fisher's normalized correlations ($-1 < Z < 2$) in an NBS framework. 93

B.1 CA1 radiatum, CA1 oriens, and DG hilus 95
B.2 Frontal neocortex 95
B.3 Olfactory bulb (Glomerular layer) 96
B.4 Basolateral amygdala 96

C.1 **The spatial activation map overlaid onto the anatomical T2 image of a representative rat.** The spatial map was computed using the temporally filtered data using a seed (arbitrarily chosen, indicated by the green crosshairs) in the left neocortex, with the aid of InstaCorr tool included with the AFNI package. Right to left indicates anterior to posterior extent of the rat brain. Pearson's correlation coefficient, r = 0.86. 97
C.2 **The spatial activation map overlaid onto the anatomical T2 image of a representative rat.** The spatial map was computed using the temporally filtered data using a seed (arbitrarily chosen, indicated by the green crosshairs) in the right neocortex, with the aid of InstaCorr tool included with the AFNI package. Right to left indicates anterior to posterior extent of the rat brain. Pearson's correlation coefficient, r = 0.86. 97
C.3 **The EPI image of a representative rat** The EPI slices serves to indicate the presence of a signal gradient that is most likely responsible for weaker signal recorded from deeper brain structures using linear coil. Right to left indicates anterior to posterior extent of the rat brain. 97
C.4 **Unfiltered spectrum:** The EPI data with no spatial smoothing or preprocessing except skull stripping. 98
C.5 **Unfiltered spectrum:** The power spectrum post-spatial smoothing, $FWHM_{xy} = 0.8 \times 0.8\ mm^2$. 98
98figure.caption.40

List of Tables

1.1 Differential distribution of KAR subtypes (Bischoff, Barhanin, Bettler, Mulle, & Heinemann, 1997; Casassus & Mulle, 2002; Davila, Houpt, & Trombley, 2007; Lerma, Paternain, Rodríguez-Moreno, & López-García, 2001; Montague & Greer, 1999; Vincent & Mulle, 2009) 13

1.2 Effects of different modes of KA administration on the survival rate, latent period duration and associated neuropathological changes < 48 hours after SE, and at > 2 days after SE (Lévesque & Avoli, 2013). 14

1.3 Graph theory network measures. See Appendix A for mathematical notation. Adapted from Bullmore and Sporns (2009), and Hutchison (2012) 20

2.1 **Seizure Assessment**: Severity of motor seizure activity according to a modified Racine scale (Ben-Ari, 1985; Dudek & Edward, 2005; Racine, 1972). 34

3.1 Statistical significant undirected edges of the functional networks – kainate-treated group > controls. See Figure 3.2 for the graph network representation. Source and target nodes do not imply causality or directional connecitivity. 53

3.2 **Regional Parameters**: Statistical comparison of the regional parameter (K_i) of the functional networks between the kainate-treated group and controls. K_i is significantly higher in the kainate group compared to saline-treated controls. Mean K_i is expressed as $K_{i,\,\text{kainate}}(K_{i,\,\text{control}})$. P is computed for Wilcoxon tests with $W > 40$. 56

List of Abbreviations

AMPA	α-Amino-3-hydroxy-5-methylisoxazole-4-propionic acid.
ANOVA	Analysis of variance.
BOLD	Blood-oxygen-level dependent.
CA1	Cornu ammonis, region 1, of the hippocampus.
CA3	Cornu ammonis, region 3, of the hippocampus.
DA	Dopamine.
Deoxy-Hb	Deoxy-haemoglobin.
DG	Dentate gyrus.
EC	Entorhinal cortex.
ED	Effective dose.
EEG	Electroencephalography.
EPI	Echo planar imaging.
EPSP	Excitatory postsynaptic potential.
fcMRI	Functional connectivity magnetic resonance imaging.
fMRI	Functional magnetic resonance imaging.
GABA	γ -Aminobutyric acid.
GFAP	Glial fibrillary acidic protein.
HC	Hippocampus.
i.c.v.	Intracerebroventicular.
IED	Interictal epileptiform discharge.
iGluR	Ionotropic glutamate receptor.
ILAE	International league against epilepsy.
i.p.	Intraperitoneal.
IPSP	Inhibitory postsynaptic potential.
i.v.	Intravenous.
KA	Kainic acid.
KAR	Kainate receptor.
LFP	Local field potential.
LORR	Loss of righting reflex.
MDL	Mediodorsal thalamic nuclei.
MEG	Magnetoencephalography.
mGluR	Metabotropic glutamate receptor.
MRI	Magnetic resonance imaging.
MSDB	Medial septum-diagonal band of Broca.
MTLE	Mesial temporal lobe epilepsy.

NMDA	N-methyl-D-aspartate.
OFT	Open field test.
Oxy-Hb	Oxy-haemoglobin.
PET	Positron emission tomography.
PPI	Prepulse inhibition.
rsfMRI	Resting-state fMRI.
s.c.	Subcutaneous.
SE	Status epileptcus.
SEM	Standard error of the mean.
SIS	Spontaneous interictal spike.
SPECT	Single-photon emission computed tomography.
SWD	Spike-wave discharge.
T1	T1 longitudinal relaxation.
T2	T2 transverse relaxation.
TE	Echo time.
TLE	Temporal lobe epilepsy.
TR	Repetition time.

Chapter 1

Introduction

Epilepsy may be defined as the the brain's pathological disposition to spontaneously generate seizures. Epilepsy is a heterogeneous disorder with diverse etiologies (metabolic, genetic, structural, immune, infectious, environmental, or unknown). This heterogeneity has prompted several re-classifications of different epilepsies, partially due to scientific and technological advances to study the epileptic phenomenon with unprecedented temporal and spatial resolution (see ILAE review: Blümcke, Coras, Miyata, & Özkara, 2012, 2013).

1.1 Mesial Temporal Lobe Epilepsy (TLE)

In Canada alone, ~42 people, are newly diagnosed with epilepsy each day (Epilepsy Canada). Long-term drug therapy is the most prescribed form of treatment. Despite the treatment and constant influx of AEDs (anti-epileptic drugs) during the past decade, approximately 20% of people living with epilepsy still develop drug resistance (Engel et al., 2012). While seizure focus localization and its resection is the one of palliative treatments available, success rate described by long-term (> 1 year) seizure free outcome is pegged at less than 50% (Thom, Mathern, Cross, & Bertram, 2010; Wieser, Ortega, Friedman, & Yonekawa, 2003) and short-term (< 1 year) seizure free outcome at ~65% (Rohan & Cunningham, 2002). Such sub-optimal success rates can be attributed to the failure to detect the extent/reach of the network dysfunction. Evidently, successful surgical treatment has been intricately linked to the resection of multiple limbic regions as opposed to a

singular focus (Thom et al., 2010). Epilepsy research has focussed on diverse themes to address and counter the neuropathology; ranging from the type of cognitive impairments, pharmacoresistance, seizure propagation pathways, to the success of epilepsy surgery (Blümcke et al., 2012).

Mesial temporal lobe epilepsy (TLE; also referred to as limbic epilepsy), characterized by focal seizures[1] originating in mesial temporal lobe regions (includes hippocampus, amygdala, parahippocampal gyrus, and entorhinal cortex), is the the most common form of drug refractory epilepsy. Hippocampal sclerosis (HS) is the hallmark histopathology of this TLE syndrome (Blümcke et al., 2013). Berg et al. (2010) defines TLE with HS as an electroclinical syndrome with distinctive constellations - with etiological and pathological variations but involving the same set of TL and extra-TL regions. While the epileptogenic area is confined to the mesial temporal lobe regions, cognitive and psychiatric deficits in other cortical/subcortical areas have been well documented. Improved surgical outcomes, however, have been attributed to resection of multiple mesial temporal regions, not any one structure in particular (Thom et al., 2010). Thus, removing hippocampus and/or other mesial structures capable of generating seizures is paramount for seizure freedom.

Epileptic phenomena can emerge in many different systems in the brain. Notably, the thalamocortical (important role in absence epilepsy) and the mesial temporal lobe (includes hippocampus and other limbic regions - play a critical role in the MTLE syndrome) systems are particularly predisposed to generating and maintaining epileptiform activity. Increasing sophistication of ultra-high field acquisition protocols has been suggested to further refine the neuroimaging correlates of HS, and inevitably improve diagnosis and prognosis (Blümcke et al., 2013).

1.1.1 Neuropathology in TLE

The partial seizures of TLE arise in limbic circuits (HC, EC, Amygdala) following an initial precipitating injury (IPI). HS is characterized by hippocampal atrophy and the progressive neuronal

[1] TLE seizures are often described as complex partial seizures – focal seizures with impairment of consciousness or awareness. Focal seizure is no longer a recommended term in ILAE terminology (see Berg et al., 2010, for review; but also see Panayiotopoulos, 2012, for critical review)

loss and gliosis in the dentate gyrus (DG) hilus, CA1, and CA3 of the hippocampal subfields. These seizures break out and spread to other areas by recruitment of adjoining/adjacent regions.

The TLE syndrome does not result from the abnormal neuronal activity in a highly circumscribed focal area; rather, it involves a tightly connected neuronal network that includes several structures of the limbic brain (Bartolomei et al., 2004; Bertram, Zhang, Mangan, Fountain, & Rempe, 1998). This paves way for the formalism that the abnormality responsible for the epileptic seizures may actually be a function of several intricately-linked networks involving multiple anatomically distinct structures.

1.1.2 Mossy fiber sprouting

Mossy fibers are axons of the DG granule cells that project onto the dentate hilus and CA3 stratum lucidum in animals and humans. These axons synapse with CA3 pyramidal cells, inhibitory interneurons, hilar mossy cells, and infrequently with other granule cells. Mossy fiber sprouting is a form of synaptic reorganization in the dentate gyrus that occurs in human TLE and animal models of epilepsy. Mossy fibers spawn collaterals that grow abnormally into the inner third of molecular layer of DG (Buckmaster, 2010; Scharfman, Sollas, Berger, & Goodman, 2003).

The causality between mossy fiber sprouting and epileptogenesis has not be clearly established, with conflicting evidence ranging from positive-feedback seizure circuitry to the preferential excitation of the inhibitory interneurons (seizure control circuitry, Buckmaster, 2010; Wu & Leung, 2001). This robust mossy fiber sprouting is a common neuropathological feature in TLE patients, adults and children alike. Besides, it is not exclusive to the TLE syndrome – evidence of sprouting has been found in non-mesial TLE, bipolar disorders, and cortical dysplasias (with or without HC damage). Moreover, experimental models of epilepsy like KA, pilocarpine, and prolonged kindling also induce mossy fiber sprouting (Buckmaster, 2010).

1.1.3 Pathological oscillations in TLE

Limbic seizures are not the only physiologically-relevant EEG anomaly (brief events lasting between few milliseconds to several seconds) in the epileptic brain. Several mechanisms have been implicated in aiding and abetting this epileptiform synchronization [in the form of interictal discharges (IEDs) and high frequency oscillations (HFOs)] to varying degrees.

Interictal discharges, initiated by large postsynaptic depolarizations (Staley & Dudek, 2006), are used as diagnostic tools for seizure localization and chronic pre-surgical monitoring (see Curtis, Jefferys, & Avoli, 2012, for review). Using a kindling model, Wadman, Lopes da Silva, and Leung (1983) showed that in addition to the after-discharges (ADs) occuring following the kindling stimulus, short transients termed spontaneous interictal spikes (SISs) may occur spontaneously between seizures. Similar transients or spikes may be found in the clinical EEG as spikes and sharp waves of certain types of epileptic patients (Niedermeyer & Lopes da Silva, 2004). Leung (1988) observed that the frequency of SISs was high during slow-wave sleep (SWS), waking immobility, face-washing and chewing while it was relatively lower during rapid-eye-movement sleep (REMS), walking and rearing. Engel and Ackermann (1980) suggested that a high SIS rate may be correlated with an increased threshold for evoking an AD and consequently, seizures. In amygdala-kindled spontaneous seizing cats, Wada, Sato, and Corcoran (1974) reported a significant increase in the SIS rate before the onset of spontaneous convulsions, while Gotman (1984) and Gotman and Marciani (1985) demonstrated in cats and humans respectively that this increase did not affect the occurrence of spontaneous seizures.

The anatomical substrate for this IED chain reaction is the extensive axon collateral network of CA3 pyramidal neurons, which project to the other CA3 neurons and onto themselves (autosynapses) (Jefferys, Jiruska, Curtis, & Avoli, 2012). Spencer (2002) suggested that studying the propagation patterns of inter-ictal spikes recordings using EEG/MEG can reveal invaluable information about epileptic neuronal ensembles and thus, the networks (and their extent) they are part of. Rodin, Constantino, Rampp, and Wong (2009, interictal EEG spikes review) and Tanaka

et al. (2010, MEG spikes) suggested that this abnormal activity may be considered biomarkers of epileptogenicity. Eventually, contributing to improving the outcome of the epilepsy surgery (Schulz et al., 2000) and clinical prognosis by shedding light on mechanisms of ictogenesis and epileptogenesis (Staley & Dudek, 2006). Jacobs et al. (2012) reviewed a novel biomarker to proxy epileptogenicity index called high frequency oscillations, i.e., HFOs (80–500 Hz range; ripples and fast ripples), piqued a lot of interest and are subject of active investigation (Stefan & Lopes da Silva, 2013).

Neuroimaging techniques like structural MRI can reveal structural abnormalities, while EEG, MEG and BOLD fMRI can reveal the underlying dynamics to fully characterize epileptogenic networks. On routine MRI, relative qualitative atrophy of the affected hippocampus decreased signal intensity on T1 imaging, and unilateral T2 signal increase are the most common findings (Liao et al., 2011). Functional connectivity mapping determines the dynamics of epileptiform activities displayed as patterns of interactions between anatomically connected neural nodes responsible for these abnormal activities.

The advent of technology facilitating faster sampling rates in the domain of clinical electrophysiology has detected high frequency activity (HFA) at the seizure onset (Buzsáki & da Silva, 2012a). Current animal research has shown that the spontaneous bursting activity of population spikes is the only defining feature that separates the pathological HFOs from a normal one (Bragin, Benassi, Kheiri, & Engel, 2011, 2007). Further research is necessitated to relate the occurrence of HFOs to different seizure types of seizures in humans and in experimental models of epilepsy to shed light on their role in seizure generation, spread and maintenance. These HFOs may be key in unlocking the mechanisms of seizure evolution and eventually aid in localizing the epileptogenic zone in the clinical practice of epilepsy surgery. Zijlmans et al. (2011) highlighted their better specificity in the seizure-onset zone than interictal HFOs or spikes while Modur, Zhang, and Vitaz (2011), Ochi et al. (2007) revealed their possible role in post-surgical outcome prediction.

Wendling, Bartolomei, Bellanger, Bourien, and Chauvel (2003), in EEG signals recorded with intracerebral electrodes in patients suffering from partial epilepsy, found evidence for decorrelation

at seizure onset as very fast (60-90 Hz band) oscillations of low amplitude in the EEG, followed by an abnormally high degree of synchronization as the seizure develops (Thom & Bertram, 2012). A substantial body of converging research has indicated that focal lesions affect brain regions beyond the epileptogenic lesion site, involving several functionally and anatomically connected neuronal populations. Temporal lobe-plus epilepsy (Harroud, Bouthillier, Weil, & Nguyen, 2012) epileptiform activity emerges from diffuse areas in the multiple lobes in addition to temporal lobe. Some promising findings, however, have been reported. In a study of patients with focal epilepsies, Jacobs et al. (2009) demonstrated that changes in BOLD signal were associated with, and preceded by a few seconds, the inter-ictal spikes recorded at the scalp. This early BOLD response may be interpreted as resulting from changes in neuronal activity in epileptogenic neuronal networks situated deep in the brain that are not reflected at the level of the low-pass filtered scalp EEG.

1.2 Competing theories of epileptogenesis

The functional anatomy of the TLE is best described by two models taken together, viz. the trisynaptic circuitry of the hippocampus, and the multiple independent generator hypothesis. The hippocentric view of the limbic epilepsy, especially in the light of characterization of the trisynaptic circuitry (EC→DG→CA3→CA1→Subiculum/EC), has been the most accepted cortical basis of TLE. Mossy fiber sprouting resulting due to the abnormal physiology of the hilar interneurons reflects aberrance in the role of DG as a gatekeeper serving to modulate the synaptic transmission from the EC to the ammon's horn. However, this construct failed to explain the emergence of broader generalization in multifocal limbic and extra-limbic sites; and has largely been corroborated by the fact that maximal surgical reprieve is achieved by resecting as many limbic regions as possible. This suggests that one-structure hypothesis to explain the development of epilepsy is largely inadequate and must involve multiple initiators and critical amplifier sites.

The multiple generator hypothesis points to extra-temporal lobe involvement with medial dorsal thalamic nuclei (MDL; with its prolonged excitatory drive) as a potent conductor orchestrating

the epileptic symphony. Tract tracing and electrophysiological studies to establish anatomical connectivity have confirmed reciprocal projections between the MDL and the HC, EC, amygdala and the olfactory cortex complex - suggesting significant physiological substrate for interaction between the thalamus and limbic system. In addition, clinical studies have reliably found thalamic atrophy specific to TLE patients. Nonetheless, the emergent phenomena of the interaction between the thalamus and limbic seizure circuitry in the development and spread of seizures has proved elusive. Clearly, the affected areas lie beyond the lesion site across areas of functional and anatomically connected neuronal ensembles, and thus, bolstering the need for therapeutic interventions inline with a network disorder rather than a focal disease (see Bertram, 2014; Thom & Bertram, 2012, for review).

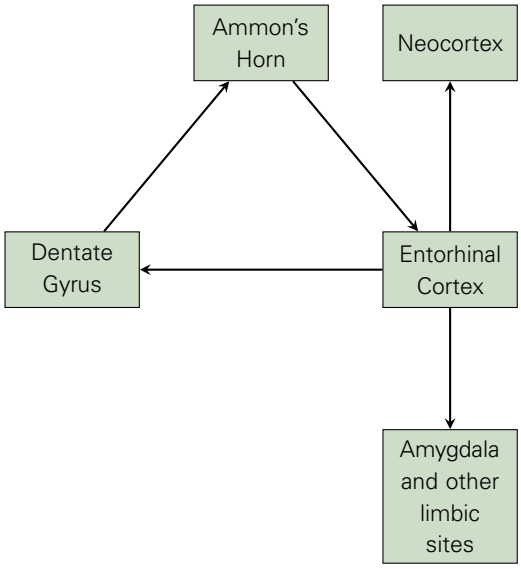

1.1.1: Trisynaptic seizures in limbic circuit.

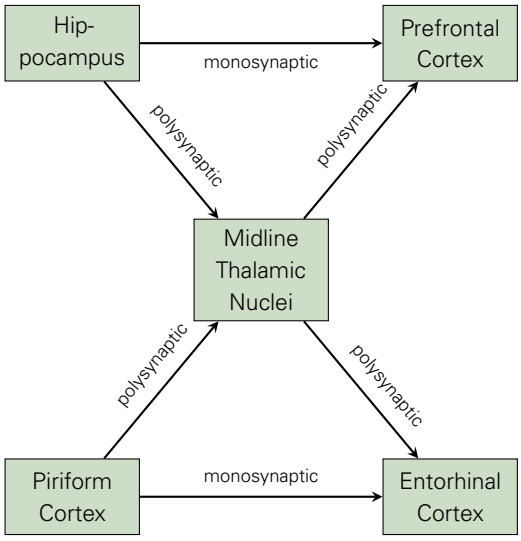

1.1.2: Medial dorsal thalamic nuclei in the divergent-convergent excitatory pathway.

Figure 1.1: Competing hypotheses in epileptogenesis.

1.3 Kainate model of TLE

Kainic acid is a cyclic L-glutamate analogue and a high affinity agonist of the ionotropic KA receptor (iGluRs: ionotropic glutamate receptors). The neuroexcitotoxic activity of the KA has been implicated in the epileptogenic character of its insult in the temporal lobe, consequently leading to symptoms that most closely imitate several behavioural, electroencephalographic, and neuropathological features of human TLE (Buckmaster, 2004; Coppola & Moshé, 2012; Dudek & Edward, 2005; Lévesque & Avoli, 2013).

High potency levels of this neurotoxin make it ideally suited to evoke robust depolarizations leading to cell death and eventually a status epilepticus state in experimental models of epilepsy. This rodent model mimics one phenomenon central to human TLE – the latent period [2] followed by the spontaneous recurrent seizures. The latent period has been regarded as an important therapeutic window for the development of antiepileptogenic strategies (Raol & Brooks-Kayal, 2012; Sloviter, 2008).

KA and pilocarpine are the preferred neurotoxins to induce acute epileptiform seizures arising in the temporal lobe; although pilocarpine results in additional selective lesions of the neocortex (Sharma et al., 2007). Systemic administration of KA leads to sustained limbic seizures lasting for several hours/days characterized by wet-dog shakes (WDS), facial and forelimb clonus, and rearing, falling and jumping (see Table 1.2, Dudek & Edward, 2005). Days, even weeks, following the status epilepticus (initial insult in TLE patients) a rather seizure-free/latent period results which inevitably leads to a significant proportion of surviving animals manifesting a chronic phase of spontaneous recurrent seizures with varying frequency but no remission during their entire lifespan (Drexel, Preidt, & Sperk, 2012; Sperk, Lassmann, Baran, Seitelberger, & Hornykiewicz, 1985).

[2] The latent period is characterized by a pre-epileptic seizure-free state following an initial insult to the brain that leads to molecular, cellular and network changes that give rise to delayed secondary processes which eventually matures, leading to spontaneous seizures

1.3.1 Kainic Acid Receptors (KARs)

KARs play an important role in the regulation, neuronal excitability and synaptic transmission in the limbic regions. Their role remains unclear in human epilepsy although their therapeutic potential in human diseases is an active topic of research (Matute, 2011). KA receptors [subunits: high-affinity GluK1, GluK2, GluK3, and low-affinity GluK4, GluK5; formerly GluR5, GluR6, GluR7, KA1, and KA2 respectively, see, Sharman et al. (2013, for revised nomenclature)] are differentially distributed throughout the brain, suggesting a specific role of each of the subunits in glutamatergic transmission: both ionotropic and metabotropic [See Table 1.1]. Functional KARs are expressed at presynaptic, postsynaptic, and extra-synaptic sites, and their activation has a plethora of effects (Lerma, Paternain, Rodríguez-Moreno, & López-García, 2001; Lerma, 2003).

KA interaction with KARs induces excessive depolarization that results in a cascade of cellular events, including excessive neuronal firing, but not limited to influx of cellular Ca^{2+}, reactive oxygen species (ROS) production, and neuronal apoptosis and necrosis as a consequence of mitochondrial dysfunction (Wang, Yu, Simonyi, Sun, & Sun, 2005).

GluK4 receptors exhibit a high expression profile in CA3 pyramidal cells but sparsely in CA1 while GluK5 is highly expressed in both CA1 and CA3 pyramidal neurons. This GluK4/K5 localization leaves CA3 region highly susceptible to KA-induced excitotoxic damage, rendering the hippocampus effectively the seizure onset zone (SOZ) in this TLE model. GluK2 is highly expressed in CA3 pyramidal cells. GluK1 is highly expressed in GABAergic interneurons of the CA1 and CA3 subfields (Lévesque & Avoli, 2013). At the presynaptic level, some KAR subtypes can effect glutamate transmission and short-term plasticity, whereas others regulate GABAergic transmission. At the postsynaptic level, KARs activated in response to endogenous release of glutamate exert an excitatory action onto both pyramidal cells and GABAergic interneurons (see Figure 1.3), and moderating neuronal excitability [by inhibiting slow afterhyperpolarization (sAHP)]. This duality in their response characteristics suggests that KARs can effectively modulate the activity of neuronal networks in either direction. Naturally, the fragile balance between excitation and

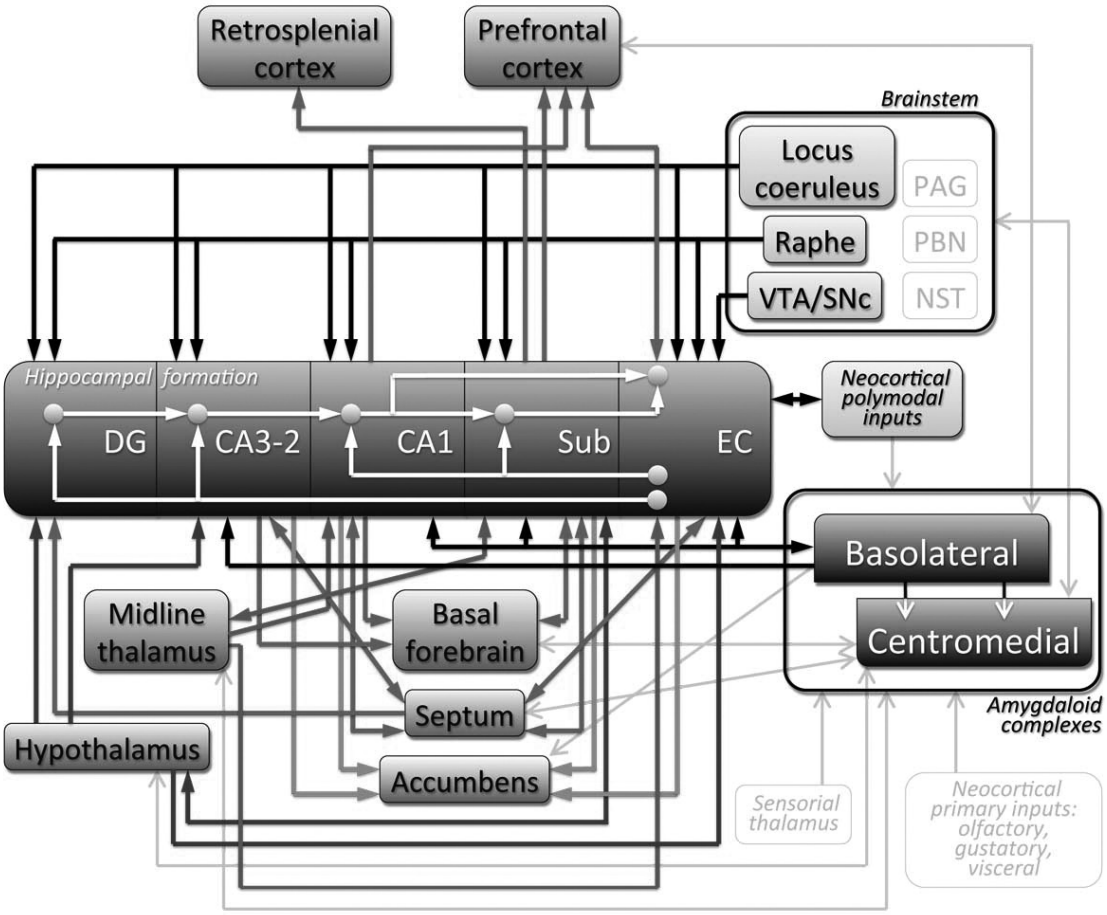

Figure 1.2: **Overview of hippocampal formation connectivity with other limbic structures.** Bold arrows depict well defined afferents and efferents of the hippocampal formation, and the entorhinal cortex. Light grey arrows/boxes represent connectivity of the amygdaloid complex. NST: nucleus of the solitary tract; PAG: periaqueductal grey; PBN: parabrachial nucleus; SNc: substantia nigra pars compacta; VTA: ventral tegmental area. Reproduced from Kandratavicius et al. (2012).

inhibition relies on the differential distribution and thus, activation of specialized KAR subtypes (O'Dell, Das, Wallace, Ray, & Banik, 2012; Vincent & Mulle, 2009). Exogenous KAR activation has been shown to potentially alter the GABA-mediated synaptic transmission in the hippocampus, amygdala, neocortex, dorsal striatum (Caudate-putamen (CPu); Chergui, Bouron, Normand, & Mulle, 2000), hypothalamus, as well as the dorsal horn (see Crowder, Ariwodola, & Weiner, 2006, for review). In addition, extrasynaptic release of glutamate from neighbouring synapses can activate KARs at GABAergic synapses and mimic the effect of exogenous KA on inhibitory synaptic transmission in the hippocampus, amygdala, and dorsal horn (Crowder et al., 2006).

The prominent neuromodulatory role of KARs is supported by the finding that these ionotropic channels can mediate slow neurotransmission through G-protein coupled receptors (GPCRs) and protein kinase C (PKC) (see Figure 1.4). This dual signalling underlies the diverse functions of KARs and defining this metabotropic component of the signalling system operated by KARs is essential in understanding the physiological contributions of glutamate receptors (Rodrigues & Lerma, 2012). This metabotropic action of KARs has been purported to physiologically support the temporal integration of glutamate transmission and synaptic plasticity, and it may be responsible for the KA-mediated epilpetogenicity. (Lerma & Marques, 2013; Rodrigues & Lerma, 2012).

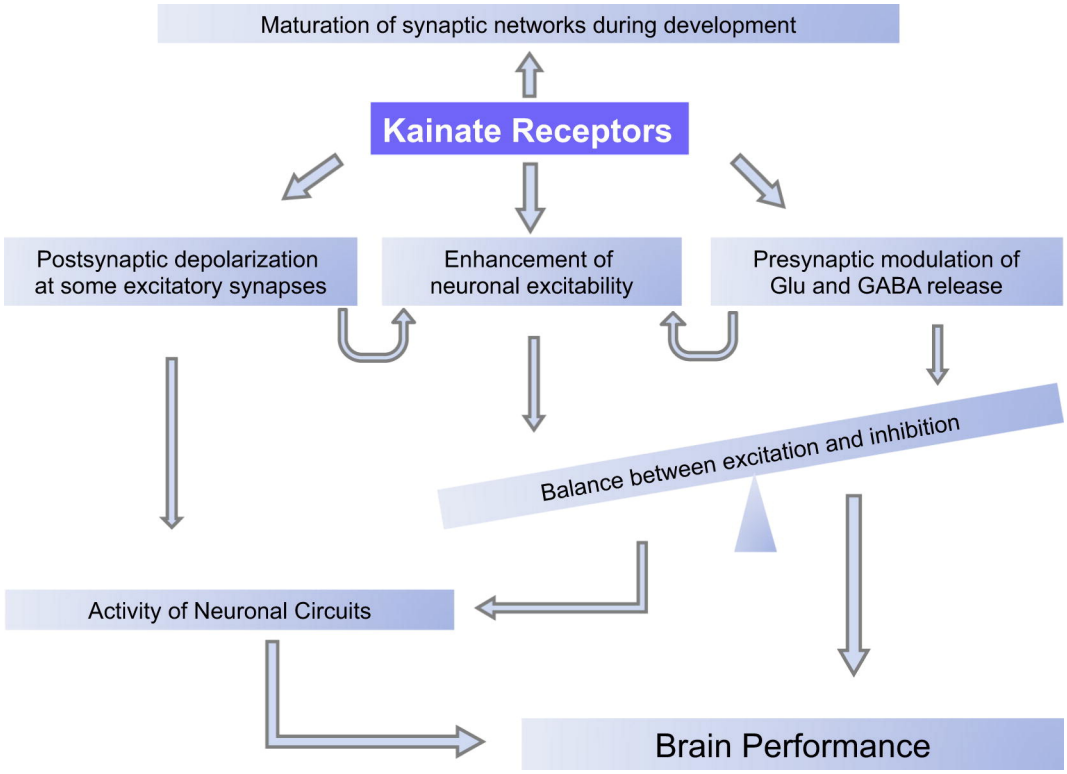

Figure 1.3: **Myriads of functional changes affected by KARs**. Any alteration in the regulation of these activities, including circuit maturation during development, may provoke sufficient disequilibrium as to lead to a disease state. Reproduced from Lerma and Marques (2013)

Lesions extraneous to the amygdala could not attributed to the toxin itself rather to the SE it induces, since diazepam injection before administering the KA in the amygdala did not affect the extent of lesions but prevented distant hippocampal damage (Lévesque & Avoli, 2013). GluK1–5 receptors are also expressed in the olfactory cortex complex – including the external plexiform layer,

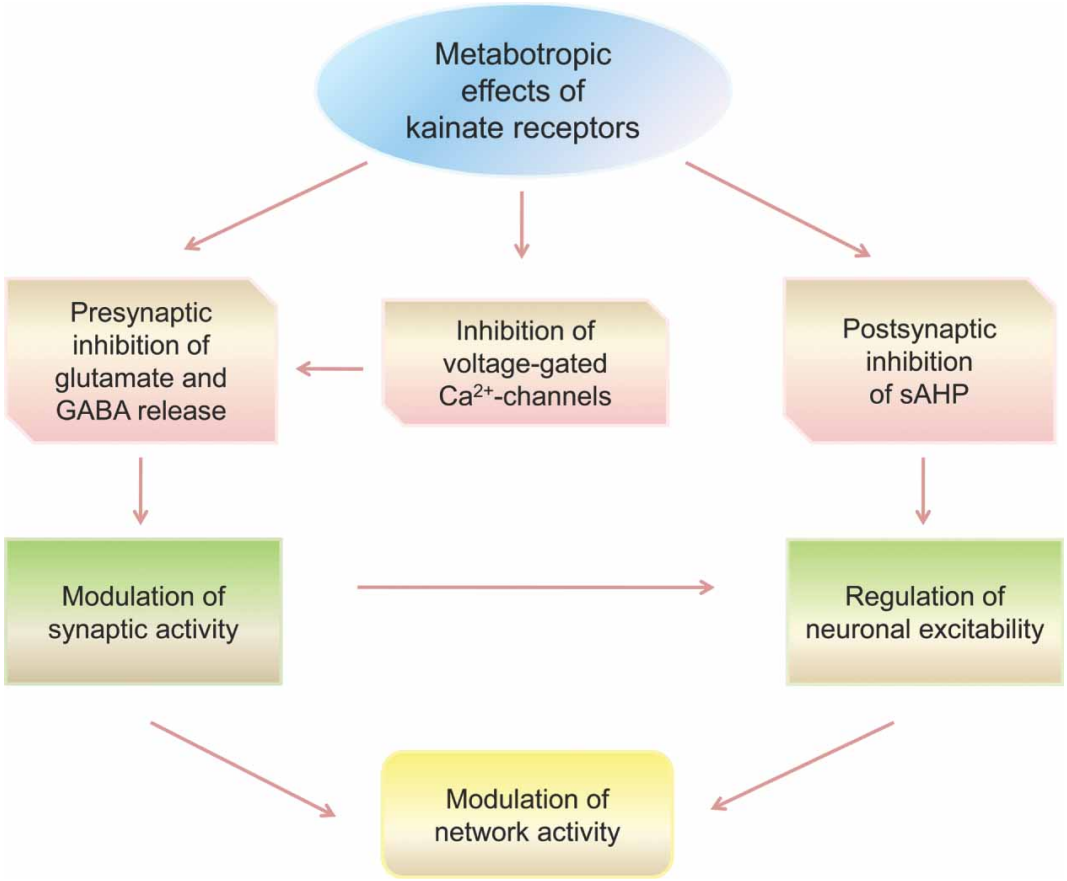

Figure 1.4: **Metabotropic action of KARs**. Presynaptic KARs can bidirectionally modulate neurotransmitter release at glutamatergic and GABAergic synapses. The inhibitory but not the facilitatory activity of KARs is most likely linked to GPCR coupled mechanisms. The inhibition of voltage-gated Ca^{2+}-channels by KARs, independent of ion flux, may contribute to the inhibitory action of KARs on neurotransmitter release. Regulation of synaptic activity is made possible via the presynaptic modulation of neurotransmitter release, and network activity control by regulating neuronal excitability. In addition, postsynaptic KARs can regulate neuronal excitability by inhibition of slow afterhyperpolarization (sAHP). Reproduced from Rodrigues and Lerma (2012)

olfactory nerve, glomerular layers, granule cells, mitral cells, and mitral/tufted dendritic processes (see Table 1.1 for differential expression). GluK1 and GluK2 mRNA levels are downregulated in response to sustained seizures (Mathern et al., 1998). However, Li, Lytle, Lan, Sandau, and Boison (2012) found contradicting evidence where GluK1 mRNA levels were upregulated in the hippocampus of TLE patients.

Mossy fiber sprouting in epileptic patients is correlated with an increase in GluR5 upregulation (Lévesque & Avoli, 2013; Li et al., 2012), and such upregulation has been shown to precede mossy fiber sprouting in KA-treated rats (Bernard et al., 1999). These data suggest that KARs may be responsible in facilitating the generation of epileptiform activity recorded from these functionally

KAR subtype	Brain region	Relative abundance in the Olfactory bulb
GluK1	Dorsal root ganglion (DRG) neurons Subiculum Septal nuclei Piriform cortex Nucleus accumbens Cingulate cortex	5
GluK2	Cerebellar granule cells Nucleus accumbens Dentate gyrus Hippocampal CA1	4
GluK3	Deep layers of cerebral cortex Striatum Inhibitory interneurons of the moleculer layer of the cerebellum	1
GluK4	Hippocampal CA3 Dentate gyrus Amygdala Nucleus accumbens Entorhinal cortex Cingulate cortex	2
GluK5	Essentially ubiquitous in the nervous system	3

5: highest abundance

Table 1.1: Differential distribution of KAR subtypes (Bischoff, Barhanin, Bettler, Mulle, & Heinemann, 1997; Casassus & Mulle, 2002; Davila, Houpt, & Trombley, 2007; Lerma, Paternain, Rodríguez-Moreno, & López-García, 2001; Montague & Greer, 1999; Vincent & Mulle, 2009)

aberrant synapses. Further, pharmacological blockade of KA receptors can effectively inhibit synchronized epileptiform transmission in the DG induced by electrical stimulation (Epsztein, Represa, Jorquera, Ben-Ari, & Crépel, 2005).

1.3.2 Neuropathological changes

Systemic administration of KA causes lesion similar to intracerebral injection, although to greater extent of neuronal damage (Lévesque & Avoli, 2013). Prominent loss of pyramidal neurons occurs in the CA1, CA3 and hilar regions of the hippocampus. (Haas, Sperber, Opanashuk, Stanton, & Moshé, 2001; Suárez et al., 2012). In addition, high sensitivity of parvalbumin-positive interneurons to KA leads to neurodegeneration in the CA1 region, the subiculum and the entorhinal cortex (Best, Mitchell, & Wheal, 1994; Drexel, Preidt, Kirchmair, & Sperk, 2011).

Fritsch et al. (2009) reported a significant reduction in the density of GABAergic (mainly

Mode of Administration	Mortality Rate	Latent period (days)	Neuropathological changes (< 48 hours after SE)	Neuropathological changes (> 2 days after SE)
Intra-amygdaloid	± 5%	10-40	Ipsilateral CA1, CA3 and DG hilar region. CA2 region and dentate granule cell resistance.	Entire hippocampus, contralateral amygdala, extra-temporal regions.
Intra-hippocampal	± 12%	5–30	Ipsilateral CA3 and DG hilar region, CA1 less sensitive.	Entire hippocampus, DG granule cell dispersion.
Systemic	± 17%	10–30	Bilateral neurodegeneration in the CA1, CA3 and DG hilar region, extrahippocampal sites.	Extensive bilateral neuronal loss in the hippocampus and extra-temporal regions, DG granule cell dispersion.

Table 1.2: Effects of different modes of KA administration on the survival rate, latent period duration and associated neuropathological changes < 48 hours after SE, and at > 2 days after SE (Lévesque & Avoli, 2013).

somatostatin-expressing) interneurons present in the basolateral amygdaloid nuclei. Drexel et al. (2012) observed, in systemically induced SE, that bilateral neuronal loss in the extra-temporal regions, neurodegeneration in entorhinal cortex (layer III), proximal subiculum, claustrum, thalamus, caudate putamen and the cerebral cortex occur within 24 hours of administration. Animals that survive relatively longer time periods (> 48 hours) after SE exhibit bilateral gliosis, neuronal shrinkage/edema in the piriform cortex, entorhinal cortex, olfactory bulb, substantia nigra, thalamus and mid brain, coupled with cell layer dispersion in the DG (Ben-Ari, Tremblay, Ottersen, & Meldrum, 1980, see Table 1.2). Interestingly, Sperk et al. (1983), Sperk et al. (1985) demonstrated that these extensive and diverse neuropathological changes are the mainstay of animals exhibiting robust convulsions during SE. Thus, bolstering the view that damage presenting in the extra-temporal/hippocampal regions is not directly caused by the toxin itself but is dependent on the propagation of epileptiform activity along monosynaptic and polysynaptic pathways.

1.3.3 Epileptogenesis

Systemic injections induce a latent period interspersed with SISs. Quite interestingly, in animals that go on to develop chronic epilepsy following SE, the interictal spike frequency during the latent period is higher relative to non-epileptic rats. Also, epileptic rats have a higher tendency to exhibit clusters of such interictal spikes, which suggests these events may serve as proxy for biomarkers

of pathological network activity in limbic networks, in the KA model of SE (White et al., 2010). These results also indicate that such patterns of interictal spikes may be a product of underlying epileptogenic or ictogenic mechanisms.

KA-induced microglial activation

Microglial/astrocytic activation accompanies neuronal death in the KA model, which is evident by the congregation of activated gliocytes in the hippocampus (Ravizza et al., 2005). However, the role of microglia in initiating the inflammatory and degenerative processes that aggravate the damage, is still scant and unclear. Gliosis has been suggested to play a neuroprotective and reparative role in MS (with its animal model) and experimental autoimmune encephalomyelitis (EAE). Microglial activation seems to be a physiological response to KA-induced excitotoxicity, but serves to aggravate the debilitating effect of neurodegeneration. Additional evidence comes from studying the glial fibrillary acidic protein (GFAP), a marker for astrogliosis, which was shown to rise steadily following local/systemic injections of KA (Vargas, Takahashi, Thomson, & Wilcox, 2013).

Non-synaptic effects of glial interaction play a role in the synchronicity of epileptic events as well. Gap junctions between astrocytes are upregulated in TLE patients, and may have a pro-epileptic effect due to glutamatergic signalling between astrocytes and neurons (Seifert, Carmignoto, & Steinhäuser, 2010). Gap junctions between interneurons in the hippocampus (Fukuda & Kosaka, 2000) are capable of enhancing coherent oscillations facilitated by their GABA mediated synaptic networks (Jefferys et al., 2012; Mancilla, Lewis, Pinto, Rinzel, & Connors, 2007).

Pathological oscillations in Kainate model of TLE

The occurrence of synchronized electrical activity across multiple bands (δ (delta), β (beta), θ (theta), α (alpha), γ (gamma), etc.) fluctuate as a function of behavioural-state or task demands (Engel, Fries, & Singer, 2001). These distributed oscillatory systems facilitate resonant communication through which discrete neuronal populations are synchronized, providing a precise timing

of discharges for information coding and transfer (Buzsáki, 2006; Buzsáki & Wang, 2012b). High frequency-band oscillations are typically confined to a relatively small area, linking local populations of neurons, whereas distributed brain regions are recruited during slow oscillations to form large-scale networks (Buzsáki & Draguhn, 2004; Csicsvari, Jamieson, Wise, & Buzsáki, 2003). The coincidence of various neuronal oscillations within the connectome permits independent information integration and processing at multiple temporal and spatial scales (Buzsáki & Draguhn, 2004).

Fisahn et al. (2004), using KAR knock-out homozygous (GluK1-K5$^{-/-}$) mice populations, established distinct roles of GluK1/K2 in support of the rhythmic activity of the healthy brain (gamma oscillations) and the pathological brain (epileptiform bursts). Ben-Ari, Riche, Tremblay, and Charton (1981) and Lothman and Collins (1981) discovered interictal spikes that first occur in the entorhinal cortex or the hippocampus following a systemic (i.p., s.c., or i.v.) injection of KA in rats, travelling to the amygdala, and then propagating to the thalamus, CA1 and the frontal cortex; without any detectable clinical signs or symptoms. In addition to interictal spikes, EEG recorded from the HC in KA model was characterized by rhythmicity of gamma (25–30 Hz) oscillations. Medvedev, MacKenzie, Hiscock, and Willoughby (2000) confirmed and characterized this phenomenon recorded from hippocampal EEG in the KA model, observing runs of gamma oscillations (30–40 Hz) followed by sporadic spikes preceded by clinical signs (Figure 1.5). Lévesque et al. (2009) also reported gamma oscillations, recorded from the HC, during seizure activity induced by KA.

Behavioural alterations in Kainate model of TLE

Comorbidities observed in TLE patients comprise major depression, anxiety disorders, psychosis and/or cognitive dysfunction (Engel, 1996; Trimble, 1991). Experimental models of epilepsy, such as the kainate/pilocarpine model of acquired epilepsy, help explore the relationship between epilepsy and behavioural deficits (Gröticke, Hoffmann, & Löscher, 2007).

TLE is often associated with schizophrenia-like symptoms, which are measured in rodents

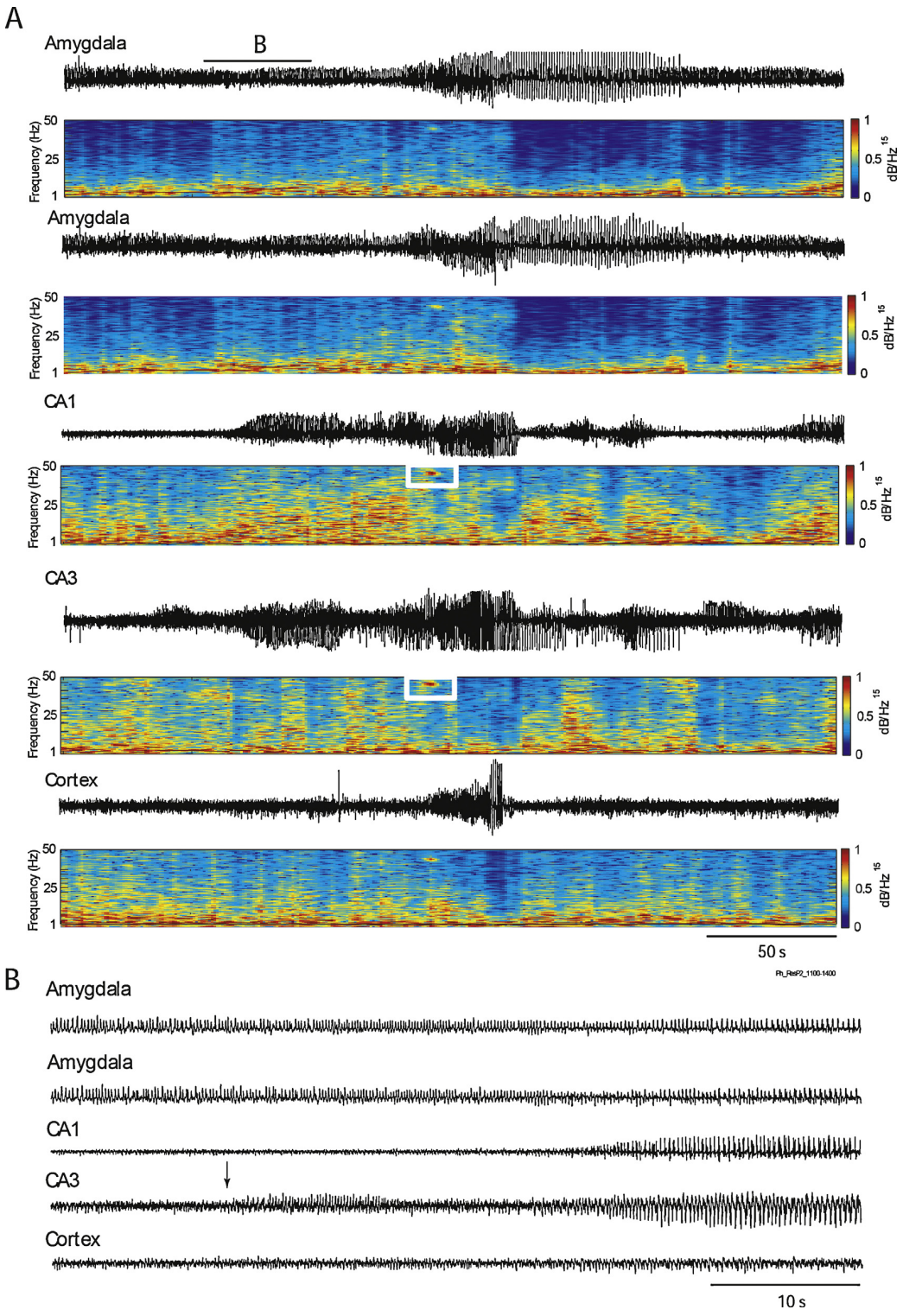

Figure 1.5: **(A)** EEG depth recordings in rat depicting a seizure recorded simultaneously in the amygdala, hippocampus and neocortex ~2 h following intra-peritoneal (systemic) administration of KA (6 mg/kg). Gamma oscillations (30–80 Hz) (white bordered rectangles) occurs in the CA1 and CA3 region. **(B)** Seizure-onset is depicted on an expanded time scale. Note: Arrow indicates the seizure start timepoint in the CA3 region. Reproduced from Lévesque and Avoli (2013).

by behavioural hyperactivity and loss of sensorimotor gating. Sensorimotor gating describes neurological processes responsible for distinguishing useful information from the background noise. A reduction in the startle amplitude is indicative of the ability of the nervous system to briefly adapt to a strong sensory stimulus when a pre-emptive attenuated signal serves as a warning to the organism. Deficits of prepulse inhibition (PPI) have been linked to abnormalities of sensorimotor gating and have been observed in psychiatric and neurodegenerative illnesses, for instance, schizophrenia (Braff, Geyer, & Swerdlow, 2001). PPI was also disrupted by kindling of the hippocampus or prefrontal cortex, and immediately after a stage 5 amygdala seizure (Koch & Ebert, 1998) or a single hippocampal seizure (Ma, Shen, Rajakumar, & Leung, 2004b). These PPI deficits are most likely due to hyperactivity within the mesolimbic dopaminergic system, or a disturbance of the glutamatergic neurotransmission in the nucleus accumbens (Koch & Schnitzler, 1997). Another schizophrenia-like symptom induced by TLE models in rats is behavioural hyperactivity, which could be recorded as hyperlocomotion in an open field, or induced by stress or drugs. Epileptic rodents exhibit deficits in cognitive and memory tasks (Ando, Morimoto, Watanabe, Ninomiya, & Suwaki, 2004), quantified by tests such as the water maze, the open-field test, and the object exploration tasks. In addition, deficits in short-term spatial memory and long-term spatial learning, a higher anxiety level (Ratté & Lacaille, 2006), and depression-like behaviors have also been observed (Gröticke, Hoffmann, & Löscher, 2008).

1.4 TLE in a graph theoretical framework

The intrinsic complexity of the organization of the anatomical and functional connectome has been considered akin to large-scale networks such as the Internet, social networks, or metabolic networks; and has been the object of network modelling based on topological properties known as the graph analysis.

The delineation of epileptogenic networks plays a substantial role in improving planning leading up to the resective surgery, and consequentially guide targeted interventions and therapies

with the aim of controlling epileptiform activity in relevant hubs and nodes within the abnormal network(s) (Lopes da Silva, Gorter, & Wadman, 2012). Functional connectivity mapping of brain networks has consistently identified sets of regions critical in enabling efficient neuronal signaling and communication. These brain hubs in anatomical and functional networks facilitate diverse functional roles across a host of cognitive tasks and both global and local dynamic coupling of functional networks (van den Heuvel & Sporns, 2013).

In a graph theoretical network framework functional networks can be objectively characterized by different mathematical measures (see Rubinov & Sporns, 2010, for a non technical review; Table 1.3). Watts and Strogatz (1998) defined small-world networks as a class of networks with significantly more clustering than random networks, while still have a similar characteristic path length as random networks. In addition, small-world networks have the property of being highly segregated and integrated, with highly connected hubs, and high modularity (Bullmore & Sporns, 2009).These networks are hypothesized to optimize rapid synchronization transfer creating a balance between local processing and global integration (Meador, 2011). Such optimal configuration of information transfer and processing is the hallmark of brain networks, and other biological networks (Stam & Reijneveld, 2007b). Random networks, on the other hand, are characterized by a low clustering coefficient and a typical short path length. In contrast, small world networks have higher absolute clustering coefficient but similar absolute path length, that is $\gamma = C_{net}/C_{random} > 1$, $\lambda = L_{net}/L_{random} \approx 1$. γ and λ can be be quantified as small-world-ness, $\sigma = \gamma/\lambda$, which is $\gg 1$ for small-world networks. To study the small world properties, the value of C_{net} and L_{net} of the functional network is compared to that of a random network (C_{random} and L_{random}).

Graph-theoretical analyses of global anatomical network organization of patients revealed increased path length in TLE (Bernhardt, Chen, He, Evans, & Bernasconi, 2011). Global integration and local segregation measures of functional networks in TLE have been reported to be significantly altered relative to controls. Most noteworthy, increased connectivity within the mesial temporal lobe (higher clustering) and decreased connectivity (longer path length) along extratemporal

Measure	Definition
Assortativity	The correlation between the degrees of connected nodes. Positive assortativity indicates that high-degree nodes tend to connect to each other
Centrality	How many of the shortest paths between all other node pairs in the network pass through a node
Clustering coefficient	Quantifies the number of connections that exist between the nearest neighbours of a node as a proportion of the maximum number of possible connections (Watts & Strogatz, 1998)
Connection density/cost	The number of edges in the graph as a proportion of the total number of possible edges
Degree	The number of connections that link a node to the rest of the network
Degree distribution	The distribution of the degree values for all of the network's nodes (Amaral, Scala, Barthelemy, & Stanley, 2000)
Efficiency	Efficiency is inversely related to path length but is numerically easier to use to estimate topological distances between elements of disconnected graphs
Hub	Hubs are nodes with high degree, or high centrality.
Modularity	Nodes that are highly interconnected and that overlap in their external connection patterns. Modules may also be functionally defined on the basis of the pattern of functional or effective connections. A given network can be decomposed into a set of non-overlapping, overlapping, or hierarchical arranged modules (Sporns, 2010, p. 328)
Motifs	A small subset of network nodes and edges forming a subgraph (Sporns, 2010, p. 328). The distribution of different motif classes in a network provides information about the types of local interactions that the network can support (Sporns & Kötter, 2004)
Path length	The minimum number of edges that must be traversed to go from one node to another.
Robustness	Robustness refers either to the structural integrity of the network following deletion of nodes or edges or to the effects of perturbations on local or global network states.
Triangle	The number of triangles around a node.

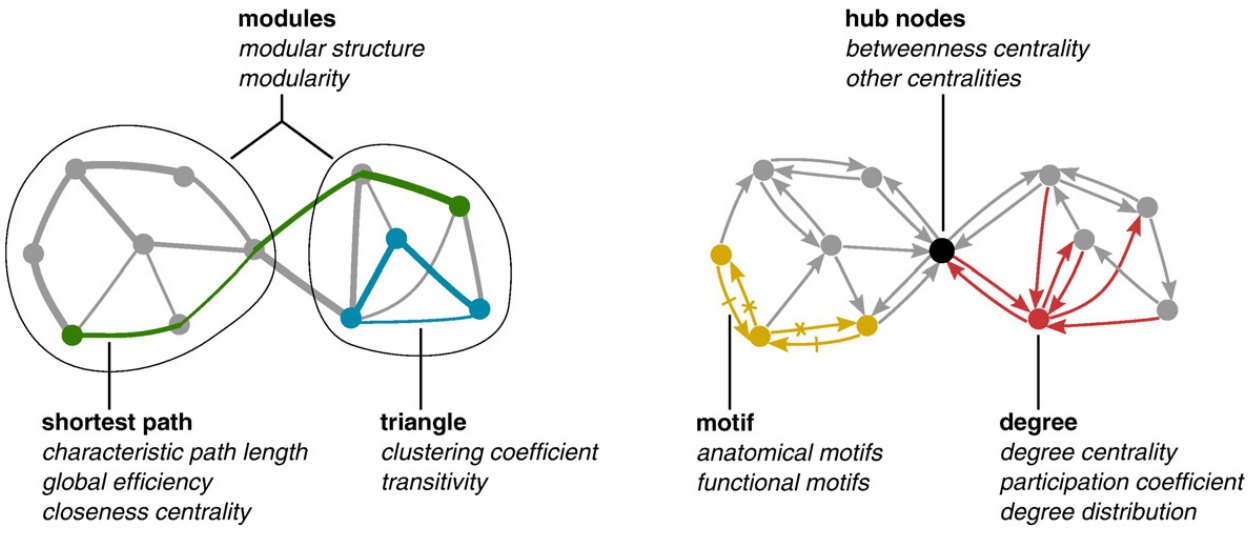

Table 1.3: Graph theory network measures. See Appendix A for mathematical notation. Adapted from Bullmore and Sporns (2009), and Hutchison (2012)

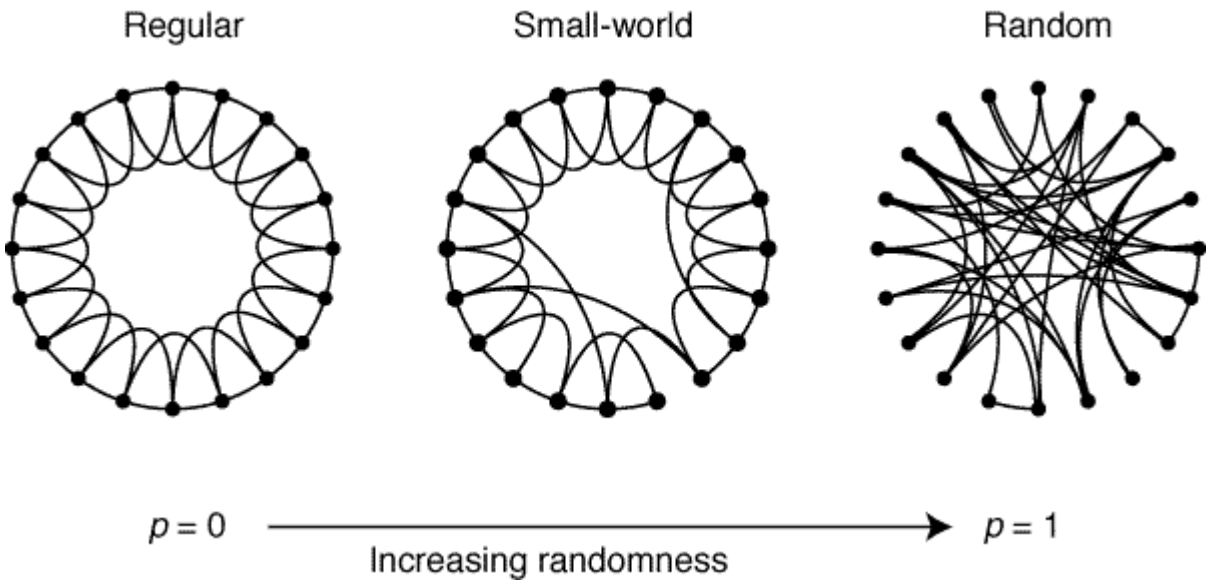

Figure 1.6: **Random rewiring in network configurations** A random rewiring procedure is dependent on the variable p, the probability of rewiring ($0 < p < 1$). This rewiring commences with a regular ring lattice with edges connecting node with probability p. As p increases, the graph becomes increasingly disordered until for p = 1, all edges are rewired randomly. For intermediate values of p, the graph is a small world network: highly clustered like a regular graph, yet with small characteristic path length, like a random graph. Three realizations of the process (for three different p values) are depicted. Reproduced from Watts and Strogatz (1998, with n = 20 vertices an average degree of k = 4 edges per vertex).

areas, including contralateral temporal regions (Cortical thickness networks; Bernhardt et al., 2011; Functional networks; Bettus et al., 2009), indicative of a reduction in global efficiency (Wang et al., 2014). Morgan, Rogers, Sonmezturk, Gore, and Abou-Khalil (2011) suggested altered bitemporal connectivity in patients with TLE. These findings suggest a deleterious impact of the epileptic lesion and the epileptogenic zone on the whole brain, potentially impacting multiple cerebral networks (Tracy et al., 2014). Liao et al. (2010) demonstrated using nodes derived from resting-state data, small world character in TLE patients along with increased connectivity in the medial temporal lobe regions and disconnection within the "default mode" network. Notably, Voets et al. (2012) explored the three-way relationship between functional network disruption, white matter disconnection, and gray matter atrophy in TLE patients. They found a lower functional connectivity between the hippocampus, anterior temporal cortex, and precentral cortex; and the DMN and sensorimotor networks.

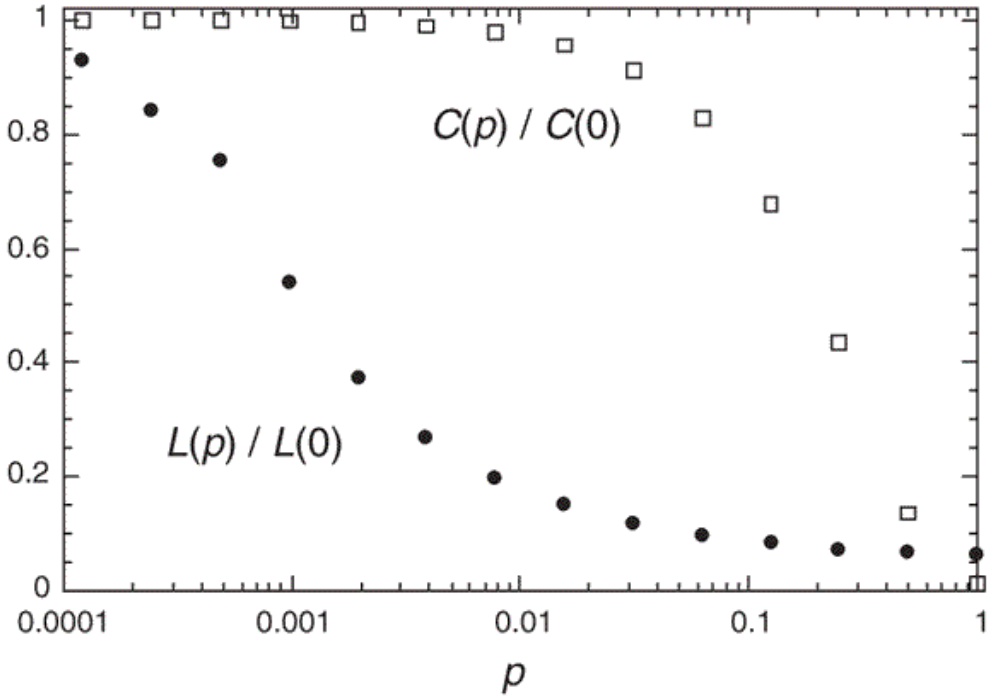

Figure 1.7: The characteristic path length $L(p)$ and clustering coefficient $C(p)$ for the family of randomly rewired graphs described in Figure 1.6 (averaged and normalized over 20 realizations). A logarithmic horizontal scale has been used to resolve the rapid drop in $L(p)$, corresponding to the onset of the small-world phenomenon. During this drop, $C(p)$ remains almost constant at its value for the regular lattice, indicating that the transition to a small world is almost undetectable at the local level.Reproduced from Watts and Strogatz (1998, n = 1,000 vertices and an average degree of k = 10 edges per vertex).

1.4.1 Resting State Networks and Multimodal Strategies

Resting-state fMRI (rsfMRI) has facilitated non-invasive visualization of the the neuronal activity in the brain at unprecedented spatial resolution, although at the cost of temporal resolution. The haemodynamic response that underlies the BOLD (Blood Oxygenation Level Dependent) signal is predominantly based on the displacement of deoxyhaemoglobin by inflowing oxygenated haemoglobin, and thus, acts as a proxy for the underlying neuronal activity. Further, Logothetis and Wandell (2004) demonstrated that the BOLD signals rely heavily on blood volume and flow, as well as on oxygen consumption, all factors which are generally positively correlated with neuronal activity (i.e., neurovascular coupling).

rsfMRI examines the spatial synchronization of intrinsic spontaneous low frequency fluctua-

tions (BOLD signal) rooted in the neuronal and synaptic activity that reflects stimulus-independent processing in the brain as opposed to an external stimulus (Kandel, Schwartz, & Jessell, 2012). Functional networks are statistical constructs that exhibit considerable variability on short timescales (temporal evolution), either spontaneously or in response to varying conditions of input and task (Sporns, 2013). These functional networks arise in the form of low-frequency oscillations (LFOs; $0.01 < f\ (\text{Hz}) < 0.1$) and are assumed to reflect the intrinsic functional architecture of the brain. Such simultaneous task-independent variations in different parts of the brain are thought to represent various networks, working in tandem to achieve a common goal of complex information processing. A growing number of studies have recognized such large-scale brain networks (Smith et al., 2009) to investigate basal brain states in health and disease (Kaiser, 2013) ever since the first RSNs were discovered within the somatosensory motor system (Biswal, Yetkin, Haughton, & Hyde, 1995). Such local and global networks have begun to serve new insights into the human connectome and the role it plays in shaping the functional dynamics (Greicius, Supekar, Menon, & Dougherty, 2009; Sporns, 2011, 2013). This realization has culminated in the setting up of BRAIN initiative (Insel, Landis, & Collins, 2013) and the Human Connectome Project (Van Essen et al., 2013) to chart the structural and functional connectome of the human brain.

The high spatial resolution of this BOLD signal complements the high temporal resolution of the EEG and better aids in the localization of focal epilepsies (Ando et al., 2004), and hence are seen today as invaluable diagnostics in the study of epileptic networks. rsfMRI connectivity also has been suggested as a good predictor of surgical outcome in TLE patients (Negishi, Martuzzi, Novotny, Spencer, & Constable, 2011). Effectively, fMRI aids in detection of various perturbations that impede the information flow and processing in the short- and long-range networks (Waites, Briellmann, Saling, Abbott, & Jackson, 2006). Hutchison, Mirsattari, Jones, Gati, and Leung (2010) identified several bilateral functional networks in the subcortical areas like the hypothalamus and the hippocampus of the rat brain. These RSNs are present in homologous brain regions in the rat, monkey and human (see Figure 1.8), indicative of an evolutionarily conserved feature.

The "default mode" network (DMN), one of several RSNs, is deactivated during goal-directed

of a non-self referential nature, while being most active in a resting state (awake with eyes closed), and involved in episodic memory processes and self-referential mental representations. Greicius et al. (2009) found structural connectivity between functionally connected parts of the default mode network (DMN), consisting of areas in dorsal/ventral medial prefrontal cortices, medial and lateral parietal cortex, and regions in the medial/lateral temporal cortices. The structural and functional substrates of the rat DMN are detailed in Lu et al. (2012). The existence of DMN in humans, nonhuman primates and rodents both under anaesthetic and conciousness states suggests that the basic role of DMN is not restricted to the self-referential behavioural constructs.

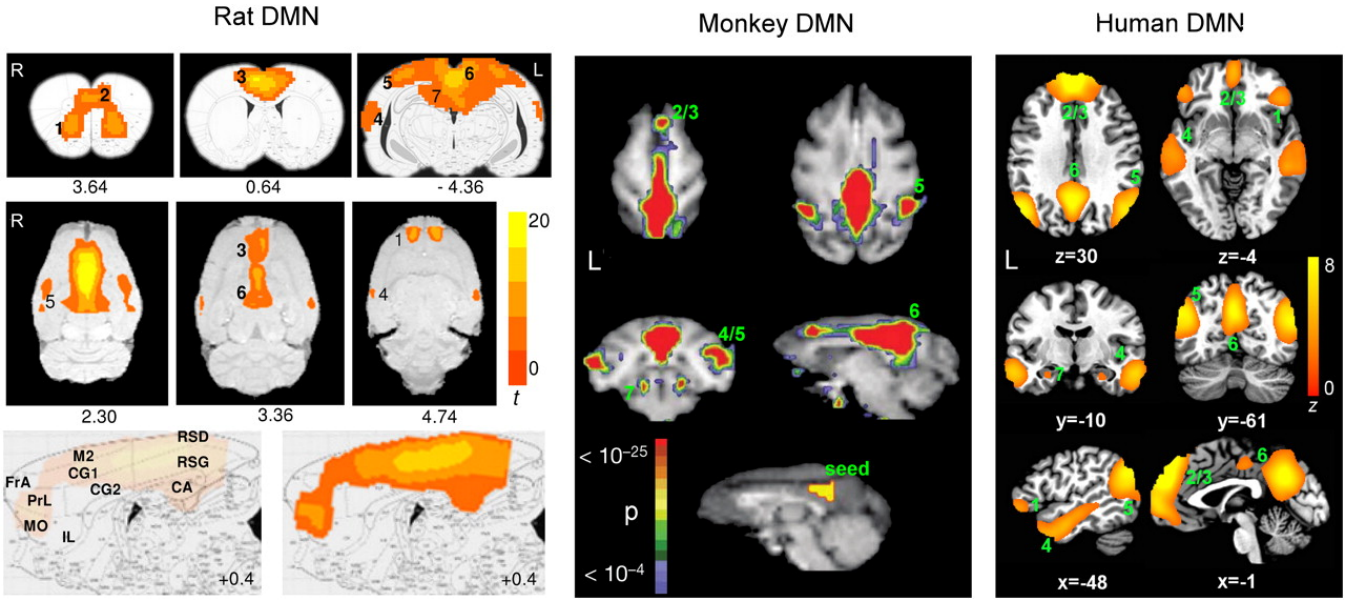

Figure 1.8: Comparison of the homologous Default Mode Network (DMN) in rat, monkey, and human.
Rat DMN, significant brain regions include: 1, orbital cortex; 2, prelimbic cortex (PrL); 3, cingulate cortex (ACC); 4, auditory/temporal association cortex (Au1, AuD, AuV, TeA); 5, posterior parietal cortex; 6, retrosplenial cortex (Rsp); 7, hippocampus. (Center) Brain spatial activation in the axial plane.
Human DMN (Right), significant clusters include: 1, orbital frontal cortex; 2/3, medial prefrontal cortex/anterior cingulate cortex; 4, lateral temporal cortex; 5, inferior parietal lobe; 6, posterior cingulate/retrosplenial cortex; 7, hippocampus/parahippocampal cortex.
Macaque (monkey) DMN: 2/3, dorsal medial prefrontal cortex; 4/5, lateral temporoparietal cortex (including area 7a and superior temporal gyrus); 6, posterior cingulate/precuneus cortex; 7, posterior parahippocampal cortex. Adapted from Lu et al. (2012) and Vincent et al. (2007).

Multimodal Strategies

EEG-fMRI has the operational advantage of both the techniques in adequately sampling the complex spatiotemporal domain of the brain networks, while being able to directly relate the BOLD response to epileptic phenomenon (Abela et al., 2014; LeVan, Tyvaert, Moeller, & Gotman, 2010; Mulert & Lemieux, 2009). Abela et al. (2014) using a spike-based evaluation of EEG-fMRI, and Huster, Debener, Eichele, and Herrmann (2012) by implementing an ICA-based approach, identified interictal discharges to be intrinsic predictors of estimating the haemodynamic responses linked to IEDs. Clinical data from multiple modalities like MRI, SPECT, PET, EEG, MEG, etc., in isolation and combination, has aided in making better estimates to localize epileptogenic foci and improve outcomes following focal resection surgery. Evidence gathered independently using several multimodal techniques is slowly converging to reveal a better network topology in epilepsy.

Evidently, the effect mesial temporal sclerosis and/or anti-epileptic drugs may have on the neurovascular coupling (prime for observing the BOLD effect) in compromising the global/local connectivity, is largely unclear (McAndrews & Cohn, 2012). However, it has been, invariably, argued that understanding the alterations in network structure and dynamics could improve diagnostic classification and identify new biomarkers and potential targets for therapy.

1.4.2 RSN Pathologies in TLE

Further impetus to investigate networks using resting-state has come from the discovery of RSN alterations across a plethora of neuropathologies. Research on experimental models of neuropathologies has significant clinical value. Need for experimental animal models in rsfMRI has been stressed several times due to the advantage of manipulability that is not possible in humans, due to obvious ethical considerations. In addition, animals models are free of multiple confounding factors and host of other factors that share a complex relationship with BOLD activation: (i) non-availability of age matched controls, (ii) estimates of structural integrity, (iii) etiology of and duration of disease state, (iv) cerebral reserve and extent of functional lateralization (Bettus et al.,

2011; McAndrews & Cohn, 2012).

Disruptions in the functional RSNs (see Greicius, 2008, for review), most notably the DMN, have been reported in several neurological and psychiatric disorders including major depression (Greicius et al., 2007; Kühn & Gallinat, 2013; Veer et al., 2010), schizophrenia (Bassett, Nelson, Mueller, Camchong, & Lim, 2012; Lynall et al., 2010), Alzheimer's disease (Damoiseaux, 2012; Wang et al., 2007), attention deficit hyperactivity disorder (ADHD) (Castellanos et al., 2008; Fair et al., 2010), epilepsy (Bettus et al., 2009; Luo et al., 2011), coma (Norton et al., 2012), chronic pain (Farmer, Baliki, & Apkarian, 2012), multiple sclerosis (Enzinger & DeLuca, 2012; Lowe et al., 2008), amyotrophic lateral sclerosis (Mohammadi et al., 2009), and Parkinson's (Prodoehl, Burciu, & Vaillancourt, 2014). Besides disruption of the DMN in TLE patients (see Cataldi, Avoli, & de Villers-Sidani, 2013, for review), several networks including attentional (Zhang et al., 2009b) and perceptual (Zhang et al., 2009a) have also been reported to be dysfunctional.

1.5 Effect of Anaesthesia

Hippocampal theta rhythm has been implicated in various phenomena that includes attention and acquisition of sensory information. The circuit of hippocampal theta synchronization includes the medial septum-diagonal band of Broca (MSDB), with cholinergic and GABAergic neurons serving as the main projections from MSDB to HC (Yoder & Pang, 2005). These neurons project to the HC through the fimbria-fornix which mediates hippocampal theta (M'Harzi & Monmaur, 1985). Electrolytic lesion of the medial septum had the effect of increasing the sensitivity to anaesthetics – propofol and isoflurane (Leung, Ma, Shen, Nachim, & Luo, 2013).

Determining LORR sensitivity to isoflurane is critical for the rsfMRI studies since isoflurane is a potent vasodilator and likely affects neurovascular coupling in the brain directly modulating the BOLD response (Farber et al., 1997; Masamoto, Fukuda, Vazquez, & Kim, 2009), warranting the use of lowest possible dose of isoflurane concentration to maintain rat immobility during the fMRI scanning session. When microinfused into the medial septum, KA acts as poison to

preferentially eliminate GABAergic neurons, while 192 IgG-saporin (SAP) selectively destroy cholinergic neurons (Yoder & Pang, 2005). Tai, Ma, and Leung (2014) recently reported that selective lesion of cholinergic neurons in the media septum mediate enhancement of isoflurane sensitivity and prolonged isoflurane anaesthesia.

Hutchison et al. (2010) discovered several coherent resting-state networks in the brains of anaesthetized rats using ICA in high-field fMRI data. However, no conclusions could be drawn on how the spatiotemporal landscape of the RSN changes with isoflurane type and concentration. Nonetheless, these RSNs have been found to exist in both awake (Becerra, Pendse, Chang, Bishop, & Borsook, 2011; Liang, King, & Zhang, 2011; Upadhyay et al., 2011) and anesthetized (Kannurpatti, Biswal, Kim, & Rosen, 2008; Liang, King, & Zhang, 2012) states in rats. Moreover, Wang et al. (2011) demonstrated that the spatiotemporal characteristics of the spontaneous BOLD signals are significantly preserved under light to mild anaesthetic levels (<2.9% isoflurane concentration). Hutchison, Hutchison, Manning, Menon, and Everling (2014) in nonhuman primates showed that the number of functional brain state transitions linearly decreases with increased isoflurane dosage. Thus, as a caveat, anaesthetic state should be carefully monitored in resting-state study, esp. when using volatile anaesthetics.

Isoflurane sensitivity is the function of ED_{50} , or the isolfurane dose that induced half the rats to lose righting reflex. Across different anaesthetics, ED_{50} in rats is highly correlated to the loss of consciousness in humans (Franks, 2008).

1.6 Olfactory System and TLE

In a fraction of patients living with TLE, olfactory hallucinations (olfactory aura) precede complex partial seizures (Acharya, Acharya, & Lüders, 1998; Chen et al., 2003; Hong, Holbrook, Leopold, & Hummel, 2012). These auras appear to involve the piriform cortex – a primary olfactory cortex. Interestingly, it is a possibility to obviate a seizure episode by smelling an odor, although with sufficient warning. Olfactory cortex is also widely being used as a model to study epileptogenesis,

to which it is highly susceptible (see Restrepo, Hellier, & Salcedo, 2013, for review). A particular intriguing aspect of this cortex is its ability to process the exceedingly complex spatial and temporal patterns of neuronal activity that constitute the olfactory code.

Olfactory bulb (OB) serves as the olfactory processing stage in the vertebrate brains. Olfactory receptor neurons in the epithelium send axonal projections to the mitral cells in the OB, which directly project to piriform cortex (PC), entorhinal cortex (EC), and other related limbic areas. Importantly, the PC projects to the amygdala and lateral EC (Nagayama et al., 2010; Shepherd, 2004), brain structures well known to be involved in limbic seizures in patients with TLE (Ben-Ari, Crepel, & Represa, 2008; Bertram, 2009; Thom et al., 2010, Figure 1.9).

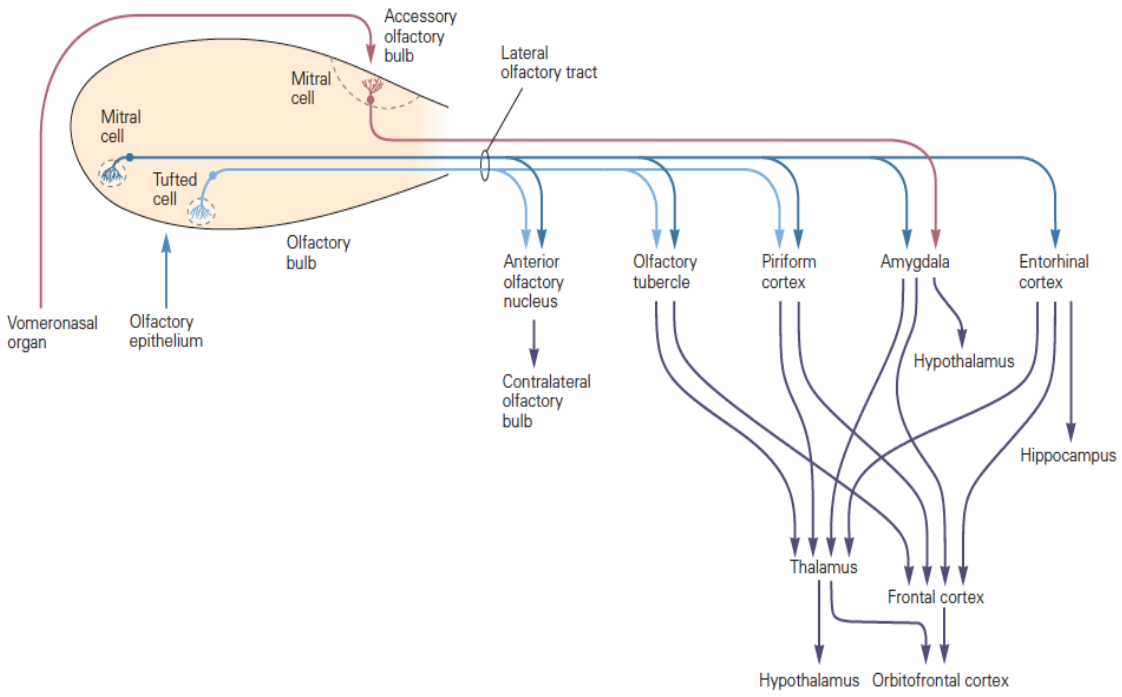

Figure 1.9: The axons of mitral and tufted relay neurons of the OB project through the lateral olfactory tract to the olfactory cortex. The olfactory cortex consists of a number of distinct areas, the largest of which is the PC. From these areas olfactory information is transmitted directly to other brain areas as well as indirectly via the thalamus. Targets include frontal and orbitofrontal areas of the neocortex, which are thought to be important for odor discrimination, and the amygdala and hypothalamus, which may be involved in emotional and physiological responses to odors. Mitral cells in the accessory olfactory bulb project to specific areas of the amygdala that transmit signals to the hypothalamus. Reproduced from Kandel, Schwartz, and Jessell (2012, p. 712).

Olfactory dysfunction in TLE patients is not quite well documented. Rather there has been a dearth of studies exploring the consequences of such sensory alterations. Some reports have suggested loss in OB volume in TLE patients, which correlated with odour threshold and discrimination abilities (Hummel et al., 2013). Hudry, Ryvlin, Royet, and Mauguière (2001) demonstrated that the human amygdala, in addition to spindles, is capable of evoking chemosensory potentials. Previous studies found evoked potentials to represent specific odour-induced responses. Lowry and Kay (2007) analysed LFPs from the olfactory bulb and anterior piriform cortex to find that the beta oscillations (15–30 Hz) in awake rats are generated specifically in response to volatile organic compounds (VOCs; vapour pressures: 1-120 mm Hg). Heale, Vanderwolf, and Leung (1995) were able to generate coherent chemosensory induced potentials in the rat olfactory bulb and the dentate gyrus with the peak frequency band of 15–20 Hz using toluene, while disrupting the coherence using KA and colchicine – pointing to the role of DG granule cells in the synchronization. These studies may potentially lend insight into how the olfactory system reorganizes following the SE in TLE patients.

1.7 Current Study

With the advances in neuroimaging techniques, it has been possible to derive the underlying neural phenomena at unprecedented spatial and temporal resolution. Kainate model of TLE displays several of the symptoms of human TLE. The behavioural patterns, encephalographic features, and pathogenesis is strikingly similar, although not the same. Therefore, it is possible to chart various features of human TLE and even validate them in the rodent model; which has obvious advantages of manipulability.

This study focusses on the disruptions in the resting-state networks, specifically the ones with the hippocampus as the hub, in the kainate model of temporal lobe epilepsy. The motivation to explore the functional network alterations stems from previous research in our laboratory, wherein Hutchison et al. (2010) discovered several functional networks in the anaesthetized rat brain.

Several RSNs have been reproduced in human TLE with varying disruptions. However, these RSNs have not been explored in the pathological state in the animal models of epilepsy.

Since, behavioural changes accompany TLE, it is crucial to establish how well it correlates with development of epilepsy at adequately spaced time intervals following SE. Heale et al. (1995) established high coherence between olfactory bulb and dentate gyrus in the β (15–20 Hz) frequency band using toluene. Such task can potentially be used to gauge the extent of damage in animal models of TLE. In addition, olfactory system dysfunction is the least characterized of all the co-morbidities associated with TLE. The olfactory deficits can be detrimental to the quality of the life of the afflicted individual. Thus, warranting inquiry into this line of research. Changes in sensitivity in response to isoflurane levels, as observed using loss of righting reflex (LORR), was tested since a higher sensitivity in response to general anaesthetics was observed by Long et al. (2009) in a pilocarpine model of TLE. Prepulse inhibition (PPI) and locomotion studies probe the role of hippocampal-accumbens circuitry in behavioural modifications. These behaviour correlates have been shown to be deficient in hippocampal kindling (Ma & Leung, 2004a) and kainate model of TLE (Ando et al., 2004).

The objective of this study was to implement resting-state fMRI to establish the disconnect between various regions of the brain, more generally the RSNs, in a kainate model of temporal lobe epilepsy. The experimental design allowed for the behaviour to be chronically recorded and changes observed as a function of the experimental variable could be recorded and analyzed. The disruptions in the BOLD signal connectivity hypothesized to be correlated with the behavioural changes were measured using PPI and open-field test (OFT).

In the first series of experiments, summarized in Figure 2.1, baseline behaviour was recorded at Day 0, followed by induction of SE using, then resting-state fMRI recording while behaviour was recorded at adequately spaced intervals following SE. We hypothesize that both the local and global functional connectivity will be significantly altered following SE in this rodent model of TLE.

In the second set of experiments, 10 weeks following the SE, rats were subjected to chronic EEG

recordings while an olfactory task was being performed. We hypothesize that the kainate-group will have lower coherence between the OB and DG in kainate group as compared to controls.

Chapter 2

Materials & Methods

2.1 Animals

Adult male Long-Evans rats (Charles River Laboratories, Canada) weighing 250-400 grams were used in these experiments. Rats were housed in standard cages and subjected to 12:12 hour light/dark cycle (7am, 7pm). Food and water was accessible *ad libitum*, in a temperature regulated environment. The study was conducted in accordance with the guidelines established by the Canadian Council on Animal Care and approved by the Animal Use Subcommittee at the University of Western Ontario (AUP # 2007-085-10, see Appendix D).

All experiments were conducted during the light phase (0800 - 1900 EST).

2.2 Sequence of Experiments

Behaviour, EEG and fMRI recordings were incorporated in the study design to reveal the effect of the independent variable (kainate/saline administration) on the dependent variable (differential cortical and sub-cortical brain activation). Figure 2.1 depicts different methods used spread across a period of 15 weeks.

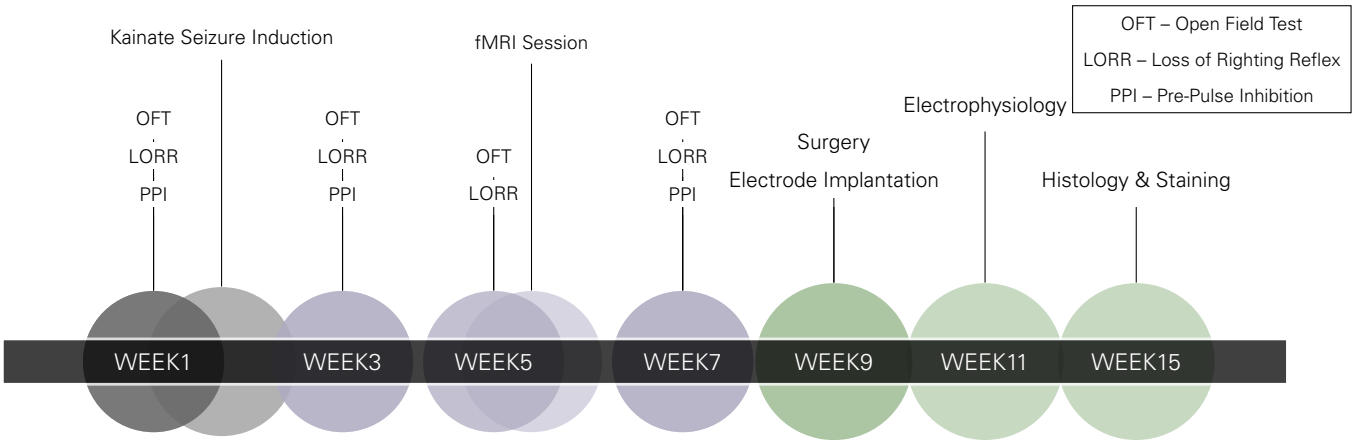

Figure 2.1: The following figure, in essence, depicts one complete cycle for the project with the timepoints chosen carefully to tentatively reflect any change/activity that can be attributed to the difference in the experimental variable, i.e. kainic acid treatment v. controls.

2.3 Induction of Spontaneous Seizures using Kainic Acid

Kainic acid (Abcam Biochemicals, Cambridge, UK) was administered systemically through the intraperitoneal (i.p.) route, with modifications of the protocol defined by Dudek and Edward (2005), to induce status epilepticus (SE) in rats. Twenty-nine male rats were randomly allocated to the experimental kainate group [n = 21; weight: 247 $\pm$ 3.9 g, mean $\pm$ standard error of the mean (SEM)] and sham saline group (n = 8; 255 $\pm$ 5.8 g,). The groups of rats did not significantly differ in weight ($P > 0.05$, Wilcoxon signed rank test). Rats were monitored for the development of behavioural seizures following an initial kainate dose of 5mg/kg i.p. (diluted to 10 mg/mL with sterile saline), with subsequent subthreshold doses administered (usually 1 hour after the initial dose) according to the stages of seizure development and motor progression (see Table 2.1). Repeated doses [Full dose (FD): 5.0 mg/kg, Half dose (HD): 2.5 mg/kg] were administered to rats until they developed fully generalized (stage 5) seizures or exhibited convulsive status epilepticus (SE) for more than 3 hours. Age matched controls were injected with the same volume of sterile saline (0.1–0.2 mL i.p.) as the volume of kainate solution in the experimental group. The differential doses delivered aim to maximize animal survival. Diazepam (Sandoz, Canada; 5 mg/mL) was administered (4 mg/kg i.p.) following $\geq$ 3 hours of stage 5 seizure manifestation to prevent any

Seizure Stage	Behavioural Correlate	Remarks
Class I	Facial Automatisms	Difficult to detect and record while an animal is grooming/exploring its environment.
Class II	Head Nodding	
Wet Dog Shakes (WDS)		WDS and the number of class III/IV/V seizures are recommended as the criteria for subsequent injections.
Class III	Forelimb clonus with a lordotic posture	
Class IV	Forelimb clonus coupled with rearing	
Class V	Class III or IV stage seizure and fall over	Fall to one side first, followed by forelimb clonus.
Jumping	Spontaneous jumping in one place or throughout the cage	

Table 2.1: **Seizure Assessment**: Severity of motor seizure activity according to a modified Racine scale (Ben-Ari, 1985; Dudek & Edward, 2005; Racine, 1972).

extraneous damage due to excessive or sustained convulsive episodes. Sterile saline (1.5–2.5 mL, 2×) was administered subcutaneously to hydrate the rats; shortly after diazepam.

Figure 2.2 depicts a hierarchical flow-chart diagram that was followed to induce SE in rats, who eventually develop chronic, spontaneous recurrent seizures that were observed for the whole duration of the study (upto 15 weeks); persisting throughout the life of the animal.

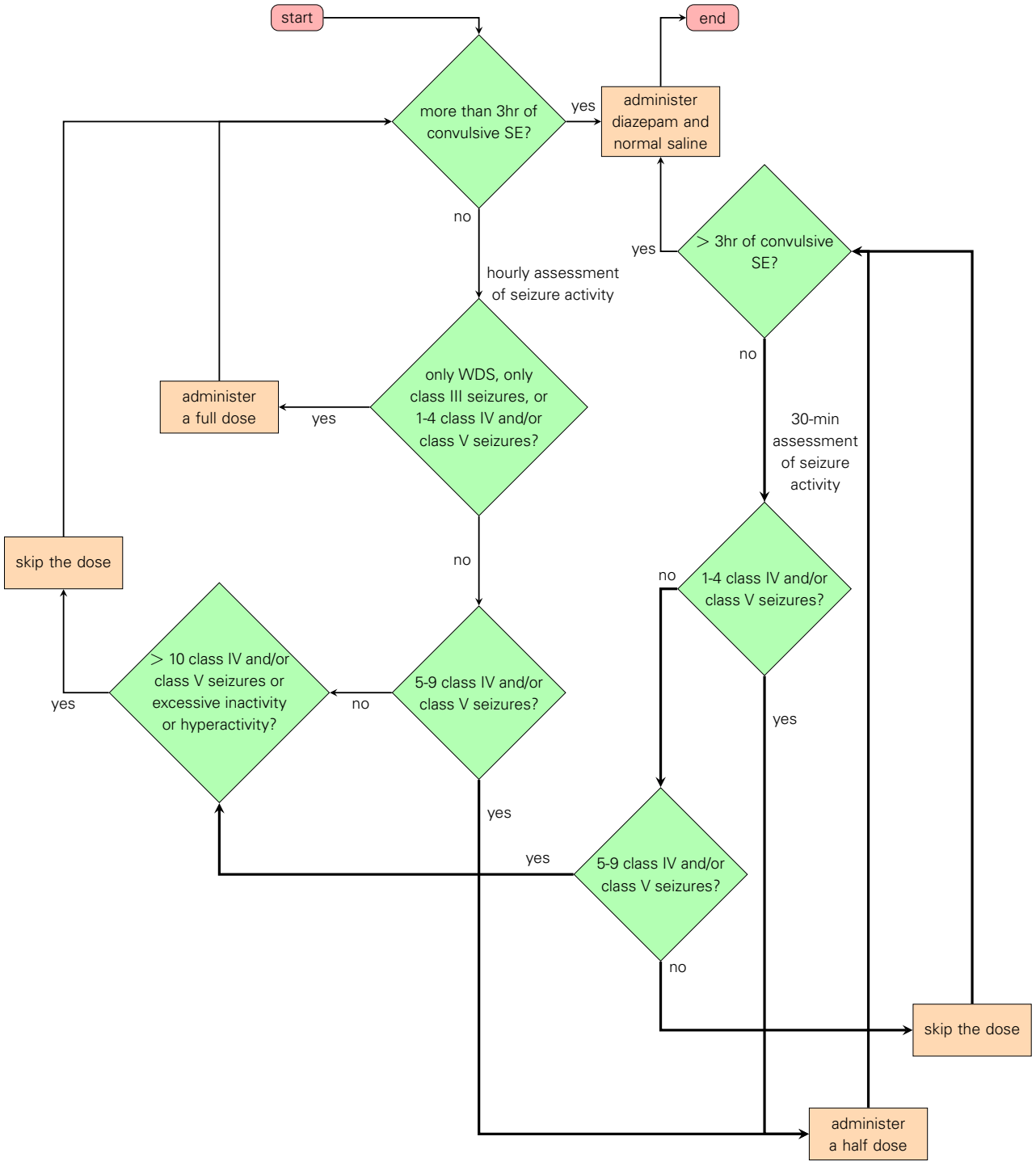

Figure 2.2: **A flowchart to determine subsequent dose administration for each kainate-treated rat.** Following the first full dose (5 mg/kg i.p.), seizure-like behaviour (see Table 2.1) is monitored and recorded for 1 hour. This recorded seizure activity along with the seizure assessment flowchart serves to establish the next course of action (full dose, half dose (2.5 mg/kg), or no dose). Two finite state loops (an hourly assessment loop—left side of figure, thin lines and a 30 minute assessment loop—right side of figure, thick lines) determine the process (rectangles) for each possible decision (diamonds). The start box represents the first hour after the initial kainate injection and all remaining hours until each rat experiences > 3 hours of convulsive SE. SE = status epilepticus; WDS = wet dog shakes. Modified from Dudek and Edward (2005).

2.4 Functional Magnetic Resonance Imaging Procedures

2.4.1 Animal Usage and Preparation

In animals (n = 15), general anaesthesia was induced with 5% isoflurane mixed with oxygen supplied at the rate of 1.5 L/min, using a calibrated vapourizer (Harvard Apparatus, Holliston, MA). Isoflurane was thereafter maintained at 2% while the rat was readied in the stereotaxic frame mounted on the MR-compatible cradle and eventually inserted into the magnet bore for image acquisition. Minimum 30 minutes were allowed for the isoflurane to equilibrate and global haemodynamics to stabilize at the 2% concentration, during which shimming and image localization were performed. The gaseous mixture was delivered via a custom nose-cone (serving partially as a bite bar) for spontaneous respiration throughout the experiment. Once under anaesthesia, the rats were secured in a custom-built nylon stereotaxic frame (Mirsattari et al., 2005) using ear bars to prevent head motion. The body temperature was measured using a rectal fiber-optic probe and maintained at 37°C via a feedback-controlled warm air system (MR compatible small animal monitoring and gating system, SA Instruments, Stoney Brook, NY) along with a heated feedback-controlled, water-circulated heating pad (TP500, Gaymar Industries, Orchard Park, NY). Respiration was monitored using a pneumatic pillow (SA Instruments) wrapped around the rat's chest wall. Heart rate and blood oxygen saturation level were measured using a pulse oximeter (MR-compatible; 8600V, Nonin Medical, Plymouth, MN) positioned on the hind-paw. Physiological parameters were in the normal range (temperature: 37 ± 0.5°C, heart rate: 250–390 beats/min, breathing rate: 60–90 breaths/min, oxygen saturation: > 95%) for the entirety of the recording/scanning session.

2.4.2 Image Acquisition

All rats ($n_{kainate}$ = 6, n_{saline} = 9) were scanned for approximately 60 minutes at 4 isoflurane concentrations (2.0%, 1.5%, 1.0%, and 0.5%), while the first scan was taken ~4-5 weeks after the kainate-treatment. The first scan was taken at 2.0% isoflurane induction and was incrementally reduced with every progressing scan (10 minutes per scan, 2×) and continued until the rat exhibited any movement, which was monitored using the heart rate and breathing rate (during the scan) and by visually inspecting the EPIs overlaid on the anatomical post-scan. Since the ED_{50} for isoflurane in Long-Evans rats was ~0.8%, very few scans were made, without movements, at 0.5% (see Results chapter; Leung et al., 2013; Tai et al., 2014).

All experiments were accomplished using a Varian DirectDrive imaging console (Palo Alto, CA), with a Magnex 31 cm actively shielded 9.4 T horizontal bore magnet equipped with an actively shielded gradient set (12 cm ID, SR 3,000 $mT\,m^{-1}\,s^{-1}$; Yarnton, UK). An optimized custom built 1.5×2.0 cm linear transmit-receive surface coil was positioned proximally to the anterior aspect of the rat's head for imaging (Hutchison, 2012). Magnetic field optimization over the volume of interest was accomplished using an automated shimming algorithm (RASTAMAP, Klassen & Menon, 2004). Thirteen coronal slices of 1-mm thickness spanning the nucleus accumbens (anterior ~2.0 mm), to the entorhinal cortex (posterior ~8.0 mm), and including the septohippocampal extent of the hippocampus were selected using the Paxinos and Watson (2007) atlas. A fast spin echo (FSE) anatomical [effective echo train (TE) 40 ms, reception time (TR) 5 s, echo train length (ETL) 4] was acquired with a 256×256 matrix and a field of view (FOV) of 25.6×25.6 mm^2. Functional images were acquired using an echo planar imaging sequence (TE 15 ms, repetition time TR 1,000 ms, flip angle 60°), with a 64×64 matrix, and a FOV of 25.6×25.6 mm^2, corresponding to an in-plane spatial resolution of 400×400 μm^2 (Hutchison, 2012). For each fMRI run, 600 images were acquired over 10 minutes (1 brain volume every second), while the rat was resting under isoflurane anaesthesia in the scanner.

2.4.3 Image Preprocessing and Analysis

Preprocessing was carried out using command-line tools bundled within the FSL (Jenkinson, Beckmann, Behrens, Woolrich, & Smith, 2012) and AFNI (Cox, 1996) framework. First 30 volumes (initial TRs) were removed to allow magnetization equilibrium (steady state), and all volumes were registered to the first volume in the fMRI datasets to correct for minor movements. Trilinear three-dimensional (3D) head motion correction and spatial smoothing using a 2D Gaussian filter (full-width at half-maximum, $\mathrm{FWHM_{xy}} = 0.8 \times 0.8\ \mathrm{mm}^2$) was applied in tandem to each EPI data set. Functional to structural space registration was achieved using FLIRT (FSL toolbox) with affine transformation (12 DOF). An eighth-order Chebyshev (Type I bandpass, ~0.01–0.1 Hz) filter with peak-to-peak passband ripple of 0.1 dB was implemented in Matlab (Mathworks, Natick, MA) and applied to all time courses on a voxel by voxel basis over the entire EPI functional (3D + time) dataset (Hampson, Peterson, Skudlarski, Gatenby, & Gore, 2002).

The standardized rat templates available could not be used owing to low degrees of freedom inherent in the data (13 slices) relative to high dimensionality ($\geq$ 100 slices with finer resolution) of the template data. Besides, the creation of the template would require the acquisition of a separate dataset that would then have to be manually labelled, negating the benefit of the template (Hutchison, 2012). To circumvent the standardization issue, the 33 regions-of-interest (ROIs) corresponding to brain regions and 2 ROIs corresponding to cerebrospinal fluid (to serve as zero/null connectivity controls) were manually drawn for each of the rats in accordance with the Paxinos and Watson (2007) rat brain atlas.

Seed regions were selected in the following medial- and extra-temporal regions in both hemispheres independently: medial frontal cortex, piriform cortex, hippocampus, mediodorsal thalamus, orbitofrontal cortex, prefrontal cortex, posterior parietal cortex, auditory/temporal association cortices, anterior/posterior cingulate cortex and amygdala (see Appendix B.1 for a complete list of ROIs). The voxels of each structure were defined according to neuroanatomical landmarks on the T2 structural scan since functional localization would be difficult and was not used. Figure

2.3 depicts the general pipeline/workflow implemented (does not illustrate preprocessing).

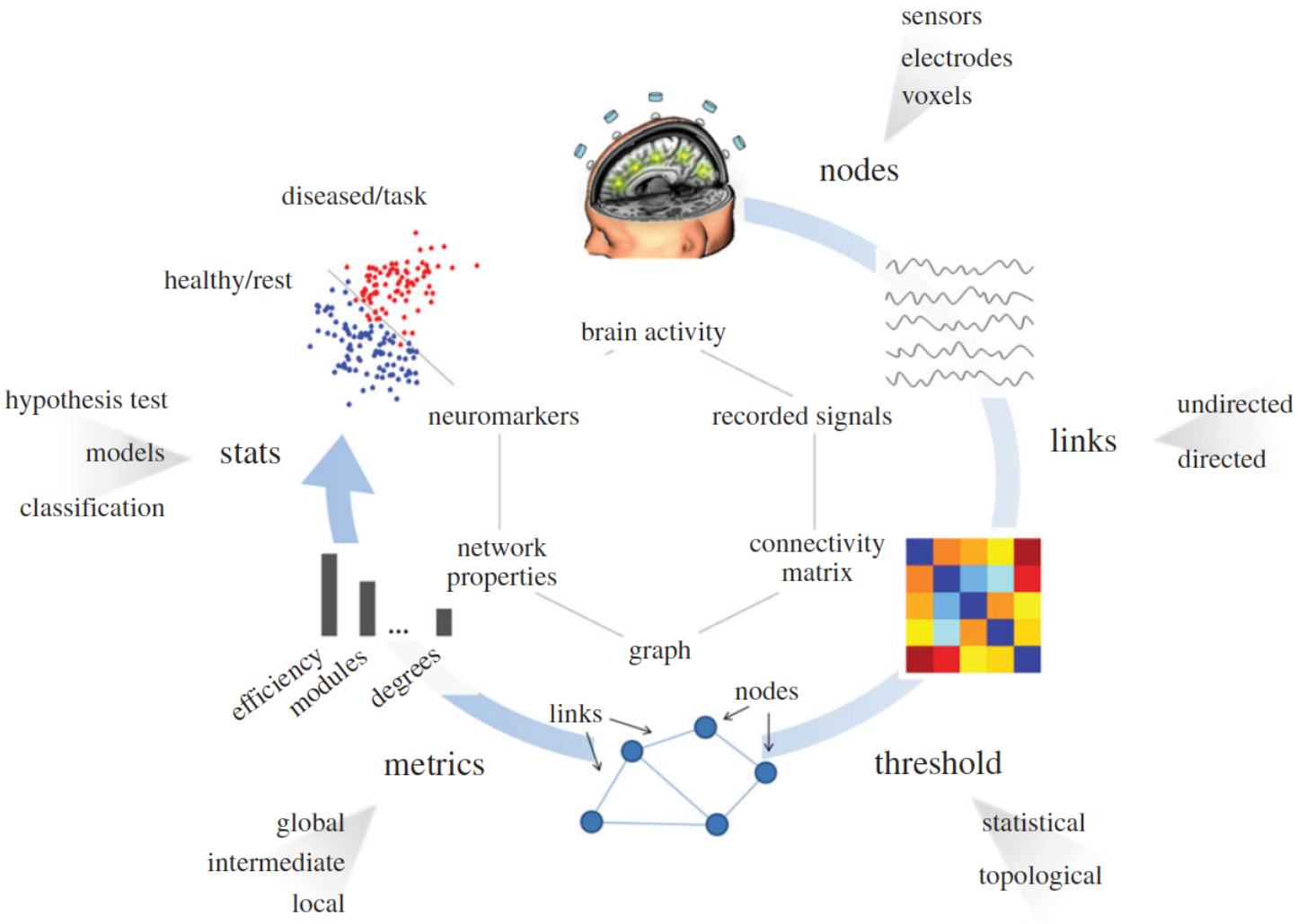

Figure 2.3: **Workflow/pipeline for graph theoretical network modelling and analysis of rsfMRI data.** Nodes correspond to a priori chosen ROIs or brain regions. The connections/links reflect the functional connectivity between the the nodes, calculated using the temporal correlation between the signals (preprocessed data: temporally filtered and spatially smoothed); this information is stored in a correlation matrix which is further thresholded (to constitute only the significant links in the brain graph) to obtain binary/sparse connectivity matrices. The brain graph topology is computed by several graph metrics to detect global integration and local segregation. Statistical analysis of the graph metrics reveals significant differences between the 2 groups. Reproduced from De Vico Fallani, Richiardi, Chavez, and Achard (2014).

Network-based Statistic

The extracted BOLD time courses averaged over the seed region was cross-correlated with all other ROIs to derive a corresponding connectivity map. For statistical analysis, the Pearson's correlation coefficients (r) were gaussianized using the Fisher's r-to-Z transformation [$Z = \frac{1}{2}\ln(\frac{1+r}{1-r})$

$= atanh(r)$]. Network-based statistic (NBS, http://www.nitrc.org/projects/nbs/) approach was implemented to localize specific connected components in which the functional connectivity was significantly different between the two groups. NBS is a method to adjust for multiple comparisons in graphs – by controlling the link-based family-wise error (FWE) rate when mass-univariate hypothesis testing is performed at each connection within the graph (Zalesky, Fornito, & Bullmore, 2010). Briefly, most consistent connections were recognized within each group. Consequently, a t-statistic is computed for each connection (node-to-node; $t \geq 3$, $P < 0.05$) to construct a subset of suprathreshold links for the most consistent connections. Connected components along with the number of links/connections present in the set of suprathreshold links were thus identified. To estimate the significance of each component, the null distribution of the connected component size was empirically derived using a nonparametric permutation approach (15,000 permutations). Ultimately, a corrected p-value for a connected component of size M found in the non-randomized data was then determined by computing the proportion of the 15,000 permutations for which the maximal connected component was significantly larger than M (Wang et al., 2013a).

Graph metrics and Random network generation

The significant supra-threshold links were visualized as a graph network using the Gephi software (Bastian, Heymann, & Jacomy, 2009). The various graph-based metrics [Weighted Clustering Coefficient (C_w), Characteristic Path Length (L_w), Global Efficiency (E_{glob}), Local Efficiency (E_{loc}), Node Degree (K_i), Betweenness Centrality (B_i) and small-world characteristics (γ , λ , σ)] were computed using the brain connectivity toolbox (BCT, http://www.brain-connectivity-toolbox.net; Rubinov & Sporns, 2010). Nonparametric Wilcoxon signed rank tests and non-parametric permutation tests (Wang et al., 2013b) were conducted to test differences in each of the graph-based metrics across the two groups.

Stam, Jones, Nolte, Breakspear, and Scheltens (2007a), Stam and Reijneveld (2007b) suggested that statistical comparisons should generally be performed between networks with equal (or at least

similar) degree sequence. However, theoretical random networks are characterized by Gaussian degree distributions, which may be incongruous with the degree distribution of the functional brain networks. Therefore, we generated, for a single threshold ($r \geq 0.3$), 100 synthetic undirected random networks with preserved degree distribution (from the KA/saline-treated brain networks) of size 35×35 using BCT. Then, we averaged across all 100 generated random networks, and binarized, to obtain a mean C_{random} [1] and a mean L_{random} [2].

2.5 Behavioural Test Procedures & Analysis

2.5.1 Open Field Test

Horizontal movements (locomotion) of a rat were measured by the number of interruptions of infrared (IR) beams in a Plexiglas® chamber ($69 \times 69 \times 49$ cm^3). Four independent IR sources, at 23 cm intervals, were located on a horizontal plane 5 cm above the base, with photodiode detectors on the opposite side. Interruptions of the IR beams were counted and transferred to a microcomputer interfaced via software (Columbus Instruments). Spontaneous locomotor activity was recorded for 45-60 minutes (at 5 mins interval, movements summed over 40 minutes) within a repeated measures design for up to 5 weeks (once before SE induction and twice after), in both experimental and control rats. Statistical differences were evaluated using 1-way repeated measures analysis of variance (ANOVA).

2.5.2 Pre-Pulse Inhibition

A Plexiglas® cylinder served as the startle chamber (8.2 cm diameter, SR-LAB, San Diego Instruments, San Diego, CA). A piezoelectric accelerometer was used to detect startle amplitude, and bursts of acoustic noise were delivered by a loudspeaker mounted 24 cm above the rat. A micro-

[1] clustering coefficient of an equivalent random network
[2] path length of an equivalent random network

computer interfaced with SR-Lab software was used to present acoustic stimuli and to record data. During PPI testing period, a rat was placed inside the startle chamber with a 68 dB background noise for a 5 minute acclimatisation. Following the acclimatisation period, the rat was presented with four types of stimuli: (i) startle pulse (120 dB – 40 ms broad band burst); and (ii) each of prepulse (73, 75, or 80 dB – 20 ms broad band) presented 100 ms prior to startle pulse. The session was designed with five trial types: startle pulse alone, each of three prepulse trials followed by a startle pulse or a period of no acoustic stimulation. For each test session, 50 trials (10 startle pulse, 10 no stimulation, and 10 of each prepulse trial types) were given in randomized order. The intertrial interval was 15 s. Each test session was repeated twice (Ma et al., 2004b).

PPI was measured as the difference of the response to the startle pulse alone and that to prepulse-startle, or PPI (in %) = $100 \times [1 - (\frac{\text{mean startle response amplitude for prepulse-startle trial}}{\text{mean amplitude of response to startle alone}})]$. In this study, mean values of the prepulse intensity of 73, 75, 80 dB (integrated prepulse intensity) and each of the three types of intensity was used for calculation of the percentage of the PPI.

A 2-way repeated measures ANOVA was conducted to reveal differences in the 2 groups across time and the type of prepulse (73, 75, 80 dB, and integrated) or startle pulse presented. Tukey multiple comparisons were conducted to establish significance.

2.5.3 Loss of Righting Reflex under Isoflurane

Loss of righting reflex (LORR) measure was selected as the behavioural endpoint to investigate the hypnotic properties of isoflurane (Forane® ; Baxter International Inc., Canada), following methods previously described albeit with slight modifications (Tai et al., 2014). To determine the isoflurane concentration that induced LORR, each rat was placed in a small Plexiglas® chamber ($23 \times 12 \times 12$ cm^3) connected to an isoflurane vaporizer with 1-1.5 L/min flow of 100% oxygen. The outlet from the chamber was fed into an infrared (IR) gas analyzer (RGM5250; Ohmeda® , Louisville, CO). Isoflurane was delivered to the chamber starting at 0.5% concentration, and was increased in 0.125% increments until LORR occurred in the rat. The concentration of isoflurane plateaued in > 10 minutes after the dose increment, which was confirmed by the IR gas analyzer. Each anaesthetic

concentration was maintained for a minimum equilibration period of 15 min, after which the chamber was rotated and tumbled to place the rat on its back. A rat was considered to show LORR if it did not return to all fours (feet) within 30 seconds, and was confirmed by a subsequent trial.

Nonparametric Wilcoxon signed rank tests were conducted to test differences in isoflurane sensitivity in the two groups.

2.6 Local Field Potentials (LFPs) Procedures

2.6.1 Surgery & Electrode Implantation

Ten rats were initially anaesthetized with sodium pentobarbital (60 mg/kg i.p.) and secured in a stereotaxic frame. The skull was exposed relative to lambda and bregma in a horizontal plane. For electrophysiology, electrodes were implanted with 4 hippocampal electrodes (bipolar-electrodes: a pair on each side but placed at different depths), and one electrode each in left frontal neocortex, left olfactory bulb, and right amygdala with 2 grounds/references over the cerebellum and the frontal cortex.

Burr holes were drilled for implantation using coordinates from a rat brain atlas (Paxinos & Watson, 2007). Rats were chronically implanted with depth electrodes [127-µm bare diameter stainless steel wires insulated with Teflon-PFA (perflouroalkoxy alkane) except at the cut ends] at the following coordinates relative to bregma: right basolateral amygdaloid nucleus (posterior 2.8 mm, lateral 5.1 mm, ventral ~8.6 mm), right dentate gyrus hilar region (posterior 3.8 mm, lateral 2.7 mm, ventral ~4.0 mm), right CA1 radiatum (posterior 3.8 mm, lateral 2.7 mm, ventral ~3.3 mm), left CA1 stratum oriens (posterior 3.8 mm, lateral 2.7 mm, ventral ~2.3 mm), left CA1 radiatum (posterior 3.8 mm, lateral 2.7 mm, ventral ~2.6 mm), and a depth electrode was positioned in the left frontal neocortex (anterior 2.0 mm, lateral 3.0 mm, ventral ~2.5 mm) and another in the olfactory bulb [(glomerular layer), anterior 7.0 mm, lateral 1.5 mm, ventral ~2.5 mm]. Approximate electrode locations are depicted in Figure 2. A jeweller's screw was

implanted in the skull over the left frontal cortex and another over the left cerebellum to serve as reference/ground electrodes in all rats; while two additional screws served to secure the head cap onto the skull. The electrodes were affixed semi-permanently to the top of the skull by moulding a head cap out of dental acrylic cement. Experiments did not commence until at least a week after surgery to allow for recovery.

2.6.2 Local Field Potential (LFP) Recordings

Bench-top experiments were conducted to characterize the TLE model of spontaneous recurrent seizures in freely moving and behaving rats. Two days prior to the recording session and ~1 week following surgery, rats were placed in a Plexiglas® cage for 1-2 hours to become accustomed to the recording environment.

Each electrode was connected to a Grass Electroencephalograph Model 8-10 system (Grass Instruments Co., Quincy, MA, USA) for EEG recordings. The LFP recording channels were filtered between 0.03 Hz and 10 kHz (first order bandpass filter). LFP signals were then fed into the Data Translation D303 analogue-to-digital converter and sampled and stored at 1 kHz using SciWorks 7 (DataWave Technologies, Loveland, CO, USA). Data acquisition was realized using custom workflows compiled using SciWorks 7 while analyses was completed using an in-house Matlab program.

LFPs - Spontaneous Behaviour

LFPs were recorded during two main wake behavioral states: awake immobility (rat holding its head against gravity), and walking (including periods of walking, body turning and rearing) and; two main sleep behavioural states: slow wave sleep (SWS) and rapid-eye movement sleep (REMS) as characterized in Leung (1998). Multiple trials extending ~5 mins were recorded for each of the four behaviours.

LFPs - Odor-Evoked Olfactory Potentials

Experimental testing began after ~1 week recovery period for chronically implanted rats. Rats were placed in a Plexiglas® cage for ~15 mins before data collection began. To elicit olfactory bulb and hilar odor-evoked oscillatory potentials, a Q-tip soaked in either toluene, water, or acetic acid [vapour pressure (at 25°C in mm Hg): 27.7, 24.0, and 15.8 respectively] was presented under the snout for at least 20 trials while taking care not to startle the rat (Heale et al., 1995). A trial was rerun if the rat exhibited any jerky movement before arrival of the cotton swab under the snout. Trials were at least 1 minute apart, and a minimum of 6 trials were performed for each solvent. The duration of odour presentation was usually 1–2 seconds, and LFPs were recorded for at least 6 seconds preceding and 30 seconds following the presentation while the time of the presentation was synchronized with the EEG data using a marker field. Further, a dry Q-tip (free of any solvent or solution) was presented multiple times before data collection began to familiarize the rats with the testing procedure, and prevented habituation to the test stimulus.

2.6.3 Perfusion & Histology

Following completion of electrophysiological recordings, rats were euthanized by administering a surgical anaesthetic dose of sodium pentobarbital (60 mg/kg i.p.). The rats were transcardially perfused with 120 mL saline followed by 120 mL of 4% paraformaldehyde solution. The brain was extracted from the cranium with the olfactory bulb intact and placed in 4% formaldehyde solution until ready for sectioning. Brains were frozen and sliced on a freezing sledge microtome (Leitz 1320) in 60 µm coronal sections. Brain slices were mounted onto slides and later stained with thionin. They were dehydrated in a series of 70, 95 and 100% ethyl alcohol, cleared in xylene (5 min, 2×), and cover-slipped with SHUR/Mount™ (TBS) mounting medium. The electrode placements for LFPs were identified and confirmed using a light microscope, and the amount of damage was qualitatively assessed (Long et al. 2009).

2.6.4 Data Analysis & Statistics

LFPs in Olfactory Task

All LFP recordings were visually inspected for artefacts using a custom Matlab (Mathworks, Natick, MA, USA) program, and only artefact-free datasets were used for further analysis. Each spectrum was constructed by averaging 6 or more segments of LFP, with each segment being 4096 points, or 4.096 s with 1 kHz sampling (Leung, Lopes da Silva, & Wadman, 1982; Leung, 1985). Each segment was tapered (10% of segment at each end) by a cosine bell function, and the auto- and cross-power (coherence and phase spectra) were obtained by Fast Fourier Transform (FFT) and smoothed across 5 adjacent frequency bins, by an elliptical function. The spectrum was filtered to remove 60 Hz line noise, and replaced with average of magnitudes from two digital frequency bins on either side of the 60 Hz peak. Each spectrum had a frequency resolution of 0.24 Hz (1/4.096 s), and statistically independent values were separated by 5 bins, or 1.22 Hz, nonetheless with $\geq$ 200 degrees of freedom. Peak power and coherence values and frequencies were obtained from the power and coherence spectra between olfactory bulb and other channels [hippocampus (CA1/DG), or amygdala] before, during, and after odour presentation. The integrated power in each channel and coherence between any of the channels against olfactory bulb was averaged between 14-20 Hz, 20-30 Hz, 30-40 Hz, 40-60 Hz, and 60-80 Hz, before, during, and after odour presentation task. Statistics were conducted on the average of these values using a linear mixed effects model. Treatment variable (Kainate v. Saline) was modelled as a fixed effect while the time of presentation (-2s,-1s, 0s, +1s, +2s), multiple trials with the same stimulus (to account for the unbalanced design, $n_{kainate} \neq n_{saline}$), and odour stimulus (water, toluene, kainic acid) were modelled as random effects. Tukey multiple comparisons were conducted to establish significance.

LFPs during Spontaneous Behaviours

For spectral analysis of LFPs during different behaviours, each spectrum was constructed by averaging 6 or more segments of LFP, with each segment being 2048 points, or 2.048 s with 1 kHz sampling (Leung et al., 1982; Leung, 1985). Auto- and cross-power (coherence and phase spectra) were obtained using FFT. The spectrum was filtered to remove 60 Hz line noise, and replaced with average of magnitudes from two digital frequency bins on either side of the 60 Hz peak. One way ANOVA (treatment as the fixed effect and repeated trials as the random error) followed by Bonferroni post-hoc tests were conducted to test differences in power and coherence across all 4 behaviours in the two groups.

All statistical testing was accomplished in R Studio (R Studio, 2012) using R (version 3.1.1; R Core Team, 2014).

2.7 Seizure Observation & Inclusion Criteria

Approximately 2-3 weeks following seizure induction, KA-treated rats were monitored, either in the lab or animal facility during the afternoons for 1-2 hours every other day, for any signs of seizure activity. Overnight video monitoring to detect seizures was conducted at 3 weeks. The observation was continued upto ~4-5 weeks, terminating just before the fMRI scanning session. This observation period was critical since this allowed identifying the rats that had been spontaneously seizing following the *status epilepticus* (SE) episode.

Of the 15 rats that were scanned, 3 rats despite being injected with kainic acid were rather resistant (Suárez et al., 2012) and did not develop any limbic/convulsive seizures either immediately after the kainate injection or during the ~1-2 months of observational period. Interestingly, these 3 rats were part of the same batch and were induced the same day.

Due to lack of any observed seizures, the resting state data from these rats was not used in the group analysis to establish changes in functional connectivity. They were also excluded from

group analysis of behavioural and electrophysiological data.

Chapter 3

Results

3.1 Functional connectivity of kainate and control rats

Rats were scanned ~4-5 weeks following kainate induction, and recorded at decremental isoflurane concentrations. However, due to missing and artefactual data, only scans recorded at 1.5% isoflurane concentration were used for subsequent analysis. To visualize the graph theory measures of functional connectivity (positive and negative correlations), the mean correlation matrix (35×35) for the 35 seed regions [33 brain regions with 2 zero connectivity controls; Figure 3.1: Correlation matrix (top)] across all the subjects within each group ($n_{kainate} = 6$, $n_{saline} = 7$) were computed from their respective time series (> 500 seconds). The correlations were arbitrarily thresholded [Figure 3.1: Connectivity matrix (bottom)] to generate sparse matrices to aid in the creation of graph networks, with each ROI serving as the node and each connection serving as the edge in an undirected (no causality) network. These sparse/binary matrices were used to derive graph theory measures [Weighted Clustering Coefficient (C_w), Characteristic Path Length (L_w), Global Efficiency (E_{glob}), Local Efficiency (E_{loc}), and small-world-ness characteristics (γ , λ , σ)] to reveal differences between the kainate and the control group. Mathematical definitions are detailed in Appendix B.2.

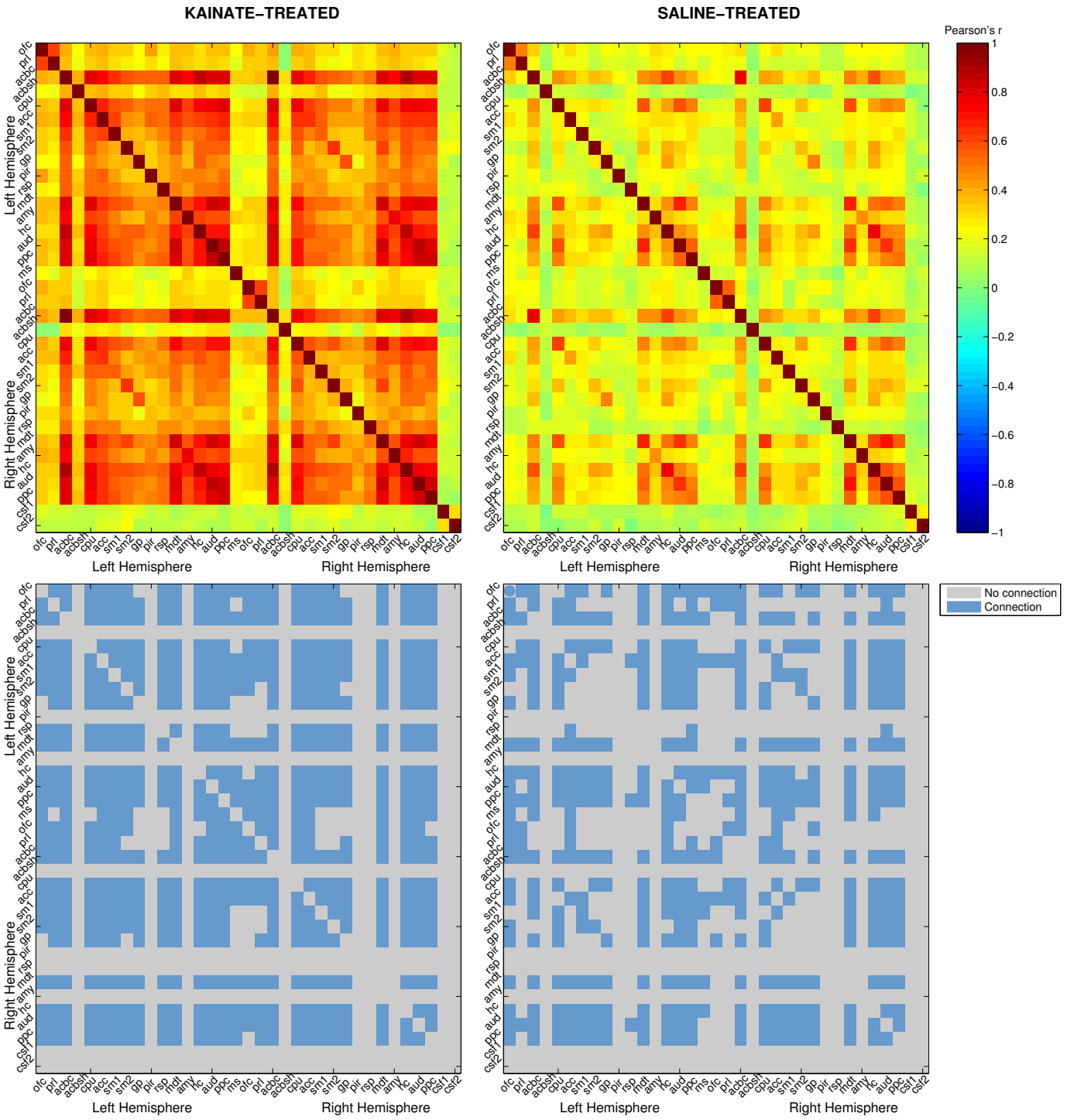

Figure 3.1: **Top: Correlation Matrix** The heatmap figure represents the significant intra-group connections in the kainate (left, P = 0.002, $n_{kainate}$ = 6) and the control (left, P = 0.014, n_{saline} = 7) group as Pearson's r correlation coefficients (-1 < r < 1) in an NBS framework. See Figure A.1 for a Fisher's r-to-Z normalized version of the matrix.

Bottom: Connectivity Matrix The binary heatmap represents the significant networks as connected and disconnected nodes .

See Table 3.1 and Appendix B.1 for edge/node abbreviations.

3.1.1 Differences in connectivity

The network based-statistic (NBS) was used to reveal nodes that were significantly well-represented (intra-group) within a group [(Kainate – edges: 303, nodes: 26, $P = 0.003$); (Controls – edges: 217, nodes: 26, $P = 0.009$)]. The NBS was further used to determine the network components that were significantly different between the two groups (inter-group). Compared to saline controls, the analysis revealed one sub-network comprising of 18 nodes and 36 edges (total possible combination of nodes = $0.5 \times {}^{33}C_2 = 264$) that was significantly higher within the kainate group (see Figure 3.2, $P = 0.016$). No nodes and edges corresponded to a reduced connectivity in the kainate group compared to controls. A significant number of nodes were localized in the medial temporal lobe regions of the hippocampus; along with other subcortical regions like the nucleus accumbens and the medial dorsal thalamus. Nodes were also identified in the components of the default mode network (ACC/Rsp/Aud/PPC) and the somatosensory system (primary/secondary somatosensory cortex). The specific ROI connections are detailed in the Table 3.1.

These 36 edges can be classified into several intra-system and inter-system connections. Most of the increased inter-system connections were between the limbic/subcortical system and the sensorimotor system and the default-mode system , while the intra-system functional connectivity within the structures of the medial temporal lobe significantly increased. However, none of the functional connections showed decreased correlations or connectivity in the kainate-group as compared to controls.

3.1.2 Global parameters of the rat brain functional networks

Statistical tests were performed to detect significant differences in the global parameters (C_w , L_w , E_{glob} , E_{loc}) of the functional networks between the two groups. Analysis revealed significantly higher values of E_{glob} ($W = 40$, $P < 0.05$, with Bonferroni adjustment), E_{loc} ($W = 40$, $P < 0.02$, with Bonferroni adjustment), C_w ($W = 43$, $P < 0.02$, with Bonferroni adjustment) while no changes were detected in L_w in the functional networks of the kainate-treated rats compared with the

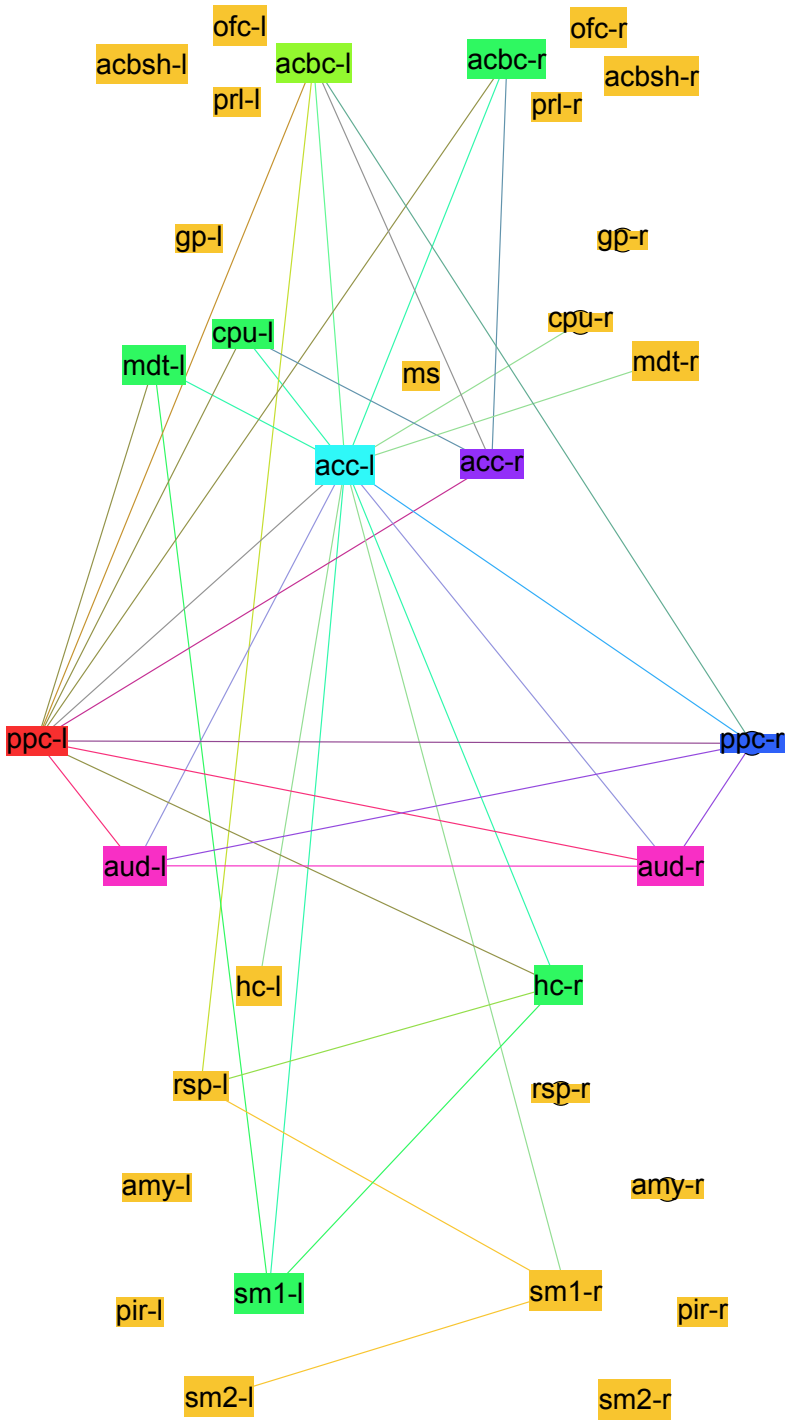

Figure 3.2: **Connectivity Graph (KA > Controls)** – The filled rectangles (overlaid with labels) represent the brain regions and the lines represent a significant supra-threshold connection between the two nodes (brain regions or seeds/ROIs). The colour scheme represent nodes with different degrees (K_i). This sub-network was thresholded at $t \geq 3.00$, with $P < 0.05$. Suffices (-r and -l) indicate right and left hemisphere. See Table 3.1 and Appendix B.1 for edge/node abbreviations.

Source Node	**Target Node**	**Edge/Connection**	**t-stat**, p = 0.016
Nucleus Accumbens Core - LH	Anterior Cingulate Cortex - LH	acbc-l⇌acc-l	3.63
Caudate Putamen - LH	Anterior Cingulate Cortex - LH	cpu-l⇌acc-l	3.33
Anterior Cingulate Cortex - LH	Primary Somatosensory Cortex - LH	acc-l⇌sm1-l	3.08
Nucleus Accumbens Core - LH	Retrospenial Cortex - LH	acbc-l⇌rsp-l	3.02
Anterior Cingulate Cortex - LH	Mediodorsal Thalamic Nuclei - LH	acc-l⇌mdt-l	3.46
Primary Somatosensory Cortex - LH	Mediodorsal Thalamic Nuclei - LH	sm1-l⇌mdt-l	3.21
Anterior Cingulate Cortex - LH	Hippocampus - LH	acc-l⇌hc-l	3.07
Anterior Cingulate Cortex - LH	Auditory/Temporal Association Cortex - LH	acc-l⇌aud-l	3.35
Nucleus Accumbens Core - LH	Posterior Parietal Cortex - LH	acbc-l⇌ppc-l	3.24
Caudate Putamen - LH	Posterior Parietal Cortex - LH	cpu-l⇌ppc-l	3.45
Anterior Cingulate Cortex - LH	Posterior Parietal Cortex - LH	acc-l⇌ppc-l	4.38
Mediodorsal Thalamic Nuclei - LH	Posterior Parietal Cortex - LH	mdt-l⇌ppc-l	3.04
Auditory/Temporal Association Cortex - LH	Posterior Parietal Cortex - LH	aud-l⇌ppc-l	4.97
Anterior Cingulate Cortex - LH	Nucleus Accumbens Core - RH	acc-l⇌acbc-r	4.01
Posterior Parietal Cortex - LH	Nucleus Accumbens Core - RH	ppc-l⇌acbc-r	3.22
Anterior Cingulate Cortex - LH	Caudate Putamen - RH	acc-l⇌cpu-r	3.38
Nucleus Accumbens Core - LH	Anterior Cingulate Cortex - RH	acbc-l⇌acc-r	3.42
Caudate Putamen - LH	Anterior Cingulate Cortex - RH	cpu-l⇌acc-r	3.55
Posterior Parietal Cortex - LH	Anterior Cingulate Cortex - RH	ppc-l⇌acc-r	3.02
Nucleus Accumbens Core - RH	Anterior Cingulate Cortex - RH	acbc-r⇌acc-r	3.02
Anterior Cingulate Cortex - LH	Primary Somatosensory Cortex - RH	acc-l⇌sm1-r	3.17
Secondary Somatosensory Cortex - LH	Primary Somatosensory Cortex - RH	sm2-l⇌sm1-r	3.08
Retrospenial Cortex - LH	Primary Somatosensory Cortex - RH	rsp-l⇌sm1-r	3.10
Anterior Cingulate Cortex - LH	Mediodorsal Thalamic Nuclei - RH	acc-l⇌mdt-r	3.14
Anterior Cingulate Cortex - LH	Hippocampus - RH	acc-l⇌hc-r	4.23
Primary Somatosensory Cortex - LH	Hippocampus - RH	sm1-l⇌hc-r	3.06
Retrospenial Cortex - LH	Hippocampus - RH	rsp-l⇌hc-r	3.27
Posterior Parietal Cortex - LH	Hippocampus - RH	ppc-l⇌hc-r	3.14
Anterior Cingulate Cortex - LH	Auditory/Temporal Association Cortex - RH	acc-l⇌aud-r	4.14
Auditory/Temporal Association Cortex - LH	Auditory/Temporal Association Cortex - RH	aud-l⇌aud-r	3.17
Posterior Parietal Cortex - LH	Auditory/Temporal Association Cortex - RH	ppc-l⇌aud-r	4.55
Nucleus Accumbens Core - LH	Posterior Parietal Cortex - RH	acbc-l⇌ppc-r	3.00
Anterior Cingulate Cortex - LH	Posterior Parietal Cortex - RH	acc-l⇌ppc-r	3.76
Auditory/Temporal Association Cortex - LH	Posterior Parietal Cortex - RH	aud-l⇌ppc-r	3.81
Posterior Parietal Cortex - LH	Posterior Parietal Cortex - RH	ppc-l⇌ppc-r	4.18
Auditory/Temporal Association Cortex - RH	Posterior Parietal Cortex - RH	aud-r⇌ppc-r	3.31

Table 3.1: Statistical significant undirected edges of the functional networks – kainate-treated group > controls. See Figure 3.2 for the graph network representation. Source and target nodes do not imply causality or directional connecitivity.

controls.

3.1.3 Regional parameters of the rat brain functional networks

Two regional parameters (degree K_i, and betweenness centrality B_i) were considered to reveal any differences in the functional networks between the two subject groups. Twenty-two brain

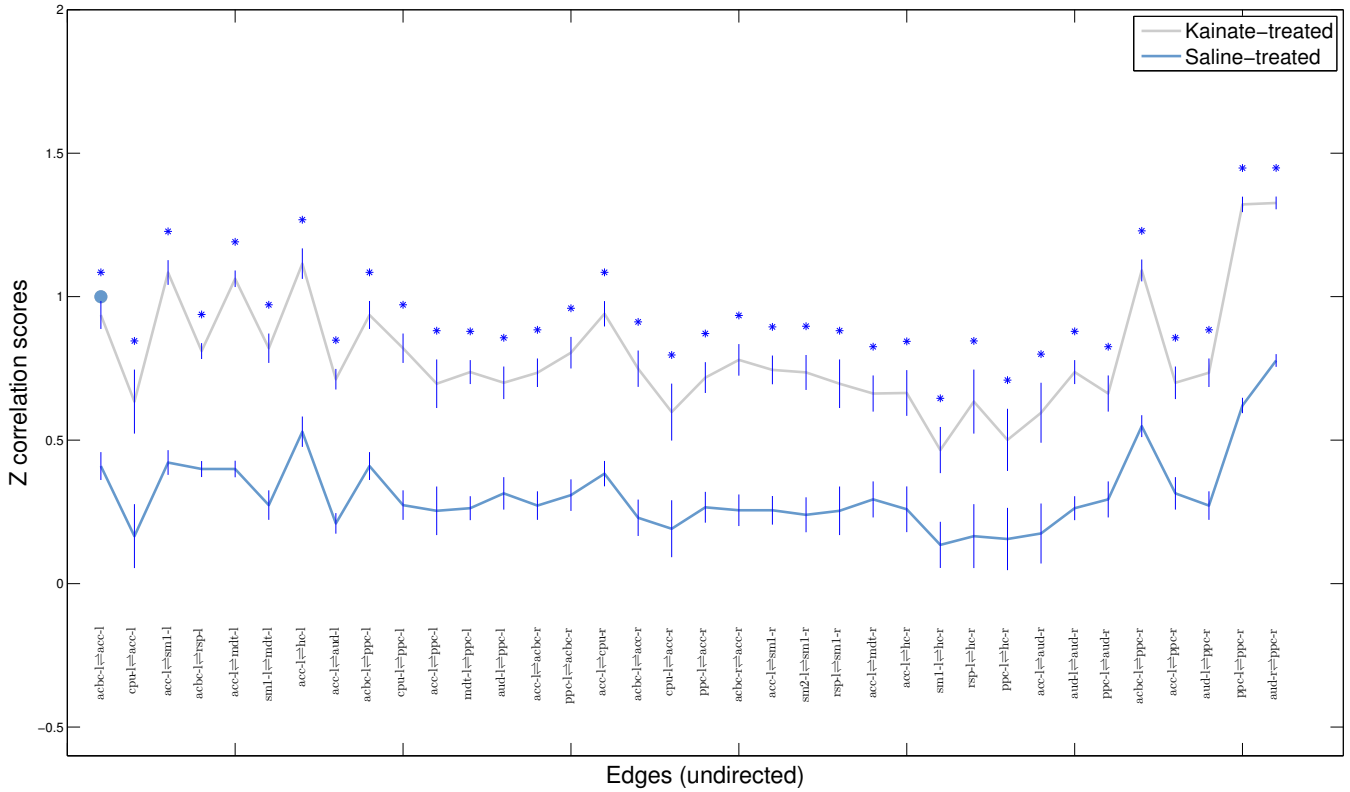

Figure 3.3: Z-correlation scores of edges (undirected connections) that are signficantly altered between the kainate groups compared to controls are illustrated as mean $\pm$ SEM. Labels corresponding to each edges (pair of 2 nodes) is mentioned along the x-axis. See Table 3.1 for edge/node abbreviations. '*' signifies $P < 0.02$.

structures were identified with a significantly higher degree, K_i(Wilcoxon test with Bonferroni correction, $P < 0.05$; see Table 3.2) in the functional network of the kainate-treated rats compared to controls. Four brain regions exhibited a significant between-group difference in betweenness centrality, including the Prelimbic cortex (PrL-LH; $W = 43$, $P = 0.012$), Caudate Putamen (CPu-LH; $W = 8$, $P = 0.042$), Posterior Parietal cortex (PPC-LH; $W = 0$, $P = 0.0006$), and Auditory/Temporal Association cortex (Aud-RH; $W = 5$, $P = 0.012$). The same structures also had significantly different degrees, K_i, between kainate-treated and control rats.

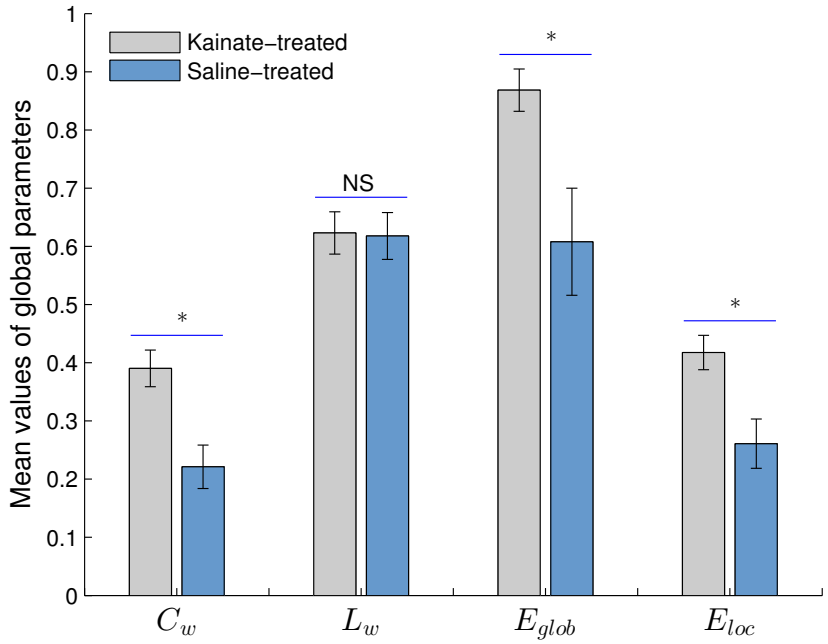

Figure 3.4: **Global Parameters**: Statistical comparison of the global parameters (C_w , L_w , E_{glob} , E_{loc}) of the functional networks between the kainate-treated group and saline-treated controls. Results are expressed as mean $\pm$ SEM. '*' signifies $P < 0.02$, and NS – not statistically significant.

3.1.4 Small-worldness of networks in TLE

Small-worldness properties of the functional networks were tested in both the groups, and small-worldness parameter, γ was found to be 1.16 ± 0.07 (mean $\pm$ SEM) for the kainate group and $\gamma = 1.16 \pm 0.04$ for the controls, indicating that the clustering coefficients were approximately 1.16 times higher than those of a comparable random network (equivalent number of vertices, N and edges, K, and same degree distribution) for both subject groups. We found $\lambda = 0.98 \pm 0.01$ for the kainate-group and $\lambda = 0.95 \pm 0.07$ for the controls. However, these small-world-ness properties did not significantly differ between the two groups. These λ values near magnitude 1 suggest that the path lengths in the two subject groups were approximately equivalent to those of random networks. The magnitudes of γ and λ were consistent with those reported by Liang et al. (2011) in awake rats. Our results showed that the functional networks corresponding to the two subject groups exhibited small-world properties, a finding which is consistent with extant literature on

ROI #	Brain region	Mean K_i	p-value (P)
1	Prelimbic Cortex - LH	13(4)	0.022
2	Nucleus Accumbens Core - LH	22(13)	0.006
3	Caudate Putamen - LH	21(12)	0.005
4	Anterior Cingulate Cortex - LH	21(7)	0.006
5	Primary Somatosensory Cortex - LH	17(6)	0.013
6	Secondary Somatosensory Cortex - LH	17(7)	0.016
7	Globus Pallidus - LH	16(7)	0.010
8	Mediodorsal Thalamic Nuclei - LH	21(13)	0.009
9	Auditory/Temporal Association Cortex - LH	21(13)	0.010
10	Posterior Parietal Cortex - LH	21(12)	0.040
11	Orbital Frontal Cortex - RH	10(3)	0.030
12	Prelimbic Cortex - RH	10(3)	0.040
13	Nucleus Accumbens Core - RH	22(13)	0.008
14	Caudate Putamen - RH	21(11)	0.002
15	Anterior Cingulate Cortex - RH	21(8)	0.004
16	Primary Somatosensory Cortex - RH	15(5)	0.036
17	Secondary Somatosensory Cortex - RH	16(6)	0.012
18	Globus Pallidus - RH	15(7)	0.020
19	Mediodorsal Thalamic Nuclei - RH	21(14)	0.010
20	Hippocampus - RH	22(13)	0.005
21	Auditory/Temporal Association Cortex - RH	21(14)	0.030
22	Posterior Parietal Cortex - RH	20(11)	0.013

Table 3.2: **Regional Parameters**: Statistical comparison of the regional parameter (K_i) of the functional networks between the kainate-treated group and controls. K_i is significantly higher in the kainate group compared to saline-treated controls. Mean K_i is expressed as $K_{i,\text{ kainate}}(K_{i,\text{ control}})$. P is computed for Wilcoxon tests with $W > 40$.

human brain functional and anatomical networks (Guye, Bettus, Bartolomei, & Cozzone, 2010; Hagmann et al., 2008; Liang et al., 2011; Liao et al., 2010).

3.2 Kainate-induced lesion enhanced anesthetic sensitivity to Isoflurane

We explored the anaesthetic sensitivity of isoflurane in kainate-treated rats and saline-treated rats by implementing a protocol of increasing isoflurane concentrations; starting at 0.375% and ending at 0.125% above the concentration after LORR (loss of righting reflex) occurred.

LORR was tested at three different times - once before the kainate/saline (to test any prior differences despite random group assignment), and two times 4 weeks apart after the treatment (to test effect of time and treatment; see Figure 2.1).

During Week 3 testing, no rats showed LORR at 0.625% or lower isoflurane concentration. However, at 0.75% isoflurane, 5 of the 13 kainate-treated rats, but none of the 12 control (sham-lesioned) rats, showed LORR. At 0.875%, 5/13 kainate-treated rats, and 2/8 control rats showed LORR. The bar plot (Figure 3.5) indicates a significantly higher isoflurane sensitivity in kainate-treated rats compared to control. The concentration at which half the rats showed LORR, or ED_{50} (LORR), was 0.81% in kainate-treated rats (95% CI, 1.000–1.09%, n = 13) and 0.99% in control rats (95% CI, 0.89–1.08%, n = 8). The ED_{50} (LORR) was significantly different between kainate-treated and saline-treated rats (Wilcoxon test with Bonferroni correction, $W = 17$, $P < 0.001$).

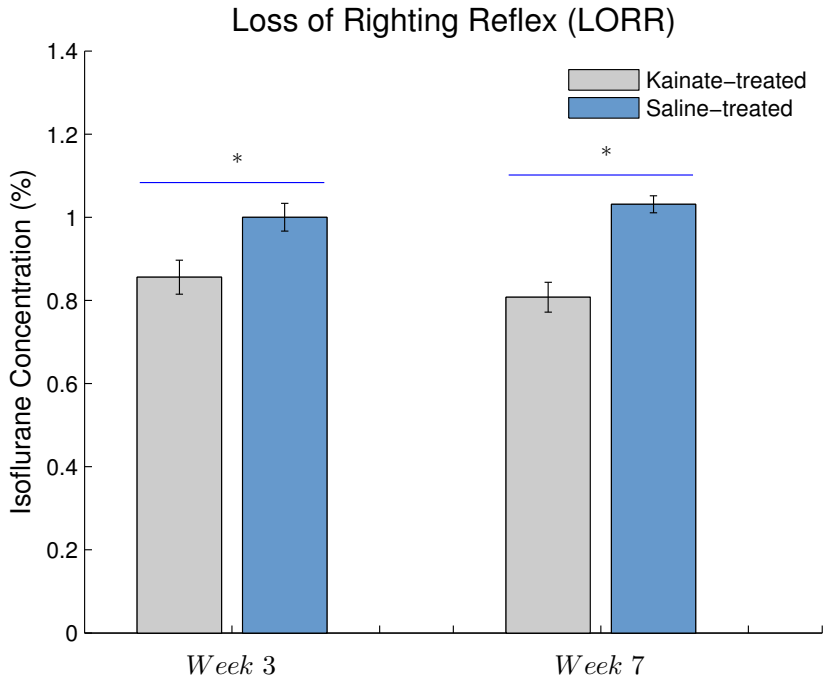

Figure 3.5: **Isoflurane concentration (% volume) of loss of righting reflex**. Kainate-treated rats have a significantly higher isolflurane sensitivity than saline-treated rats. Results are expressed as mean ± SEM. '*' signifies $P < 0.001$.

During Week 7 testing, no rats showed LORR at 0.625% or lower isoflurane concentration. However, at 0.75% isoflurane, 8/13 kainate-treated rats, but none of the 12 control (sham-lesioned) rats, showed LORR. At 0.875%, 4/13 kainate-treated rats, but none of the control rats showed LORR. The bar plot (Figure 3.5) indicates a significantly higher isoflurane sensitivity in kainate-treated

rats compared to saline-treated controls. The concentration at which half the rats showed LORR, or ED_{50} (LORR), was 0.80% in kainate-treated rats (95% CI, 0.78–0.90%, n = 13) and 1.02% in saline-treated rats (95% CI, 0.854–1.063%, n = 8). The ED_{50} (LORR) was significantly different between kainate-treated and saline-treated rats (Wilcoxon test with Bonferroni correction, W = 23.5, $P < 0.03$).

No significant interaction of treatment and time was found when comparing the Week 3 and Week 7 data.

3.3 Kainate did not affect sensorimotor gating

Prepulse inhibition was tested as a proxy for impairment of sensorimotor gating at 2 time points (Week 3 and Week 7). The kainate group did not significantly differ in the PPI or the startle amplitude [$F(1, 11) = 0.61$, NS] compared to saline-treated controls (Figure 3.6). PPI computed at prepulse intensity of 73 dB [$F(1, 11) = 1.10$, NS], 75 dB [$F(1, 11) = 0.40$, NS], 80 dB [$F(1, 11) = 0.31$, NS], and integrated prepulse [$F(1, 11) = 0.57$, NS] did not statistically reveal any significant improvement (increase) or impairment (decrease). Moreover, there was no significant treatment$\times$time interaction between the two groups.

3.4 No behavioural hyperactivity was observed

Open field test was conducted twice, during Week 3 and Week 7, after kainate/saline treatment. Locomotor activity tested in a freely behaving rat did not significantly differ between the two groups [$F(1, 17) = 0.63$, NS]. No significant treatment$\times$time interaction was identified (Figure 3.7).

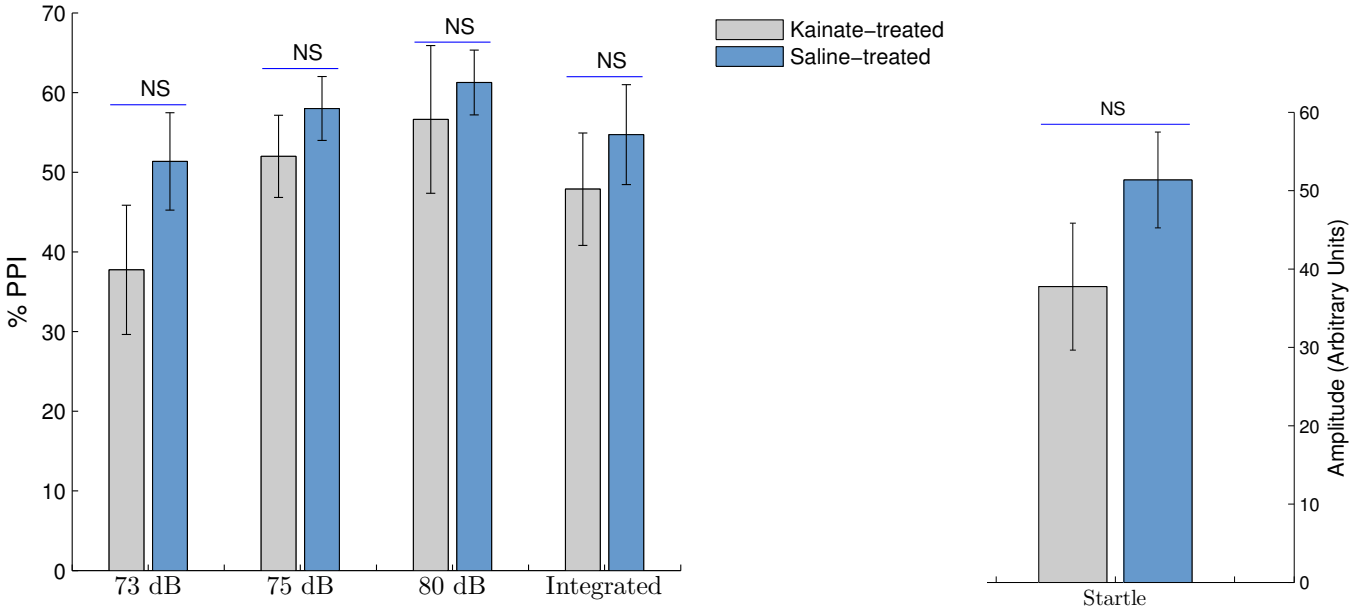

Figure 3.6: **Prepulse Inhibition at Week 3**. PPI did not significantly differ between the kainate-treated and saline-treated control rats, or across time (Week 3 v. Week 7). Results are expressed as mean ± SEM. NS signifies not statistically significant.

3.5 Effect of Kainate treatment on LFP coherence of olfactory bulb with the limbic system

Because of the extensive hippocampal atrophy, revealed by histological analysis in the epileptic rats, hippocampal electrodes in 4 of 6 epileptic rats, implanted in accordance with the standard rat stereotaxic atlas (Paxinos & Watson, 2007), missed the targeted locations.

Based on the limited number of rats, the DG-OB coherence ($n_{kainate} = 2$, $n_{saline} = 4$) or CA1-OB coherence ($n_{kainate} = 2$, $n_{saline} = 4$), or amygdala-OB coherence ($n_{kainate} = 3$, $n_{saline} = 2$) were not significantly different between kainate-treated and control rats.

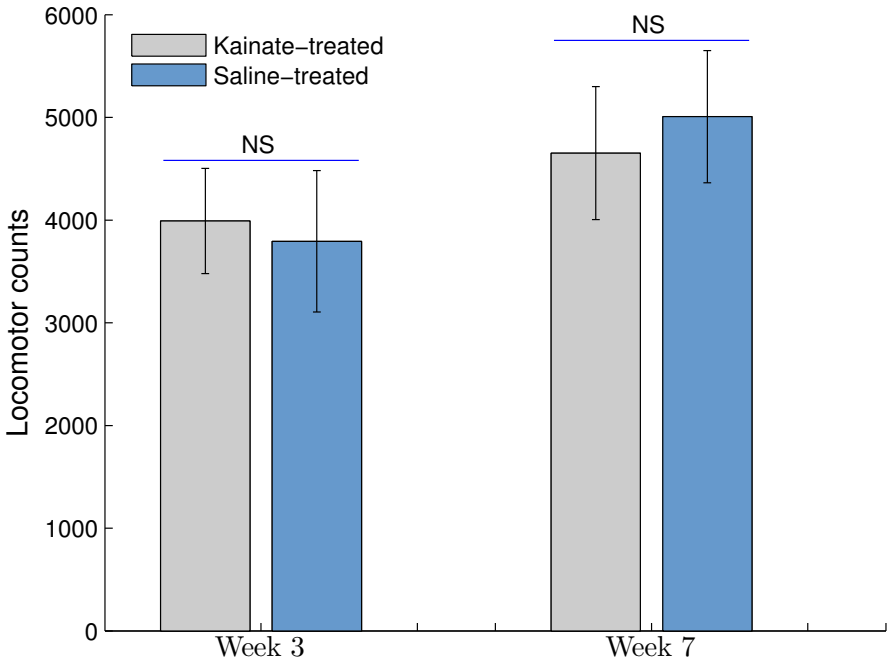

Figure 3.7: **Behavioural hyperactivity**. Locomotor activity indicated by counts of interrupted infrared beams in a horizontal plane within 40 minutes in a chamber did not significantly differ between the kainate-treated and saline-treated control rats ($n_{kainate}$ = 6, n_{saline} = 6), or across time (Week 3 v. Week 7). Results are expressed as mean ± SEM. NS signifies not statistically significant.

3.6 Effect of Kainate treatment on LFP power of olfactory bulb

OB log-power, recorded during the awake immobility state, was not significantly different between the kainate-group and saline-treated controls [$n_{kainate}$ = 3 (observations = 6), n_{saline} = 3 (observations = 6)] in any of the frequency bands: 14-20 Hz [$F(1,4) = 0.60$, NS], 20-30 Hz [$F(1,4) = 0.42$, NS], 30-40 Hz [$F(1,4) = 0.11$, NS], 40-60 Hz [$F(1,4) = 0.62$, NS] and 60-80 Hz [$F(1,4) = 0.85$, NS].

Chapter 4

Discussion

The primary objective of this thesis was to investigate how the hippocampal functional network disruptions manifest following a systemic injection of kainic acid in a rat model of TLE, during the interictal period. We investigated this hippocampal dysfunction using resting-state fMRI within a graph statistical modelling framework. It has been hypothesized that the intra-hemispheric, inter-hemispheric resting-state functional networks involving the hippocampus, and resting-state activity within the medial temporal lobe region will be altered (increased or reduced connectivity) in this pharmacological model of TLE. In addition to the resting-state connectivity, we also aimed at establishing behavioural and electrographic correlates of the hippocampal dysfunction. In behaviour, we hypothesized that locomotor activity would be higher; prepulse inhibition lowered, and isoflurane sensitivity higher in epileptic rats as compared to saline-injected rats. We tested this hypothesis using a battery of behavioural tests – open-field test, prepulse inhibition, and LORR test respectively. For LFP correlates, we tested a functional network involving the hippocampus using LFP recordings while an olfactory-stimulus (toluene) task is performed, and during spontaneous behaviours; to test the hypothesis that olfactory LFP would present with disruption of the fast oscillations (15–20 Hz) between the OB and DG.

4.1 Differences in Functional Connectivity

4.1.1 Increased Connectivity within the Limbic Networks

To reiterate briefly, the regions participating in the medial temporal/limbic networks include the cortical, subcortical, and bilateral regions of the hippocampus, amygdala, the entorhinal and temporal neocortices, inferior frontal lobes and the extra-TL components of the medial thalamus (Spencer, 2002).

Specifically, increased connectivity is observed between the hippocampus and the ACC on both the right and the left hemisphere. In addition, right hippocampus shows signs of increased connectivity with left retrosplenial cortex and left primary somatosensory cortex. No direct functional connections were observed between the mediodorsal thalamus (MDL), however, indirect functional connections were mediated by left ACC to connect both the right and left hippocampus with their MDL counterparts. ACC projects to the hippocampus via the lateral entorhinal cortex (Jones & Witter, 2007).

MDL/ACC and HC connectivity with the primary somatosensory cortex is also higher in the kainate-treated than the control group. Since seizure activity spreads from hippocampus to the extrapyramidal system and other cortical areas, it may be suggestive of the increased frequency of motor seizures coupled with a decreased seizure threshold in the status epilepticus (SE) rats. Moreover, somatosensory auras/hallucinations (Erickson, Clapp, Ford, & Jabbari, 2006), similar to olfactory auras, are rare manifestations in refractory TLE patients. Wu and Leung (2003) documented recurrent excitation of CA1 following CA3b stimulation in kainate-treated but not control rats as an evidence of reverberation of hippocampo-entorhinal activity, suggestive of increased glutamatergic transmission. This apparent prolonged disinhibition in a kainate model of TLE can affect widespread behaviour alterations in light of the hippocampal connectivity with other nodes of the limbic system. Ullal, Fahnestock, and Racine (2005) demonstrated upregulation of GluK1 mRNA and its protein product in the KA-induced systemic SE model, while GluK2 and GluK3

remained unaffected, at 180 days after the SE. GluK1 has been shown to suppress GABA-mediated inhibition and GluK2 reduces neuronal excitability (Vincent & Mulle, 2009); taken together, this illustrates their clear role in facilitating spontaneous seizures occurring months later. An increase in defensiveness was seen in cats post-partial kindling of the amygdala or ventral hippocampus (Adamec, 1991). These behavioural changes persisted anywhere from weeks to months, and correlated with an enhanced transmission of the amygdala-ventromedial hypothalamic pathway. Although no change in amygdalal connectivity was observed, it is quite relevant in the light of intimate limbic connectivity. The dynamic progression of morphological and molecular changes that affect the KAR expression profile seems like an attractive target in investigating the substrates of epileptogenesis.

4.1.2 Increased Activity within the DMN

We found increased connectivity within the components of the DMN, including the ACC, Rsp, Aud, PPC, and the hippocampus, in kainate rats as compared to controls. Liao et al. (2010) in a graph theory study in TLE patients demonstrated results seemingly contrary to ours – not suggesting a decreased/increased connectivity but rather that the number of DMN components participating in TLE patients are lower than those in controls. This would be rather difficult to explain since we tested the connectivity for only a single threshold while Liao et al. (2010) varied threshold a several hundred times to generate connectivity matrices to reliably arrive at that conclusion. Retrosplenial cortex has been shown to be one of the hub regions in the anaesthetized rat brain (Lu et al., 2012). Although our results suggests this hub status does not significantly change across groups, ACC, on the left and right side, however, emerge as the hub regions not only for the DMN but for entirety of the network with limited nodes considered. This dynamic change may reflect a change in functional reorganization following the status epilepticus, in light of the various reciprocal direct/indirect projections shared with the hypersynchronous/epileptic hippocampus. In addition, the intercalated (ITC) cells of the amygdala exert GABAergic inhibitory control over the amygdala, and share strong reciprocal projections with the infralimbic cortex (prefrontal

cortex; a subcomponent of the DMN) (Quirk & Mueller, 2008). Amygdala or the prefrontal cortex were not affected by the treatment, serving to validate our results since presence of one and not the other could be interpreted as spurious connections, to some extent. Corticocortical connectivity (anterior and posterior DMN) and thalamocortical (MDL and DMN) connectivity is also upregulated.

Other bilateral components of the DMN that include the posterior parietal cortex (PPC), and auditory/temporal association cortex (Aud) are significantly more functionally connected than in the epileptic rats as compared to controls. DMN disruptions have been reported during the interictal (Liao et al., 2010) as well ictal (Laufs et al., 2007) states with consistent reports of disconnection with other parts of the brain in TLE patients – citing reduced connection density as the precipitating factor. The changes in DMN connectivity, taken together, suggest a global reorganization of functional networks. However, we report increased connectivity within the DMN components of PPC, Aud, ACC, Rsp and hippocampus. There is no refuting the fact that in addition to temporal lobe sclerosis, the loss of white matter tracts would occur in the TLE rat model. However, the reparative mechanisms promote the increase of aberrant connections leading to re-entrant (mossy fiber sprouting in the DG) and autoassociative (CA3 auto synapses) pathways and consequently, leading to the increase in the observed functional connectivity. Considering the extent of the network in the TLE, this effect can be easily propagated to other local and distant structures. This compensatory increase may be supported by short-term and long term plasticity, considering the neuroplasticity of the medial temporal lobe structures.

Canals, Beyerlein, Merkle, and Logothetis (2009) reported a greater degree of interhemispheric connectivity by means of an increase in the BOLD signal and recruitment of limbic and neocortical circuits following LTP induction within the hippocampus following perforant path stimulation. They reported significant activations in the perirhinal cortex (PRh), the prefrontal cortex (PFC), the nucleus accumbens (Acb), and the anterior olfactory nucleus (AON). Parallels can be drawn between the LTP-induced by means of the electrical stimulation, and the intermittent epileptiform activity within the hippocampus. KA-treated rats are known to spontaneously seize even months

after the treatment. Villers, Godaux, and Ris (2012) established that long-lasting LTP can be induced either by single or repeated stimulations. A single IED originating in the hippocampus can propagate via monosynaptic pathways, and possibly through polysynaptic pathways, to induce short-term or long-term plasticity. This phenomena may tend to integrate in time with multiple IEDs spread across time to induce LTP in various structures which may eventually manifest as the increase in connectivity that we observed. The efficiency of KARs in the regulation of neuronal excitability seems to rely on repetitive synaptic activation rather than on single impulses, indicating that postsynaptic KARs are designed to modulate the temporal integration of excitatory circuits (Lerma & Marques, 2013). White matter reorganization as a result of axonal sprouting and neurite growth in spite of the excessive neurodegeneration are completely plausible explanations supported by the paradoxical increase in the structural connectivity within the medial temporal lobe (Bonilha et al., 2012). The concept of functional reserve and lateralization are particularly important in clinical literature. Studies have determined the transfer of visual and memory functions to the hemisphere contralateral to the lesion, without any surgery (Figueiredo et al., 2008; Powell et al., 2007). This gives weight to our functional reorganization argument, while the mechanisms facilitating such changes remains to be understood. Vaudano, Legg, and Glickstein (1991) suggested that the rat temporal association cortex bridges visual/auditory cortex with the limbic system via the amygdala and perirhinal cortex. Also, besides the usual sensory afferents (cortical areas), perirhinal cortex is the limbic afferent to the PPC (Lu et al., 2012). Biagini et al. (2013) showed that the perirhinal cortex is hyperexcitable in a pilocarpine model of TLE, and is intimately connected with several limbic structures. This interconnectedness of limbic systems with the PPC and "Aud" may be critical in relaying the epileptic activity to these cortical structures. This may eventually provoke molecular changes and morphological rearrangements responsible for the increase in connectivity observed between these structures.

4.1.3 Changes in the Dopaminergic Mesolimbic System

In support of our findings, the mesolimbic dopaminergic system has been shown to be sensitized by kindling (Csernansky, Kerr, Pruthi, & Prosser, 1988) was also inferred to be altered in the kainate (Ando et al., 2004) TLE model. The change observed in the nucleus accumbens (NAC) connectivity is particularly interesting. The nucleus accumbens manifests a significant degree increase in KA-treated rats compared to controls. This can be justified since strong projections between the hippocampus and the nucleus accumbens (Groenewegen, Vermeulen-Van der Zee, te Kortschot, & Witter, 1987; Groenewegen & Trimble, 2007) have been shown to increase the dopaminergic receptors in a hippocampal kindling model (Csernansky et al., 1988). This density increase in the KA model – systemic administration can be regarded as a non-specific pharmacological model of kindling – may spawn increased connectivity with regions it has connections with. In addition, medium spiny GABAergic neurons in the nucleus accumbens can achieve the same dysfunction through LTD as is achieved with LTP in the glutamatergic system. Therefore, an excitation/imbalance may cause the network dysregulation associated with mesolimbic dopamine system. The nucleus accumbens also projects to the medial part of the globus pallidus, but this connection seems to affect no group-level change. Contrary to our findings, reduced connectivity between the DMN and the dopaminergic mesolimbic network has been reported in TLE patients (Pittau, Grova, Moeller, Dubeau, & Gotman, 2012).

ACC and caudate nucleus are anatomically connected and are key recipients of dopaminergic projections from the ventral tegmental area (VTA) (Fallon, 1981; Groenewegen & Trimble, 2007). The observation that the ACC and CPu are connected significantly can be explained in the context of the hippocampal-VTA functional loop disruption. This DA-ergically mediated functional loop affecting the long-term potentiation in the hippocampus has been suggested to be critical component of the brain's memory system (Lisman & Grace, 2005); and an apparent dysfunction of this connection may be responsible for the observed upregulation. Lee, Hunsaker, and Kesner (2005) cited the hippocampus as the center of novelty detection; with the CA1 subfield as the

putative locus and serving as the "comparator" that computes novelty (Lisman & Grace, 2005). Since the hippocampal circuit is compromised in KA model of TLE, this can induce changes in the dopaminergic circuitry through the subiculum–accumbens projection that participates in the hippocampal-VTA loop. This possible dopaminergic dysfunction can account for an increased activity between the CPu and ACC. VTA also sends dopaminergic projections to the hippocampus, the NAC and prefrontal cortex (PFC); and its kindling results in schizophrenia-like behavioural changes (Glenthøj, Mogensen, Laursen, Holm, & Hemmingsen, 1993). Ma and Leung (2010) demonstrated that postictal hyperactivity and gamma oscillatory activity after prelimbic cortical kindling is mediated by the PrL-NAC connection via the hippocampus; and may help explain the increased NAC activity in the KA model of TLE. Furthermore, Chergui et al. (2000) demonstrated that exogenous KAR activation can depress the GABAergically mediated synaptic transmission in the CPu. Even though GluK4 receptors are expressed in the cingulate cortex, there is no evidence of KAR upregulation in the ACC. The associated functional and anatomical loop, however, may be responsible for the chronic disruption in the excitatory/inhibitory neurotransmission.

4.1.4 Change in Graph Metrics

In considering the global network alterations, it is important to consider how the graph topology and related graph metrics change in human subjects. These graph topological properties to measure the integration, segregation and centrality were significantly altered in epileptic rats compared to controls. Liang et al. (2011) demonstrated small worldness characterized by high clustering coefficient and a low characteristic path length, the configuration optimizing information transfer at low wiring cost, in awake rat brains. Both metrics are suggestive of the high information segregation and integration in the brain networks. Our graph metrics illustrate the same, in the rat brain, with the network being more connected or cliquish than the random network.

In terms of global parameters, we found significantly higher magnitudes of clustering coefficient (C_w), global efficiency (E_{glob}), and local efficiency (E_{loc}) in epileptic rats compared to controls. High C_w implies relatively high local connectedness of brain regions with metrics far from that of

a random network. The path length was quite similar and short in the two groups. The shorter absolute path lengths have been shown to promote effective interactions across cortical centres of processing; also indicating faster information transfer between inter-connected regions. The higher activity within the medial temporal lobe regions seems to corroborate our finding.

In a human study (Liao et al., 2010), the authors found that the values for C_w were significantly lower, while no significant change in L_w was observed in the TLE patients compared to controls. It is hard to reconcile the differences between the human and animal functional connectivity literature. It is possible that the KA systemic administration, as opposed to localized to hippocampus/amygdala, has far reaching consequences that modulate the network properties differently in rats, as compared to the unknown etiology in human TLE.

Global and local efficiency were significantly higher in the epileptic rats compared to controls. The global increase is especially obvious considering the increased interconnectivity of the DMN substructures (anterior and posterior DMN). Even though the MDL is anatomically connected to the ACC, it is functionally excluded from the DMN (Lu et al., 2012). MDL acts as the interface between the limbic structures and the neocortex, and due to its connectivity with the limbic structures acts as a major synchronizer of seizure activity. Thus, this compromised structure might be responsible for induced potentiation in the neocortex, which results in the observed increased functional connectivity of the limbic system with the DMN. The local efficiency can be attributed to the increased connectivity within the limbic network. In a computational study investigating DG epileptogenesis, Dyhrfjeld-Johnsen et al. (2007) found both local and long range connections, in support of our increased clustering coefficient, and small world findings for local computations and efficient global relay.

Similar to a study in TLE patients (Bonilha et al., 2012), we report in epileptic rats a global reorganisation of the DMN and local/global reorganisation of the limbic circuitry. The KA model of TLE is associated with regional loss of connections in the hippocampus. However, rsfMRI spatial resolution limits detection of changes within the hippocampus, i.e, between the CA1, CA3, DG, etc. Hippocampus, taken as a whole, is associated with higher clustering coefficient and consequently,

a higher influence of specific nodes over the network, as demonstrated by the higher efficiency, clustering and degree of various hubs in addition to the hippocampus. The global efficiency of the network was also significantly higher. Bonilha et al. (2012) also suggested that the global increase in clustering coefficient may indicate a higher fraction of reentrant to original connections (esp. axonal sprouting in DG) that do not alter the ability of the whole network to transfer information with high fidelity. Recent and past literature would suggest that the core of network alterations in this TLE model are restricted to the medial temporal regions; however, we reported additional alterations of the DMN.

4.2 Behavioural Alterations in KA Model of TLE

4.2.1 Increased Isoflurane Sensitivity in Epileptic Rats

Kainate-treated rats exhibited a higher sensitivity to the isoflurane anaesthesia, compared to controls. Multiple brain areas that included wake-active neurons and the limbic system are known to affect sensitivity to general anaesthesia (Leung, Luo, Ma, & Herrick, 2014). In particular, inactivation of the hippocampus (Ma, Shen, Stewart, Herrick, & Leung, 2002) and inactivation (Ma et al., 2002) or lesion of the medial septum (Leung et al., 2013; Tai et al., 2014) increased sensitivity to isoflurane anaesthesia. Thus, isoflurane sensitivity in kainate-treated rats may be the consequence of lesions in the hippocampus and limbic areas. The decrease in anaesthetic sensitivity was found despite an inferred increase in resting state functional connectivity within the limbic system and DMN. A similar increase in anaesthetic sensitivity has been observed in a pilocarpine model of TLE (Long et al., 2009). Also, septal cholinergic system has been shown to mediate and regulate the effects of anaesthesia on arousal systems (Leung et al., 2013; Tai et al., 2014). Evidentally, septal GABAergic system is prone to KA-damage and is closely related to the former system (Lévesque & Avoli, 2013).

4.2.2 PPI Deficits and Hyperlocomotion are not observed in Epileptic Rats

The two measures of schizophrenia-like symptoms in rats, PPI deficit and hyperlocomotion, were not different between epileptic and control rats in the present study. Increase in hippocampal or prefrontal glutamatergic inputs to the nucleus accumbens may be expected to enhance dopamine release from VTA terminals in the nucleus accumbens (Mogenson et al., 1993), and mediate locomotion increase and deficit in PPI (Swerdlow et al., 2001). Kindling of the hippocampus or prefrontal cortex, to a stage without behavioural convulsions, resulted in PPI deficit for up to 2 weeks after hippocampal kindling (Ma and Leung, 2004), and 3 days after prefrontal cortex kindling (Ma et al., 2010). PPI deficit was also observed immediately after a stage 5 amygdala seizure Koch and Ebert (1998), and after a non-convulsive hippocampal seizure (Ma et al., 2004). Our results were consistent with Koch and Ebert (1998), where the KA-treated rats tended to have a non-trivial increase in startle amplitude but no significant change under prepulse exposure.

Nucleus accumbens acts as the interface between the limbic and the motor systems (Groenewegen & Trimble, 2007; Mogenson, Jones, & Yim, 1980). In a previous study, Ando et al. (2004) reported higher locomotor activity induced by methamphetamine in kainate-treated as compared to control rats. Hyperlocomotion is considered a schizophrenia-like behavior that can be induced by a single or repeated seizures (Leung, Ma, & McLachlan, 2000), dopamine release in the nucleus accumbens after hippocampal or temporal lobe seizure. However, spontaneous locomotor activity in our study did not differ between epileptic and control rats, suggesting the baseline hippocampal and accumbens dopaminergic activity are not inducing hyperlocomotion.

4.3 Electrographic Characterization of the KA Model of TLE

4.3.1 No Significant Change in Olfactory Bulb Power

We observed no change in power in the olfactory bulb in any of the 5 frequency bands investigated during the awake immobile state, in the epileptic rats compared to controls, most likely on account of very limited data points. The odour-evoked beta oscillations in the range ~14–30 Hz are thought to be responsible for odor learning while high power in the olfactory gamma oscillations (~40–100 Hz) have been implicated in the optimal discrimination of closely related odorants (Kay et al., 2009). This finding, however, is not consistent with loss of OB volume in kainate-treated rats (Davila, Houpt, & Trombley, 2007; Lévesque & Avoli, 2013). Also, the loss of neurons can not be confirmed due to lack of immunohistochemical staining. The olfactory function deficit was not empirically determined through additional experiments. Nonetheless, such olfactory deficits correlated with reduction in OB volume have been reported in TLE patients (Hummel et al., 2013). However, further research is warranted in regards to olfactory neuropathology and concomitant dysfunction to better characterize this comorbidity in the KA model of TLE.

An attempt was made to obtain depth recordings from the hippocampus. However, due to extensive hippocampal atrophy (revealed by histological analysis) in the epileptic rats, the electrodes that were implanted according to the standard rat stereotaxic atlas (Paxinos & Watson, 2007) missed the targeted locations. Hence, we could not make any conclusions and interpretations concerning the OB-DG coherence levels following toluene stimulus in the epileptic rats.

4.4 Disparity with Human Literature

We reported results in our study that both support and apparently contradict the human literature. No study, to the best of our knowledge, has explored resting-state network disruptions in the KA model of TLE. Besides, there is a paucity of research investigating pathological small-world networks in small animals. In the same vein, the TLE models do not precisely replicate the human symptomatology and neuropathology, but have enough similarities to allow appropriate questions that may lend insight into the human condition, and thus, should be viewed as such.

There are potential pitfalls in drawing parallels between the TLE models and patients. Etiology of human TLE is quite different from KA-treated epileptic rats, and most TLE patients, thus, do not arise from a *status epilepticus*. TLE patients have large variability, but they do not uniformly have the pathology in EC, CA3, piriform cortex, unlike KA-treated rats. However, this may account for a lot of variability observed in the TLE patient population. This disparity could result from a number of reasons. Firstly, the seizure focus can either be in the hippocampus, amygdala, entorhinal or the perirhinal cortex in the TLE patients. In contrast, in the systemic administration of KA, the focus mostly lies in the hippocampus (Lévesque & Avoli, 2013). Secondly, the human results can easily be confounded due to a number of factors that include: (i) the cerebral functional reserve in unilateral (more common in humans) TLE (bilateral onset in rats), (ii) age, (iii) gender, (iv) drug load and drug interactions (rats not treated with AEDs), (v) etiology of and duration of disease state, and (vi) initial injury cause and site.

4.5 Study Limitations

Firstly, the coarse resolution of 800×800 μm^2 (400×400 μm^2 before spatial smoothing) with 1 mm slice thickness considerably limits our ability to differentiate between small yet distinct brain structures close together. Second, no causality or effective connectivity could be determined since we used undirected networks. Third, although the resting state networks have been discovered in

rodents under anaesthesia, a certain degree of bias may be introduced in the results; since isoflurane has been known to affect neurovascular coupling. Fourth, we manually defined seed regions in each of the rats. Since this manual node definition is prone to human error, an ICA-optimized approach – that recognizes the spatiotemporal activations inherent in the data to define seed regions – may be a good choice. Still, to avoid averaging signals from 2 distinct brain regions, it was made sure that they were at least 2 voxels ($1 \times$FWHM or 0.8 mm) apart. Lastly, a surface coil placed atop the rat head/skull was used to record the BOLD contrast. This surface coil, however, does not capture the BOLD signals from deeper subcortical with high fidelity. Volumetric coil, with a higher curvature and better contrast-to-noise ratio (CNR), can help improve the BOLD signal. However, the volumetric coil was not available to use until after half way through the study; and will be used in future studies.

4.6 Conclusion

In conclusion, we have demonstrated that the KA model of TLE, far from a perfect model, is adept at replicating several features of the TLE neuropathology that has been increasingly complex at defining and diagnosing. We found increase in functional connectivity within the medial temporal regions and the limbic network. In addition, the anterior and posterior DMN share a better connection. Furthermore, our results suggest that the increased clustering coefficient, short path length and higher level of global and local efficiency along with the small world properties, are altered in this disorder. The network-level interaction of three main neurotransmission systems – glutamate, dopamine, and GABA – is unequivocally the most crucial one in teasing apart the effects of diverse symptomatology of TLE disorder. How KARs affect various actions under conditions of physiological activation (canonical and noncanonical) and its behavioural consequences is still an enigma, and naturally, an area of active research (see Figure 1.4). A better understanding of KAR physiology would go a long way in interpreting the network effects of TLE.

Our understanding of the brain structure, function, and network-level pathology has grown

leaps and bounds from the small animal investigations using neuroimaging techniques. The present study systematically investigated the resting-state functional networks in the anaesthetized rat brain. TLE has progressed in its definition from being a focal pathology to a network disorder. This has led to shifting of the focus away from the hippocampus and to the limbic network. Resolving the temporal character of these neuroplastic processes may be key in defining a more suitable and effective methodology for treatment of TLE. Although this still requires a significant amount of resting-state research in the animal models of epilepsy, we suggest that the alterations observed in the functional connectivity and network topological properties could be potentially used as tentative biomarkers of TLE in the near future.

References

Abela, E., Rummel, C., Hauf, M., Weisstanner, C., Schindler, K., & Wiest, R. (2014). Neuroimaging of epilepsy: lesions, networks, oscillations. *Clinical neuroradiology*, 24:(1): 5–15.

Acharya, V., Acharya, J., & Lüders, H. (1998). Olfactory epileptic auras. *Neurology*, 51: 56–61.

Adamec, R. E. (1991). Partial kindling of the ventral hippocampus: Identification of changes in limbic physiology which accompany changes in feline aggression and defense. *Physiology & Behavior*, 49:(3): 443–453.

Amaral, L. A., Scala, A., Barthelemy, M., & Stanley, H. E. (2000). Classes of small-world networks. *Proceedings of the National Academy of Sciences of the United States of America*, 97:(21): 11149–52.

Ando, N., Morimoto, K., Watanabe, T., Ninomiya, T., & Suwaki, H. (2004). Enhancement of central dopaminergic activity in the kainate model of temporal lobe epilepsy: implication for the mechanism of epileptic psychosis. *Neuropsychopharmacology : official publication of the American College of Neuropsychopharmacology*, 29:(7): 1251–8.

Bartolomei, F., Wendling, F., Régis, J., Gavaret, M., Guye, M., & Chauvel, P. (2004). Pre-ictal synchronicity in limbic networks of mesial temporal lobe epilepsy. *Epilepsy Research*, 61: 89–104.

Bassett, D. S., Nelson, B. G., Mueller, B. A., Camchong, J., & Lim, K. O. (2012). Altered resting state complexity in schizophrenia. *NeuroImage*, 59: 2196–2207.

Bastian, M., Heymann, S., & Jacomy, M. (2009). Gephi: An Open Source Software for Exploring and Manipulating Networks. *Third International AAAI Conference on Weblogs and Social Media*: 361–362.

Becerra, L., Pendse, G., Chang, P.-C., Bishop, J., & Borsook, D. (2011). Robust reproducible resting state networks in the awake rodent brain. *PloS one*, 6:(10): e25701.

Ben-Ari, Y. (1985). Limbic seizure and brain damage produced by kainic acid: mechanisms and relevance to human temporal lobe epilepsy. *Neuroscience*, 14:(2): 375–403.

Ben-Ari, Y., Riche, D., Tremblay, E., & Charton, G. (1981). Alterations in local glucose consumption following systemic administration of kainic acid, bicuculline or metrazol. *European neurology*, 20: 173–175.

Ben-Ari, Y., Tremblay, E., Ottersen, O. P., & Meldrum, B. S. (1980). The role of epileptic activity in hippocampal and 'remote' cerebral lesions induced by kainic acid. *Brain Research*, 191: 79–97.

Ben-Ari, Y., Crepel, V., & Represa, A. (2008). Seizures Beget Seizures in Temporal Lobe Epilepsies: The Boomerang Effects of Newly Formed Aberrant Kainatergic Synapses. *Epilepsy Currents*, 8: 68–72.

Berg, A. T., Berkovic, S. F., Brodie, M. J., Buchhalter, J., Cross, J. H., Van Emde Boas, W., … Scheffer, I. E. (2010). Revised terminology and concepts for organization of seizures and epilepsies: Report of the ILAE Commission on Classification and Terminology, 2005-2009. *Epilepsia*, 51: 676–685.

Bernard, A., Ferhat, L., Dessi, F., Charton, G., Represa, A., Ben-Ari, Y., & Khrestchatisky, M. (1999). Q/R editing of the rat GluR5 and GluR6 kainate receptors in vivo and in vitro: Evidence for independent developmental, pathological and cellular regulation. *European Journal of Neuroscience*, 11: 604–616.

Bernhardt, B. C., Chen, Z., He, Y., Evans, A. C., & Bernasconi, N. (2011). Graph-theoretical analysis reveals disrupted small-world organization of cortical thickness correlation networks in temporal lobe epilepsy. *Cerebral Cortex*, 21: 2147–2157.

Bertram, E. H. (2009). Temporal lobe epilepsy: Where do the seizures really begin? *Epilepsy and Behavior*, 14: 32–37.

Bertram, E. H. (2014). Extratemporal lobe circuits in temporal lobe epilepsy. *Epilepsy & Behavior : E&B*, 34: 1036–1046.

Bertram, E. H., Zhang, D. X., Mangan, P., Fountain, N., & Rempe, D. (1998). Functional anatomy of limbic epilepsy: A proposal for central synchronization of a diffusely hyperexcitable network. In *Epilepsy research* (Vol. 32, pp. 194–205).

Best, N., Mitchell, J., & Wheal, H. V. (1994). Ultrastructure of parvalbumin-immunoreactive neurons in the CA1 area of the rat hippocampus following a kainic acid injection. *Acta Neuropathologica*, 87: 187–195.

Bettus, G., Guedj, E., Joyeux, F., Confort-Gouny, S., Soulier, E., Laguitton, V., … Guye, M. (2009). Decreased basal fMRI functional connectivity in epileptogenic networks and contralateral compensatory mechanisms. *Human Brain Mapping*, 30: 1580–1591.

Bettus, G., Ranjeva, J.-P., Wendling, F., Bénar, C. G., Confort-Gouny, S., Régis, J., … Guye, M. (2011). Interictal functional connectivity of human epileptic networks assessed by intracerebral EEG and BOLD signal fluctuations. *PloS one*, 6:(5): e20071.

Biagini, G., D'Antuono, M., Benini, R., de Guzman, P., Longo, D., & Avoli, M. (2013). Perirhinal cortex and temporal lobe epilepsy. *Frontiers in cellular neuroscience*, 7: 130.

Bischoff, S., Barhanin, J., Bettler, B., Mulle, C., & Heinemann, S. (1997). Spatial distribution of kainate receptor subunit mRNA in the mouse basal ganglia and ventral mesencephalon. *Journal of Comparative Neurology*, 379: 541–562.

Biswal, B., Yetkin, F. Z., Haughton, V. M., & Hyde, J. S. (1995). Functional connectivity in the motor cortex of resting human brain using echo-planar MRI. *Magnetic resonance in medicine : official journal of the Society of Magnetic Resonance in Medicine / Society of Magnetic Resonance in Medicine*, 34:(4): 537–41.

Blümcke, I., Coras, R., Miyata, H., & Özkara, C. (2012). Defining clinico-neuropathological subtypes of mesial temporal lobe epilepsy with hippocampal sclerosis. In *Brain pathology* (Vol. 22, pp. 402–411).

Blümcke, I., Thom, M., Aronica, E., Armstrong, D. D., Bartolomei, F., Bernasconi, A., … Spreafico, R. (2013). International consensus classification of hippocampal sclerosis in temporal lobe epilepsy: A Task Force report from the ILAE Commission on Diagnostic Methods. *Epilepsia*, 54: 1315–1329.

Bonilha, L., Nesland, T., Martz, G. U., Joseph, J. E., Spampinato, M. V., Edwards, J. C., & Tabesh, A. (2012). Medial temporal lobe epilepsy is associated with neuronal fibre loss and paradoxical increase in structural connectivity of limbic structures. *Journal of neurology, neurosurgery, and psychiatry*, 83:(9): 903–9.

Braff, D. L., Geyer, M. A., & Swerdlow, N. R. (2001). Human studies of prepulse inhibition of startle: normal subjects, patient groups, and pharmacological studies. *Psychopharmacology*, 156:(2-3): 234–258.

Bragin, A., Benassi, S. K., Kheiri, F., & Engel, J. (2011). Further evidence that pathologic high-frequency oscillations are bursts of population spikes derived from recordings of identified cells in dentate gyrus. *Epilepsia*, 52: 45–52.

Bragin, A., Wilson, C. L., & Engel, J. (2007). Voltage depth profiles of high-frequency oscillations after kainic acid-induced status epilepticus. *Epilepsia*, 48 Suppl 5: 35–40.

Buckmaster, P. S. (2004). Laboratory animal models of temporal lobe epilepsy. *Comparative medicine*, 54:(5): 473–85.

Buckmaster, P. S. (2010). Mossy fiber sprouting in the dentate gyrus. In Jasper's basic mechanisms of the epilepsies (4th, Vol. 51, p. 39). Bethesda, MD: NCBI.

Bullmore, E. & Sporns, O. (2009). Complex brain networks: graph theoretical analysis of structural and functional systems. *Nature reviews. Neuroscience*, 10:(3): 186–98.

Buzsáki, G. (2006). *Rhythms of the Brain*. Oxford University Press.

Buzsáki, G. & da Silva, F. L. (2012a). High frequency oscillations in the intact brain. *Progress in neurobiology*, 98:(3): 241–9.

Buzsáki, G. & Draguhn, A. (2004). Neuronal oscillations in cortical networks. *Science*, 304: 1926–1929.

Buzsáki, G. & Wang, X.-J. (2012b). Mechanisms of gamma oscillations. *Annual review of neuroscience*, 35: 203–25.

Canals, S., Beyerlein, M., Merkle, H., & Logothetis, N. K. (2009). Functional MRI Evidence for LTP-Induced Neural Network Reorganization. *Current Biology*, 19: 398–403.

Casassus, G. & Mulle, C. (2002). Functional characterization of kainate receptors in the mouse nucleus accumbens. *Neuropharmacology*, 42: 603–611.

Castellanos, F. X., Margulies, D. S., Kelly, C., Uddin, L. Q., Ghaffari, M., Kirsch, A., … Milham, M. P. (2008). Cingulate-Precuneus Interactions: A New Locus of Dysfunction in Adult Attention-Deficit/Hyperactivity Disorder. *Biological Psychiatry*, 63: 332–337.

Cataldi, M., Avoli, M., & de Villers-Sidani, E. (2013). Resting state networks in temporal lobe epilepsy. *Epilepsia*, 54:(12): 2048–59.

Chen, C., Shih, Y.-H., Yen, D.-J., Lirng, J.-F., Guo, Y.-C., Yu, H.-Y., & Yiu, C.-H. (2003). Olfactory auras in patients with temporal lobe epilepsy. *Epilepsia*, 44:(2): 257–60.

Chergui, K., Bouron, A., Normand, E., & Mulle, C. (2000). Functional GluR6 kainate receptors in the striatum: indirect downregulation of synaptic transmission. *The Journal of neuroscience : the official journal of the Society for Neuroscience*, 20:(6): 2175–82.

Coppola, A. & Moshé, S. L. (2012). Animal models. *Handbook of clinical neurology*, 107: 63–98.

Cox, R. W. (1996). AFNI: software for analysis and visualization of functional magnetic resonance neuroimages. *Computers and biomedical research, an international journal*, 29: 162–173.

Crowder, T. L., Ariwodola, O. J., & Weiner, J. L. (2006). Kainate receptor activation potentiates GABAergic synaptic transmission in the nucleus accumbens core. *Brain research*, 1088:(1): 73–82.

Csernansky, J. G., Kerr, S., Pruthi, R., & Prosser, E. S. (1988). Mesolimbic dopamine receptor increases two weeks following hippocampal kindling. *Brain Research*, 449:(1-2): 357–360.

Csicsvari, J., Jamieson, B., Wise, K. D., & Buzsáki, G. (2003). Mechanisms of gamma oscillations in the hippocampus of the behaving rat. *Neuron*, 37: 311–322.

Curtis, M. D., Jefferys, J. G. R., & Avoli, M. (2012). Interictal Epileptiform Discharges in Partial Epilepsy : Complex Neurobiological Mechanisms Based on Experimental and Clinical Evidence. In Jasper's basic mechanisms of the epilepsies (4th). Bethesda, MD: NCBI.

Damoiseaux, J. S. (2012). Resting-state fMRI as a biomarker for Alzheimer's disease? *Alzheimer's research & therapy*, 4:(2): 8.

Davila, N. G., Houpt, T. a., & Trombley, P. Q. (2007). Expression and function of kainate receptors in the rat olfactory bulb. *Synapse (New York, N.Y.)* 61:(5): 320–34.

De Vico Fallani, F., Richiardi, J., Chavez, M., & Achard, S. (2014). Graph analysis of functional brain networks: practical issues in translational neuroscience. *Philosophical transactions of the Royal Society of London. Series B, Biological sciences*, 369:(1653).

Drexel, M., Preidt, A. P., Kirchmair, E., & Sperk, G. (2011). Parvalbumin interneurons and calretinin fibers arising from the thalamic nucleus reuniens degenerate in the subiculum after kainic acid-induced seizures. *Neuroscience*, 189: 316–329.

Drexel, M., Preidt, A. P., & Sperk, G. (2012). Sequel of spontaneous seizures after kainic acid-induced status epilepticus and associated neuropathological changes in the subiculum and entorhinal cortex. *Neuropharmacology*, 63:(5): 806–17.

Dudek, J. L. H. & Edward, F. (2005). Chemoconvulsant Model of Chronic Spontaneous Seizures - Kainic Acid Protocol. *Current Protocols in Neuroscience*, Supplement: 1–12.

Dyhrfjeld-Johnsen, J., Santhakumar, V., Morgan, R. J., Huerta, R., Tsimring, L., & Soltesz, I. (2007). Topological determinants of epileptogenesis in large-scale structural and functional models of the dentate gyrus derived from experimental data. *Journal of neurophysiology*, 97: 1566–1587.

Engel, A. K., Fries, P., & Singer, W. (2001). Dynamic predictions: oscillations and synchrony in top-down processing. *Nature reviews. Neuroscience*, 2: 704–716.

Engel, J. (1996). Surgery for seizures. *The New England journal of medicine*, 334: 647–652.

Engel, J. & Ackermann, R. F. (1980). Interictal EEG spikes correlate with decreased, rather than increased, epileptogenicity in amygdaloid kindled rats. *Brain Research*, 190:(2): 543–548.

Engel, J., McDermott, M. P., Wiebe, S., Langfitt, J. T., Stern, J. M., Dewar, S., … Kieburtz, K. (2012). Early surgical therapy for drug-resistant temporal lobe epilepsy: a randomized trial. *JAMA : the journal of the American Medical Association*, 307: 922–30.

Enzinger, C. & DeLuca, J. (2012). Large-scale neuronal network dysfunction in multiple sclerosis?: Evidence from resting-state fMRI. *Neurology*, 79:(14): 1416–7.

Epsztein, J., Represa, A., Jorquera, I., Ben-Ari, Y., & Crépel, V. (2005). Recurrent mossy fibers establish aberrant kainate receptor-operated synapses on granule cells from epileptic rats. *The Journal of neuroscience : the official journal of the Society for Neuroscience*, 25: 8229–8239.

Erickson, J. C., Clapp, L. E., Ford, G., & Jabbari, B. (2006). Somatosensory auras in refractory temporal lobe epilepsy. *Epilepsia*, 47: 202–206.

Fair, D. A., Posner, J., Nagel, B. J., Bathula, D., Dias, T. G. C., Mills, K. L., … Nigg, J. T. (2010). Atypical default network connectivity in youth with attention-deficit/hyperactivity disorder. *Biological psychiatry*, 68: 1084–1091.

Fallon, J. H. (1981). Collateralization of monoamine neurons: mesotelencephalic dopamine projections to caudate, septum, and frontal cortex. *The Journal of neuroscience : the official journal of the Society for Neuroscience*, 1:(12): 1361–8.

Farber, N. E., Harkin, C. P., Niedfeldt, J., Hudetz, A. G., Kampine, J. P., & Schmeling, W. T. (1997). Region-specific and agent-specific dilation of intracerebral microvessels by volatile anesthetics in rat brain slices. *Anesthesiology*, 87: 1191–1198.

Farmer, M. A., Baliki, M. N., & Apkarian, A. V. (2012). A dynamic network perspective of chronic pain. *Neuroscience letters*, 520:(2): 197–203.

Figueiredo, P., Santana, I., Teixeira, J., Cunha, C., Machado, E., Sales, F., … Castelo-Branco, M. (2008). Adaptive visual memory reorganization in right medial temporal lobe epilepsy. *Epilepsia*, 49: 1395–1408.

Fisahn, A., Contractor, A., Traub, R. D., Buhl, E. H., Heinemann, S. F., & McBain, C. J. (2004). Distinct roles for the kainate receptor subunits GluR5 and GluR6 in kainate-induced hippocampal gamma oscillations. *The Journal of neuroscience : the official journal of the Society for Neuroscience*, 24:(43): 9658–68.

Franks, N. P. (2008). General anaesthesia: from molecular targets to neuronal pathways of sleep and arousal. *Nature reviews. Neuroscience*, 9: 370–386.

Fritsch, B., Qashu, F., Figueiredo, T. H., Aroniadou-Anderjaska, V., Rogawski, M. A., & Braga, M. F. M. (2009). Pathological alterations in GABAergic interneurons and reduced tonic inhibition in the basolateral amygdala during epileptogenesis. *Neuroscience*, 163: 415–429.

Fukuda, T. & Kosaka, T. (2000). Gap junctions linking the dendritic network of GABAergic interneurons in the hippocampus. *The Journal of neuroscience : the official journal of the Society for Neuroscience*, 20: 1519–1528.

Glenthøj, B., Mogensen, J., Laursen, H., Holm, S., & Hemmingsen, R. (1993). Electrical sensitization of the meso-limbic dopaminergic system in rats: a pathogenetic model for schizophrenia. *Brain research*, 619:(1-2): 39–54.

Gotman, J. (1984). Relationships between triggered seizures, spontaneous seizures, and interictal spiking in the kindling model of epilepsy. *Experimental neurology*, 84:(2): 259–73.

Gotman, J. & Marciani, M. G. (1985). Electroencephalographic spiking activity, drug levels, and seizure occurrence in epileptic patients. *Annals of neurology*, 17:(6): 597–603.

Greicius, M. (2008). Resting-state functional connectivity in neuropsychiatric disorders. *Current opinion in neurology*, 21: 424–430.

Greicius, M. D., Flores, B. H., Menon, V., Glover, G. H., Solvason, H. B., Kenna, H., … Schatzberg, A. F. (2007). Resting-State Functional Connectivity in Major Depression: Abnormally Increased Contributions from Subgenual Cingulate Cortex and Thalamus. *Biological Psychiatry*, 62: 429–437.

Greicius, M. D., Supekar, K., Menon, V., & Dougherty, R. F. (2009). Resting-state functional connectivity reflects structural connectivity in the default mode network. *Cerebral cortex (New York, N.Y. : 1991)*, 19:(1): 72–8.

Groenewegen, H. J., Vermeulen-Van der Zee, E., te Kortschot, A., & Witter, M. P. (1987). Organization of the projections from the subiculum to the ventral striatum in the rat. A study using anterograde transport of Phaseolus vulgaris leucoagglutinin. *Neuroscience*, 23:(1): 103–20.

Groenewegen, H. J. & Trimble, M. (2007). The ventral striatum as an interface between the limbic and motor systems. *CNS spectrums*, 12: 887–892.

Gröticke, I., Hoffmann, K., & Löscher, W. (2007). Behavioral alterations in the pilocarpine model of temporal lobe epilepsy in mice. *Experimental Neurology*, 207: 329–349.

Gröticke, I., Hoffmann, K., & Löscher, W. (2008). Behavioral alterations in a mouse model of temporal lobe epilepsy induced by intrahippocampal injection of kainate. *Experimental Neurology*, 213: 71–83.

Guye, M., Bettus, G., Bartolomei, F., & Cozzone, P. J. (2010). Graph theoretical analysis of structural and functional connectivity MRI in normal and pathological brain networks. *Magma (New York, N.Y.)* 23:(5-6): 409–21.

Haas, K. Z., Sperber, E. F., Opanashuk, L. A., Stanton, P. K., & Moshé, S. L. (2001). Resistance of immature hippocampus to morphologic and physiologic alterations following status epilepticus or kindling. *Hippocampus*, 11: 615–625.

Hagmann, P., Cammoun, L., Gigandet, X., Meuli, R., Honey, C. J., Van Wedeen, J., & Sporns, O. (2008). Mapping the structural core of human cerebral cortex. *PLoS Biology*, 6: 1479–1493.

Hampson, M., Peterson, B. S., Skudlarski, P., Gatenby, J. C., & Gore, J. C. (2002). Detection of functional connectivity using temporal correlations in MR images. *Human Brain Mapping*, 15: 247–262.

Harroud, A., Bouthillier, A., Weil, A. G., & Nguyen, D. K. (2012). Temporal lobe epilepsy surgery failures: a review. *Epilepsy research and treatment*, 2012: 201651.

Heale, V. R., Vanderwolf, C. H., & Leung, L. S. (1995). The neurotoxins colchicine and kainic acid block odor-induced fast waves and olfactory-evoked potentials in the dentate gyrus of the behaving rat. *Brain research*, 690:(2): 157–66.

Hong, S.-C., Holbrook, E. H., Leopold, D. A., & Hummel, T. (2012). Distorted olfactory perception: a systematic review. *Acta oto-laryngologica*, 132 Suppl: S27–31.

Hudry, J., Ryvlin, P., Royet, J. P., & Mauguière, F. (2001). Odorants elicit evoked potentials in the human amygdala. *Cerebral cortex (New York, N.Y. : 1991)*, 11:(7): 619–27.

Hummel, T., Henkel, S., Negoias, S., Galván, J. R. B., Bogdanov, V., Hopp, P., … Haehner, A. (2013). Olfactory bulb volume in patients with temporal lobe epilepsy. *Journal of neurology*, 260:(4): 1004–8.

Huster, R. J., Debener, S., Eichele, T., & Herrmann, C. S. (2012). Methods for simultaneous EEG-fMRI: an introductory review. *The Journal of neuroscience : the official journal of the Society for Neuroscience*, 32:(18): 6053–60.

Hutchison, R. M. (2012). *Brain connectivity studied by fMRI : homologous network organization in the rat, monkey, and human* (Doctoral dissertation, University of Western Ontario).

Hutchison, R. M., Hutchison, M., Manning, K. Y., Menon, R. S., & Everling, S. (2014). Isoflurane induces dose-dependent alterations in the cortical connectivity profiles and dynamic properties of the brain's functional architecture. *Human brain mapping*, 00:(07).

Hutchison, R. M., Mirsattari, S. M., Jones, C. K., Gati, J. S., & Leung, L. S. (2010). Functional networks in the anesthetized rat brain revealed by independent component analysis of resting-state FMRI. *Journal of neurophysiology*, 103:(6): 3398–406.

Insel, T., Landis, S., & Collins, F. (2013). The NIH brain initiative. *Science*, 340: 687–688.

Jacobs, J., Staba, R., Asano, E., Otsubo, H., Wu, J. Y., Zijlmans, M., … Gotman, J. (2012). High-frequency oscillations (HFOs) in clinical epilepsy. *Progress in neurobiology*, 98:(3): 302–15.

Jacobs, J., LeVan, P., Moeller, F., Boor, R., Stephani, U., Gotman, J., & Siniatchkin, M. (2009). Hemodynamic changes preceding the interictal EEG spike in patients with focal epilepsy investigated using simultaneous EEG-fMRI. *NeuroImage*, 45: 1220–1231.

Jefferys, J. G. R., Jiruska, P., Curtis, M. D., & Avoli, M. (2012). Limbic Network Synchronization and Temporal Lobe Epilepsy. In Jasper's basic mechanisms of the epilepsies (4th, pp. 1–18). Bethesda, MD: NCBI.

Jenkinson, M., Beckmann, C. F., Behrens, T. E. J., Woolrich, M. W., & Smith, S. M. (2012). FSL. *NeuroImage*, 62:(2): 782–90.

Jones, B. F. & Witter, M. P. (2007). Cingulate cortex projections to the parahippocampal region and hippocampal formation in the rat. *Hippocampus*, 17: 957–976.

Kaiser, M. (2013). The potential of the human connectome as a biomarker of brain disease. *Frontiers in human neuroscience*, 7: 484.

Kandel, E. R., Schwartz, J. H., & Jessell, T. M. (2012). *Principles of Neural Science* (5th). McGraw-Hill Professional.

Kandratavicius, L., Lopes-Aguiar, C., Bueno-Júnior, L. S., Romcy-Pereira, R. N., Hallak, J. E. C., & Leite, J. P. (2012). Psychiatric Comorbidities in Temporal Lobe Epilepsy: Possible Relationships between Psychotic Disorders and Involvement of Limbic Circuits. *Revista Brasileira de Psiquiatria*, 35:(1): 107.

Kannurpatti, S. S., Biswal, B. B., Kim, Y. R., & Rosen, B. R. (2008). Spatio-temporal characteristics of low-frequency BOLD signal fluctuations in isoflurane-anesthetized rat brain. *NeuroImage*, 40:(4): 1738–47.

Kay, L. M., Beshel, J., Brea, J., Martin, C., Rojas-Líbano, D., & Kopell, N. (2009). Olfactory oscillations: the what, how and what for. *Trends in neurosciences*, 32:(4): 207–14.

Klassen, L. M. & Menon, R. S. (2004). Robust Automated Shimming Technique Using Arbitrary Mapping Acquisition Parameters (RASTAMAP). *Magnetic Resonance in Medicine*, 51: 881–887.

Koch, M. & Ebert, U. (1998). Deficient sensorimotor gating following seizures in amygdala-kindled rats. *Biological psychiatry*, 44:(4): 290–7.

Koch, M. & Schnitzler, H.-U. (1997). The acoustic startle response in rats—circuits mediating evocation, inhibition and potentiation. *Behavioural Brain Research*, 89:(1-2): 35–49.

Kühn, S. & Gallinat, J. (2013). Resting-state brain activity in schizophrenia and major depression: A quantitative meta-analysis. *Schizophrenia Bulletin*, 39: 358–365.

Laufs, H., Hamandi, K., Salek-Haddadi, A., Kleinschmidt, A. K., Duncan, J. S., & Lemieux, L. (2007). Temporal lobe interictal epileptic discharges affect cerebral activity in "default mode" brain regions. *Human Brain Mapping*, 28: 1023–1032.

Lee, I., Hunsaker, M. R., & Kesner, R. P. (2005). The role of hippocampal subregions in detecting spatial novelty. *Behavioral neuroscience*, 119: 145–153.

Lerma, J., Paternain, a. V., Rodríguez-Moreno, A., & López-García, J. C. (2001). Molecular physiology of kainate receptors. *Physiological reviews*, 81:(3): 971–98.

Lerma, J. (2003). Roles and rules of kainate receptors in synaptic transmission. *Nature reviews. Neuroscience*, 4:(6): 481–95.

Lerma, J. & Marques, J. M. (2013). Kainate receptors in health and disease. *Neuron*, 80:(2): 292–311.

Leung, L. S. (1998). Generation of theta and gamma rhythms in the hippocampus. *Neuroscience and biobehavioral reviews*, 22:(2): 275–90.

Leung, L. S., Lopes da Silva, F. H., & Wadman, W. J. (1982). Spectral characteristics of the hippocampal EEG in the freely moving rat. *Electroencephalography and Clinical Neurophysiology*, 54: 203–219.

Leung, L. S., Luo, T., Ma, J., & Herrick, I. (2014). Brain areas that influence general anesthesia. *Progress in neurobiology*, 84: 450–455.

Leung, L. S., Ma, J., Shen, B., Nachim, I., & Luo, T. (2013). Medial septal lesion enhances general anesthesia response. *Experimental neurology*, 247: 419–28.

Leung, L. W. (1988). Hippocampal interictal spikes induced by kindling: relations to behavior and EEG. *Behavioural brain research*, 31: 75–84.

Leung, L. W. S. (1985). Spectral analysis of hippocampal EEG in the freely moving rat: Effects of centrally active drugs and relations to evoked potentials. *Electroencephalography and Clinical Neurophysiology*, 60: 65–77.

Leung, L., Ma, J., & McLachlan, R. (2000). Behaviors induced or disrupted by complex partial seizures. *Neuroscience & Biobehavioral Reviews*, 24:(7): 763–775.

LeVan, P., Tyvaert, L., Moeller, F., & Gotman, J. (2010). Independent component analysis reveals dynamic ictal BOLD responses in EEG-fMRI data from focal epilepsy patients. *NeuroImage*, 49: 366–378.

Lévesque, M. & Avoli, M. (2013). The kainic acid model of temporal lobe epilepsy. *Neuroscience and biobehavioral reviews*, 37:(10 Pt 2): 2887–99.

Lévesque, M., Langlois, J. M. P., Lema, P., Courtemanche, R., Bilodeau, G. A., & Carmant, L. (2009). Synchronized gamma oscillations (30-50 Hz) in the amygdalo-hippocampal network in relation with seizure propagation and severity. *Neurobiology of Disease*, 35: 209–218.

Li, T., Lytle, N., Lan, J.-Q., Sandau, U. S., & Boison, D. (2012). Local disruption of glial adenosine homeostasis in mice associates with focal electrographic seizures: a first step in epileptogenesis? *Glia*, 60:(1): 83–95.

Liang, Z., King, J., & Zhang, N. (2011). Uncovering intrinsic connectional architecture of functional networks in awake rat brain. *The Journal of neuroscience : the official journal of the Society for Neuroscience*, 31:(10): 3776–83.

Liang, Z., King, J., & Zhang, N. (2012). Intrinsic organization of the anesthetized brain. *The Journal of neuroscience : the official journal of the Society for Neuroscience*, 32:(30): 10183–91.

Liao, W., Zhang, Z., Pan, Z., Mantini, D., Ding, J., Duan, X., … Chen, H. (2010). Altered functional connectivity and small-world in mesial temporal lobe epilepsy. *PloS one*, 5:(1): e8525.

Liao, W., Zhang, Z., Pan, Z., Mantini, D., Ding, J., Duan, X., … Chen, H. (2011). Default mode network abnormalities in mesial temporal lobe epilepsy: a study combining fMRI and DTI. *Human brain mapping*, 32:(6): 883–95.

Lisman, J. E. & Grace, A. A. (2005). The hippocampal-VTA loop: controlling the entry of information into long-term memory. *Neuron*, 46:(5): 703–13.

Logothetis, N. K. & Wandell, B. A. (2004). Interpreting the BOLD signal. *Annual review of physiology*, 66: 735–769.

Long, J. J. A., Shen, B., Luo, T., Stewart, L., McMurran, T. J. A., & Leung, L. S. (2009). Pilocarpine model of temporal lobe epilepsy shows enhanced response to general anesthetics. *Experimental Neurology*, 219: 308–318.

Lopes da Silva, F. H., Gorter, J. a., & Wadman, W. J. (2012). Epilepsy as a dynamic disease of neuronal networks. *Handbook of clinical neurology*, 107:(31): 35–62.

Lothman, E. W. & Collins, R. C. (1981). Kainic acid induced limbic seizures: metabolic, behavioral, electroencephalographic and neuropathological correlates. *Brain research*, 218: 299–318.

Lowe, M. J., Beall, E. B., Sakaie, K. E., Koenig, K. A., Stone, L., Marrie, R. A., & Phillips, M. D. (2008). Resting state sensorimotor functional connectivity in multiple sclerosis inversely correlates with transcallosal motor pathway transverse diffusivity. *Human Brain Mapping*, 29: 818–827.

Lowry, C. a. & Kay, L. M. (2007). Chemical factors determine olfactory system beta oscillations in waking rats. *Journal of neurophysiology*, 98:(1): 394–404.

Lu, H., Zou, Q., Gu, H., Raichle, M. E., Stein, E. a., & Yang, Y. (2012). Rat brains also have a default mode network. *Proceedings of the National Academy of Sciences of the United States of America*, 109:(10): 3979–84.

Luo, C., Qiu, C., Guo, Z., Fang, J., Li, Q., Lei, X., … Yao, D. (2011). Disrupted functional brain connectivity in partial epilepsy: a resting-state fMRI study. *PloS one*, 7:(1): e28196.

Lynall, M.-E., Bassett, D. S., Kerwin, R., McKenna, P. J., Kitzbichler, M., Muller, U., & Bullmore, E. (2010). Functional connectivity and brain networks in schizophrenia. *The Journal of neuroscience : the official journal of the Society for Neuroscience*, 30: 9477–9487.

Ma, J. & Leung, L. S. (2010). Kindled seizure in the prefrontal cortex activated behavioral hyperactivity and increase in accumbens gamma oscillations through the hippocampus. *Behavioural brain research*, 206:(1): 68–77.

Ma, J. & Leung, L. (2004a). Schizophrenia-like behavioral changes after partial hippocampal kindling. *Brain Research*, 997:(1): 111–118.

Ma, J., Shen, B., Rajakumar, N., & Leung, L. S. (2004b). The medial septum mediates impairment of prepulse inhibition of acoustic startle induced by a hippocampal seizure or phencyclidine. *Behavioural brain research*, 155:(1): 153–66.

Ma, J., Shen, B., Stewart, L. S., Herrick, I. A., & Leung, L. S. (2002). The septohippocampal system participates in general anesthesia. *The Journal of neuroscience : the official journal of the Society for Neuroscience*, 22: RC200.

Mancilla, J. G., Lewis, T. J., Pinto, D. J., Rinzel, J., & Connors, B. W. (2007). Synchronization of electrically coupled pairs of inhibitory interneurons in neocortex. *The Journal of neuroscience : the official journal of the Society for Neuroscience*, 27: 2058–2073.

Masamoto, K., Fukuda, M., Vazquez, A., & Kim, S.-G. (2009). Dose-dependent effect of isoflurane on neurovascular coupling in rat cerebral cortex. *The European journal of neuroscience*, 30:(2): 242–50.

Mathern, G. W., Pretorius, J. K., Kornblum, H. I., Mendoza, D., Lozada, A., Leite, J. P., … Adelson, P. D. (1998). Altered hippocampal kainate-receptor mRNA levels in temporal lobe epilepsy patients. *Neurobiology of disease*, 5: 151–176.

Matute, C. (2011). Therapeutic potential of kainate receptors. *CNS neuroscience & therapeutics*, 17:(6): 661–9.

McAndrews, M. P. & Cohn, M. (2012). Neuropsychology in temporal lobe epilepsy: influences from cognitive neuroscience and functional neuroimaging. *Epilepsy research and treatment*, 2012: 925238.

Meador, K. J. (2011). Networks, cognition, and epilepsy. *Neurology*, 77:(10): 930–1.

Medvedev, A., MacKenzie, L., Hiscock, J. J., & Willoughby, J. O. (2000). Kainic acid induces distinct types of epileptiform discharge with differential involvement of hippocampus and neocortex. *Brain Research Bulletin*, 52: 89–98.

M'Harzi, M. & Monmaur, P. (1985). Selective lesions of the fimbria and the fornix in the rat: differential effects on CA1 and dentate theta. *Experimental neurology*, 89: 361–371.

Mirsattari, S. M., Ives, J. R., Bihari, F., Leung, L. S., Menon, R. S., & Bartha, R. (2005). Real-time display of artifact-free electroencephalography during functional magnetic resonance imaging and magnetic resonance spectroscopy in an animal model of epilepsy. *Magnetic resonance in medicine : official journal of the Society of Magnetic Resonance in Medicine / Society of Magnetic Resonance in Medicine*, 53:(2): 456–64.

Modur, P. N., Zhang, S., & Vitaz, T. W. (2011). Ictal high-frequency oscillations in neocortical epilepsy: Implications for seizure localization and surgical resection. *Epilepsia*, 52: 1792–1801.

Mogenson, G. J., Jones, D. L., & Yim, C. Y. (1980). From motivation to action: functional interface between the limbic system and the motor system. *Progress in neurobiology*, 14: 69–97.

Mohammadi, B., Kollewe, K., Samii, A., Krampfl, K., Dengler, R., & Münte, T. F. (2009). Changes of resting state brain networks in amyotrophic lateral sclerosis. *Experimental Neurology*, 217: 147–153.

Montague, A. A. & Greer, C. A. (1999). Differential distribution of ionotropic glutamate receptor subunits in the rat olfactory bulb. *The Journal of comparative neurology*, 405:(2): 233–46.

Morgan, V. L., Rogers, B. P., Sonmezturk, H. H., Gore, J. C., & Abou-Khalil, B. (2011). Cross hippocampal influence in mesial temporal lobe epilepsy measured with high temporal resolution functional magnetic resonance imaging. *Epilepsia*, 52: 1741–1749.

Mulert, C. & Lemieux, L. (2009). *EEG - fMRI: Physiological Basis, Technique, and Applications* (2010th ed.). Springer.

Nagayama, S., Enerva, A., Fletcher, M. L., Masurkar, A. V., Igarashi, K. M., Mori, K., & Chen, W. R. (2010). Differential axonal projection of mitral and tufted cells in the mouse main olfactory system. *Frontiers in neural circuits*, 4:

Negishi, M., Martuzzi, R., Novotny, E. J., Spencer, D. D., & Constable, R. T. (2011). Functional MRI connectivity as a predictor of the surgical outcome of epilepsy. *Epilepsia*, 52: 1733–1740.

Niedermeyer, E. & Lopes da Silva, F. H. (2004). *Electroencephalography: Basic Principles, Clinical Applications, and Related Fields*.

Norton, L., Hutchison, R. M., Young, G. B., Lee, D. H., Sharpe, M. D., & Mirsattari, S. M. (2012). Disruptions of functional connectivity in the default mode network of comatose patients. *Neurology*, 78: 175–181.

Ochi, A., Otsubo, H., Donner, E. J., Elliott, I., Iwata, R., Funaki, T., … Snead, O. C. (2007). Dynamic changes of ictal high-frequency oscillations in neocortical epilepsy: Using multiple band frequency analysis. *Epilepsia*, 48: 286–296.

O'Dell, C. M., Das, A., Wallace, G., Ray, S. K., & Banik, N. L. (2012). Understanding the basic mechanisms underlying seizures in mesial temporal lobe epilepsy and possible therapeutic targets: a review. *Journal of neuroscience research*, 90:(5): 913–24.

Panayiotopoulos, C. P. (2012). The new ILAE report on terminology and concepts for the organization of epilepsies: critical review and contribution. *Epilepsia*, 53:(3): 399–404.

Paxinos, G. & Watson, C. (2007). The Rat Brain in Stereotaxic Coordinates Sixth Edition. *Elsevier Academic Press*, 170: 547–612.

Pittau, F., Grova, C., Moeller, F., Dubeau, F., & Gotman, J. (2012). Patterns of altered functional connectivity in mesial temporal lobe epilepsy. *Epilepsia*, 53:(6): 1013–23.

Powell, H. W. R., Richardson, M. P., Symms, M. R., Boulby, P. A., Thompson, P. J., Duncan, J. S., & Koepp, M. J. (2007). Reorganization of verbal and nonverbal memory in temporal lobe epilepsy due to unilateral hippocampal sclerosis. *Epilepsia*, 48:(8): 1512–25.

Prodoehl, J., Burciu, R. G., & Vaillancourt, D. E. (2014). Resting state functional magnetic resonance imaging in Parkinson's disease. *Current neurology and neuroscience reports*, 14:(6): 448.

Quirk, G. J. & Mueller, D. (2008). Neural mechanisms of extinction learning and retrieval. *Neuropsychopharmacology : official publication of the American College of Neuropsychopharmacology*, 33: 56–72.

R Core Team. (2014). R: A language and environment for statistical computing. Vienna, Austria.: R Foundation for Statistical Computing.

R Studio. (2012). RStudio: Integrated development environment for R. Boston, MA: RStudio.

Racine, R. J. (1972). Modification of seizure activity by electrical stimulation. II. Motor seizure. *Electroencephalography and clinical neurophysiology*, 32: 281–294.

Raol, Y. H. & Brooks-Kayal, A. R. (2012). Experimental models of seizures and epilepsies. *Progress in molecular biology and translational science*, 105: 57–82.

Ratté, S. & Lacaille, J.-C. (2006). Selective degeneration and synaptic reorganization of hippocampal interneurons in a chronic model of temporal lobe epilepsy. *Advances in neurology*, 97: 69–76.

Ravizza, T., Rizzi, M., Perego, C., Richichi, C., Velíská, J., Moshé, S. L., … Vezzani, A. (2005). Inflammatory response and glia activation in developing rat hippocampus after status epilepticus. In *Epilepsia* (Vol. 46, pp. 113–117).

Restrepo, D., Hellier, J. L., & Salcedo, E. (2013). Complex metabolically demanding sensory processing in the olfactory system: Implications for epilepsy. *Epilepsy & behavior : E&B*.

Rodin, E., Constantino, T., Rampp, S., & Wong, P. K. (2009). Spikes and epilepsy. *Clinical EEG and neuroscience : official journal of the EEG and Clinical Neuroscience Society (ENCS)*, 40: 288–299.

Rodrigues, R. J. & Lerma, J. (2012). Metabotropic signaling by kainate receptors. *Wiley Interdisciplinary Reviews: Membrane Transport and Signaling*, 1:(4): 399–410.

Rohan, D. & Cunningham, A. J. (2002). A Randomized, Controlled Trial of Surgery for Temporal-Lobe Epilepsy. *Survey of Anesthesiology*, 46:(3): 142–143.

Rubinov, M. & Sporns, O. (2010). Complex network measures of brain connectivity: uses and interpretations. *NeuroImage*, 52:(3): 1059–69.

Scharfman, H. E., Sollas, A. L., Berger, R. E., & Goodman, J. H. (2003). Electrophysiological evidence of monosynaptic excitatory transmission between granule cells after seizure-induced mossy fiber sprouting. *Journal of neurophysiology*, 90:(4): 2536–47.

Schulz, R., Lüders, H. O., Hoppe, M., Tuxhorn, I., May, T., & Ebner, A. (2000). Interictal EEG and ictal scalp EEG propagation are highly predictive of surgical outcome in mesial temporal lobe epilepsy. *Epilepsia*, 41: 564–570.

Seifert, G., Carmignoto, G., & Steinhäuser, C. (2010). Astrocyte dysfunction in epilepsy. *Brain research reviews*, 63:(1-2): 212–21.

Sharma, A. K., Reams, R. Y., Jordan, W. H., Miller, M. a., Thacker, H. L., & Snyder, P. W. (2007). Mesial temporal lobe epilepsy: pathogenesis, induced rodent models and lesions. *Toxicologic pathology*, 35:(7): 984–99.

Sharman, J. L., Benson, H. E., Pawson, A. J., Lukito, V., Mpamhanga, C. P., Bombail, V., … Harmar, A. J. (2013). IUPHAR-DB: Updated database content and new features. *Nucleic Acids Research*, 41:

Shepherd, G. (2004). *The Synaptic Organization of the Brain* (5th). Oxford University Press.

Sloviter, R. S. (2008). Hippocampal epileptogenesis in animal models of mesial temporal lobe epilepsy with hippocampal sclerosis: the importance of the "latent period" and other concepts. *Epilepsia*, 49 Suppl 9: 85–92.

Smith, S. M., Fox, P. T., Miller, K. L., Glahn, D. C., Fox, P. M., Mackay, C. E., … Beckmann, C. F. (2009). Correspondence of the brain's functional architecture during activation and rest. *Proceedings of the National Academy of Sciences of the United States of America*, 106:(31): 13040–5.

Spencer, S. S. (2002). Neural Networks in Human Epilepsy: Evidence of and Implications for Treatment. *Epilepsia*, 43:(3): 219–227.

Sperk, G., Lassmann, H., Baran, H., Kish, S. J., Seitelberger, F., & Hornykiewicz, O. (1983). Kainic acid induced seizures: neurochemical and histopathological changes. *Neuroscience*, 10: 1301–1315.

Sperk, G., Lassmann, H., Baran, H., Seitelberger, F., & Hornykiewicz, O. (1985). Kainic acid-induced seizures: Dose-relationship of behavioural, neurochemical and histopathological changes. *Brain Research*, 338: 289–295.

Sporns, O. (2010). *Networks of the Brain*. MIT press.

Sporns, O. (2011). The human connectome: a complex network. *Annals of the New York Academy of Sciences*, 1224: 109–25.

Sporns, O. (2013). The Human Connectome. Linking Structure and Function in the Human Brain. In Diffusion mri: from quantitative measurement to in vivo neuroanatomy: second edition (pp. 401–428).

Sporns, O. & Kötter, R. (2004). Motifs in brain networks. *PLoS biology*, 2:(11): e369.

Staley, K. J. & Dudek, F. E. (2006). Interictal Spikes and Epileptogenesis. *Epilepsy Currents*, 6: 199–202.

Stam, C. J., Jones, B. F., Nolte, G., Breakspear, M., & Scheltens, P. (2007a). Small-world networks and functional connectivity in Alzheimer's disease. *Cerebral cortex (New York, N.Y. : 1991)*, 17: 92–99.

Stam, C. J. & Reijneveld, J. C. (2007b). Graph theoretical analysis of complex networks in the brain. *Nonlinear biomedical physics*, 1:(1): 3.

Stefan, H. & Lopes da Silva, F. H. (2013). Epileptic neuronal networks: methods of identification and clinical relevance. *Frontiers in neurology*, 4:(3): 8.

Suárez, L. M., Cid, E., Gal, B., Inostroza, M., Brotons-Mas, J. R., Gómez-Domínguez, D., … Solís, J. M. (2012). Systemic injection of kainic acid differently affects LTP magnitude depending on its epileptogenic efficiency. *PloS one*, 7:(10): e48128.

Tai, S. K., Ma, J., & Leung, L. S. (2014). Medial septal cholinergic neurons modulate isoflurane anesthesia. *Anesthesiology*, 120:(2): 392–402.

Tanaka, N., Hämäläinen, M. S., Ahlfors, S. P., Liu, H., Madsen, J. R., Bourgeois, B. F., … Stufflebeam, S. M. (2010). Propagation of epileptic spikes reconstructed from spatiotemporal magnetoencephalographic and electroencephalographic source analysis. *NeuroImage*, 50: 217–222.

Thom, M. & Bertram, E. H. (2012). Temporal lobe epilepsy. *Handbook of Clinical Neurology*, 107: 225–240.

Thom, M., Mathern, G. W., Cross, J. H., & Bertram, E. H. (2010). Mesial temporal lobe epilepsy: How do we improve surgical outcome? *Annals of neurology*, 68:(4): 424–34.

Tracy, J. I., Osipowicz, K., Spechler, P., Sharan, A., Skidmore, C., Doucet, G., & Sperling, M. R. (2014). Functional connectivity evidence of cortico-cortico inhibition in temporal lobe epilepsy. *Human brain mapping*, 35:(1): 353–66.

Trimble, M. R. (1991). *The psychoses of epilepsy*. Raven Press, NY.

Ullal, G., Fahnestock, M., & Racine, R. (2005). Time-dependent effect of kainate-induced seizures on glutamate receptor GluR5, GluR6, and GluR7 mRNA and Protein Expression in rat hippocampus. *Epilepsia*, 46:(5): 616–23.

Upadhyay, J., Baker, S. J., Chandran, P., Miller, L., Lee, Y., Marek, G. J., … Day, M. (2011). Default-mode-like network activation in awake rodents. *PloS one*, 6:(11): e27839.

van den Heuvel, M. P. & Sporns, O. (2013). Network hubs in the human brain. *Trends in cognitive sciences*, 17:(12): 683–96.

Van Essen, D. C., Smith, S. M., Barch, D. M., Behrens, T. E. J., Yacoub, E., & Ugurbil, K. (2013). The WU-Minn Human Connectome Project: An overview. *NeuroImage*, 80: 62–79.

Vargas, J. R., Takahashi, D. K., Thomson, K. E., & Wilcox, K. S. (2013). The expression of kainate receptor subunits in hippocampal astrocytes after experimentally induced status epilepticus. *Journal of neuropathology and experimental neurology*, 72:(10): 919–32.

Vaudano, E., Legg, C. R., & Glickstein, M. (1991). Afferent and Efferent Connections of Temporal Association Cortex in the Rat: A Horseradish Peroxidase Study. *European Journal of Neuroscience*, 3: 317–330.

Veer, I. M., Beckmann, C. F., van Tol, M.-J., Ferrarini, L., Milles, J., Veltman, D. J., … Rombouts, S. A. R. B. (2010). Whole brain resting-state analysis reveals decreased functional connectivity in major depression. *Frontiers in systems neuroscience*, 4:

Villers, A., Godaux, E., & Ris, L. (2012). Long-lasting LTP requires neither repeated trains for its induction nor protein synthesis for its development. *PloS one*, 7:(7): e40823.

Vincent, J. L., Patel, G. H., Fox, M. D., Snyder, A. Z., Baker, J. T., Van Essen, D. C., … Raichle, M. E. (2007). Intrinsic functional architecture in the anaesthetized monkey brain. *Nature*, 447: 83–86.

Vincent, P. & Mulle, C. (2009). Kainate receptors in epilepsy and excitotoxicity. *Neuroscience*, 158:(1): 309–23.

Voets, N. L., Beckmann, C. F., Cole, D. M., Hong, S., Bernasconi, A., & Bernasconi, N. (2012). Structural substrates for resting network disruption in temporal lobe epilepsy. *Brain : a journal of neurology*, 135:(8): 2350–7.

Wada, J. A., Sato, M., & Corcoran, M. E. (1974). Persistent seizure susceptibility and recurrent spontaneous seizures in kindled cats. *Epilepsia*, 15:(4): 465–78.

Wadman, W. J., Lopes da Silva, F. H., & Leung, L. W. (1983). Two types of interictal transients of reversed polarity in rat hippocampus during kindling. *Electroencephalography and clinical neurophysiology*, 55:(3): 314–9.

Waites, A. B., Briellmann, R. S., Saling, M. M., Abbott, D. F., & Jackson, G. D. (2006). Functional connectivity networks are disrupted in left temporal lobe epilepsy. *Annals of neurology*, 59:(2): 335–43.

Wang, B., Fan, Y., Lu, M., Li, S., Song, Z., Peng, X., … Huang, R. (2013a). Brain anatomical networks in world class gymnasts: a DTI tractography study. *NeuroImage*, 65: 476–87.

Wang, J., Zuo, X., Dai, Z., Xia, M., Zhao, Z., Zhao, X., … He, Y. (2013b). Disrupted functional brain connectome in individuals at risk for Alzheimer's disease. *Biological psychiatry*, 73:(5): 472–81.

Wang, J., Qiu, S., Xu, Y., Liu, Z., Wen, X., Hu, X., … Huang, R. (2014). Graph theoretical analysis reveals disrupted topological properties of whole brain functional networks in temporal lobe epilepsy. *Clinical neurophysiology : official journal of the International Federation of Clinical Neurophysiology*, 125:(9): 1744–56.

Wang, K., Liang, M., Wang, L., Tian, L., Zhang, X., Li, K., & Jiang, T. (2007). Altered functional connectivity in early Alzheimer's disease: A resting-state fMRI study. *Human Brain Mapping*, 28: 967–978.

Wang, K., van Meer, M. P. A., van der Marel, K., van der Toorn, A., Xu, L., Liu, Y., … Dijkhuizen, R. M. (2011). Temporal scaling properties and spatial synchronization of spontaneous blood oxygenation level-dependent (BOLD) signal fluctuations in rat sensorimotor network at different levels of isoflurane anesthesia. *NMR in biomedicine*, 24:(1): 61–7.

Wang, Q., Yu, S., Simonyi, A., Sun, G. Y., & Sun, A. Y. (2005). Kainic acid-mediated excitotoxicity as a model for neurodegeneration. *Molecular neurobiology*, 31: 3–16.

Watts, D. J. & Strogatz, S. H. (1998). Collective dynamics of 'small-world' networks. *Nature*, 393: 440–442.

Wendling, F., Bartolomei, F., Bellanger, J. J., Bourien, J., & Chauvel, P. (2003). Epileptic fast intracerebral EEG activity: Evidence for spatial decorrelation at seizure onset. *Brain*, 126: 1449–1459.

White, A., Williams, P. A., Hellier, J. L., Clark, S., Dudek, F. E., & Staley, K. J. (2010). EEG spike activity precedes epilepsy after kainate-induced status epilepticus. *Epilepsia*, 51: 371–383.

Wieser, H. G., Ortega, M., Friedman, A., & Yonekawa, Y. (2003). Long-term seizure outcomes following amygdalohippocampectomy. *Journal of neurosurgery*, 98: 751–763.

Wu, K. & Leung, L. S. (2001). Enhanced but fragile inhibition in the dentate gyrus in vivo in the kainic acid model of temporal lobe epilepsy: A study using current source density analysis. *Neuroscience*, 104: 379–396.

Wu, K. & Leung, L. (2003). Increased dendritic excitability in hippocampal ca1 in vivo in the kainic acid model of temporal lobe epilepsy: a study using current source density analysis. *Neuroscience*, 116:(2): 599–616.

Yoder, R. M. & Pang, K. C. H. (2005). Involvement of GABAergic and cholinergic medial septal neurons in hippocampal theta rhythm. *Hippocampus*, 15: 381–392.

Zalesky, A., Fornito, A., & Bullmore, E. T. (2010). Network-based statistic: Identifying differences in brain networks. *NeuroImage*, 53: 1197–1207.

Zhang, Z., Lu, G., Zhong, Y., Tan, Q., Liao, W., Chen, Z., … Liu, Y. (2009a). Impaired perceptual networks in temporal lobe epilepsy revealed by resting fMRI. *Journal of Neurology*, 256: 1705–1713.

Zhang, Z., Lu, G., Zhong, Y., Tan, Q., Yang, Z., Liao, W., … Liu, Y. (2009b). Impaired attention network in temporal lobe epilepsy: A resting FMRI study. *Neuroscience Letters*, 458: 97–101.

Zijlmans, M., Jacobs, J., Kahn, Y. U., Zelmann, R., Dubeau, F., & Gotman, J. (2011). Ictal and interictal high frequency oscillations in patients with focal epilepsy. *Clinical Neurophysiology*, 122: 664–671.

Appendix A

Graph Theory Analysis

A.1 Mathematical Notation

1. Edge,

$$e_{ij} = \begin{cases} 1 & \text{if } |t_{ij}| > T; \\ 0 & \text{otherwise.} \end{cases}$$

Edge, e_{ij} is the connection status between i and j: $e_{ij} = 1$ when link (i, j) exists (when i and j are neighbors); $e_{ij} = 0$ otherwise ($e_{ii} = 0$ for all i).
N is the set of all nodes in the network, and n is the number of nodes. L is the set of all links in the network, and l is number of links. (i, j) is a link between nodes i and j, $(i, j \in N)$.

2. Degree of a Node,

$$K_i = \sum_{j \in N} e_{ij}$$

Degree – number of links connected to a node. e_{ij} is the connection status between i and j.

3. Shortest Path Length,

$$d_{ij} = \sum_{a_{uv} \in_{gi \leftrightarrow j}} a_{uv}$$

A basis for measuring integration.

4. Number of triangles,

$$t_i = \frac{1}{2} \sum_{j,h \in N} a_{ij} a_{ih} a_{jh}$$

A basis for measuring segregation.

5. Clustering Coefficient,

$$C = C\frac{1}{n} \sum_{i \in N} C_i = \frac{1}{n} \sum_{i \in N} \frac{2t_i}{k_i(k_i - 1)}$$

where C_i is the clustering coefficient of node i ($C_i = 0$ for $k_i < 2$).

6. Local Efficiency,

$$E_{loc} = \frac{1}{n}\sum_{i\in N} E_{loc,i} = \frac{1}{n}\sum_{i\in N}\frac{\sum_{j,h\in N, j\neq i} a_{ij}a_{ih}\left[d_{jh}(N_i)\right]^{-1}}{k_i(k_i-1)}$$

where $E_{loc,i}$ is the local efficiency of node i, and $d_{jh}(N_i)$ is the length of the shortest path between j and h that contains only neighbours of i.

7. Betweenness Centrality,

$$b_i = \frac{1}{(n-1)(n-2)}\sum_{\substack{h,j\in N\\ h\neq j, h\neq i, j\neq i,}}\frac{\rho_{hj}(i)}{\rho_{hj}}$$

where ρ_{hj} is the number of shortest paths between h and j, and $\rho_{hj}(i)$ is the number of shortest paths between h and j that pass through i.

8. Characteristic Path Length,

$$L = \frac{1}{n}\sum_{i\in N} L_i = \frac{1}{n}\sum_{i\in N}\frac{\sum_{j\in N, j\neq i} d_{ij}}{n-1}$$

where L_i is the average distance between node i and all other nodes.

9. Global Efficiency,

$$E = \frac{1}{n}\sum_{i\in N} E_i = \frac{1}{n}\sum_{i\in N}\frac{\sum_{j\in N, j\neq i}(1/d_{ij})}{n-1}$$

where E_i is the efficiency of node i.

10. Measure of network small-worldness,

$$\sigma = \frac{C/C_{rand}}{L/L_{rand}}$$

where C and C_{rand} are the clustering coefficients, and L and L_{rand} are the characteristic path lengths of the respective tested network and a random network. Small-world networks often have $\sigma \gg 1$.

Graph theoretical measures and notations adapted from Rubinov and Sporns (2010)

A.2 Fisher's r-to-Z Normalized Map

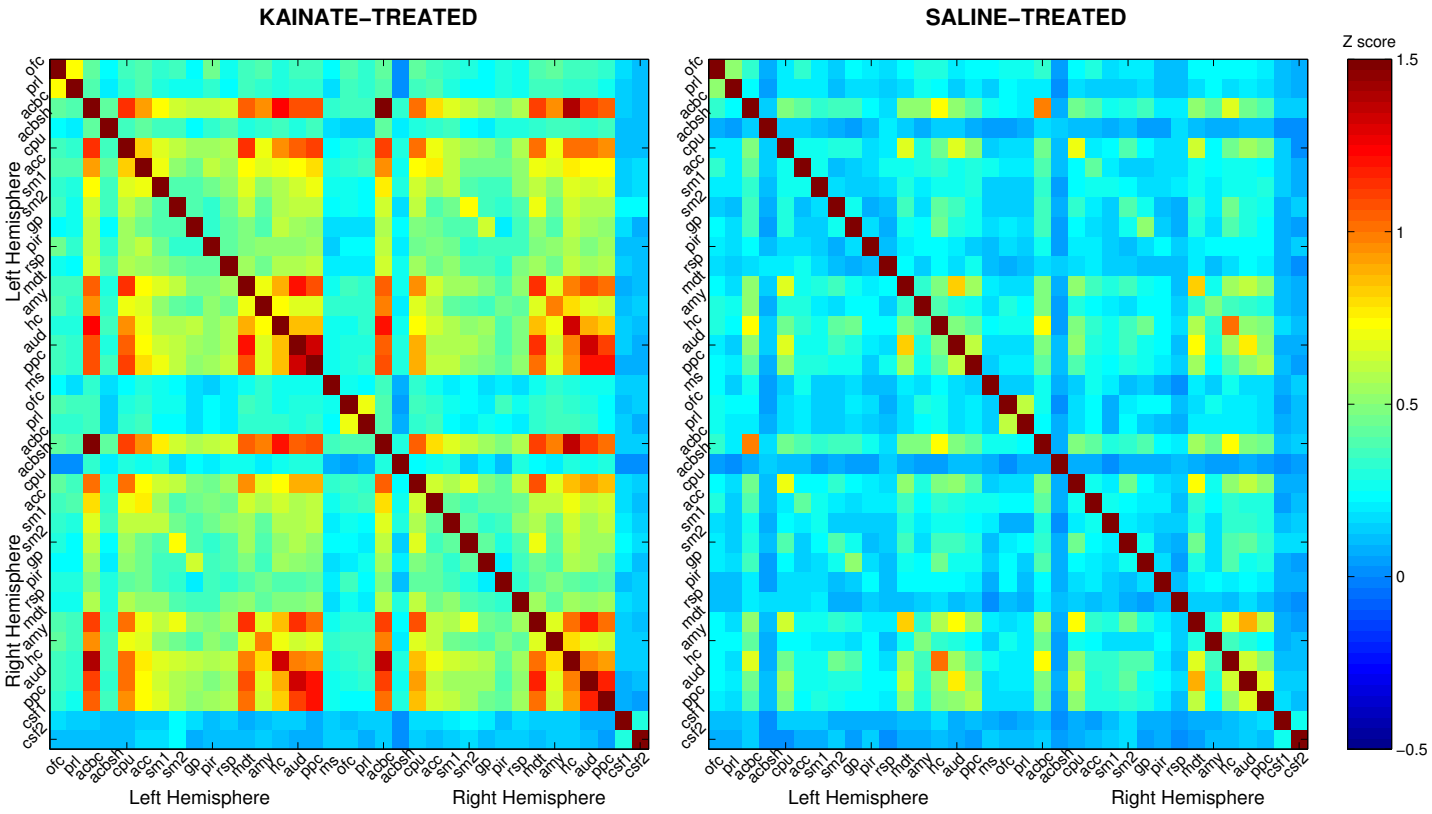

Figure A.1: **Correlation Matrix** The heatmap figure represents the significant intra-group connections in the kainate (left, P = 0.002, $n_{kainate}$ = 6) and the control (left, P = 0.014, n_{saline} = 7) group as Fisher's normalized correlations (-1 < Z < 2) in an NBS framework.

Appendix B

Node Definitions

B.1 Resting-state fMRI

ROI #	Node	Abbreviation	**Substructures** (see Paxinos & Watson, 2007, rat brain atlas)
1	Orbital Frontal Cortex - LH	ofc-l	LO, VO
2	Prelimbic Cortex - LH	prl-l	PrL
3	Nucleus Accumbens Shell - LH	acbc-l	AcbC
4	Nucleus Accumbens Core - LH	acbsh-l	AcbSh
5	Caudate Putamen - LH	cpu-l	CPu
6	Anterior Cingulate Cortex - LH	acc-l	Cg1, Cg2
7	Primary Somatosensory Cortex - LH	sm1-l	S1BF
8	Secondary Somatosensory Cortex - LH	sm2-l	S2
9	Globus Pallidus - LH	gp-l	GP
10	Piriform Cortex - LH	pir-l	Pir
11	Retrospenial Cortex - LH	rsp-l	RSD, RSGc
12	Mediodorsal Thalamic Nuclei - LH	mdt-l	MDL, MDM
13	Amygdala - LH	amy-l	BLA, BLP
14	Hippocampus - LH	hc-l	CA1, CA3
15	Auditory/Temporal Association Cortex - LH	aud-l	Au1, AuD, AuV, TeA
16	Posterior Parietal Cortex - LH	ppc-l	PtPD, PtPR
17	Medial Septum	ms	MS
18	Orbital Frontal Cortex - RH	ofc-r	LO, VO
19	Prelimbic Cortex - RH	prl-r	PrL
20	Nucleus Accumbens Shell - RH	acbc-r	AcbC
21	Nucleus Accumbens Core - RH	acbsh-r	AcbSh
22	Caudate Putamen - RH	cpu-r	CP
23	Anterior Cingulate Cortex - RH	acc-r	Cg1, Cg2
24	Primary Somatosensory Cortex - RH	sm1-r	S1BF
25	Secondary Somatosensory Cortex - RH	sm2-r	S2
26	Globus Pallidus - RH	gp-r	GP
27	Piriform Cortex - RH	pir-r	Pir
28	Retrospenial Cortex - RH	rsp-r	RSD, RSGc
29	Mediodorsal Thalamic Nuclei - RH	mdt-r	MDL, MDM
30	Amygdala - RH	amy-r	BLA, BLP
31	Hippocampus - RH	hc-r	CA1, CA3
32	Auditory/Temporal Association Cortex - RH	aud-r	Au1, AuD, AuV, TeA
33	Posterior Parietal Cortex - RH	ppc-r	PtPD, PtPR
34	Cerebrospinal Fluid (Ventricles) - 1	csf1	choroid plexus (chp, cerebrospinal fluid)
35	Cerebrospinal Fluid (Ventricles) - 2	csf2	choroid plexus (chp, cerebrospinal fluid)

B.2 Electrophysiology

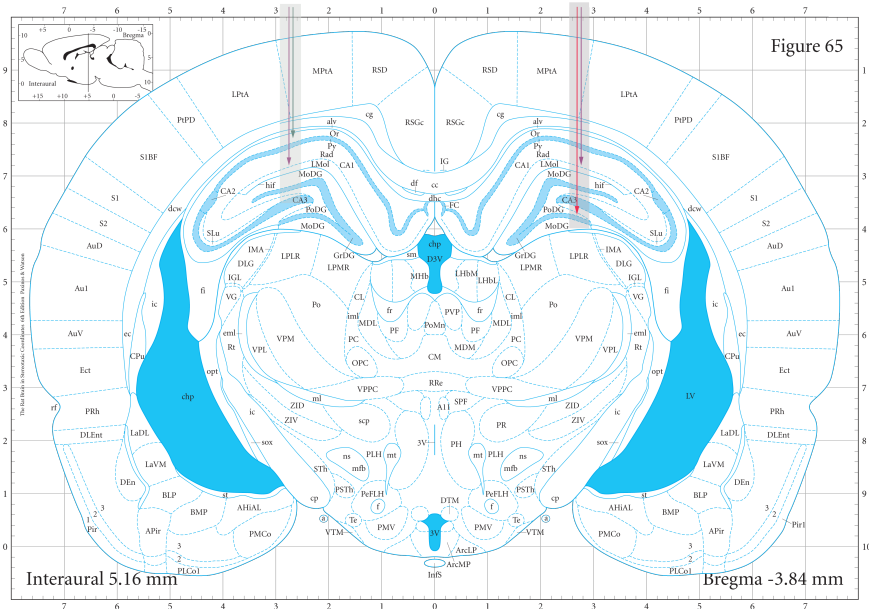

Figure B.1: CA1 radiatum, CA1 oriens, and DG hilus

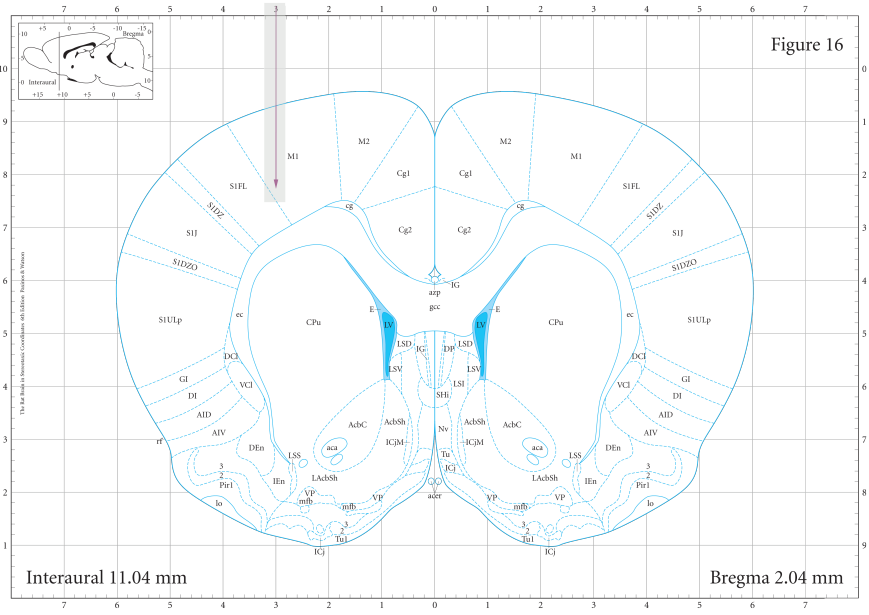

Figure B.2: Frontal neocortex

Approximate electrode locations. Images reproduced from Paxinos and Watson (2007)

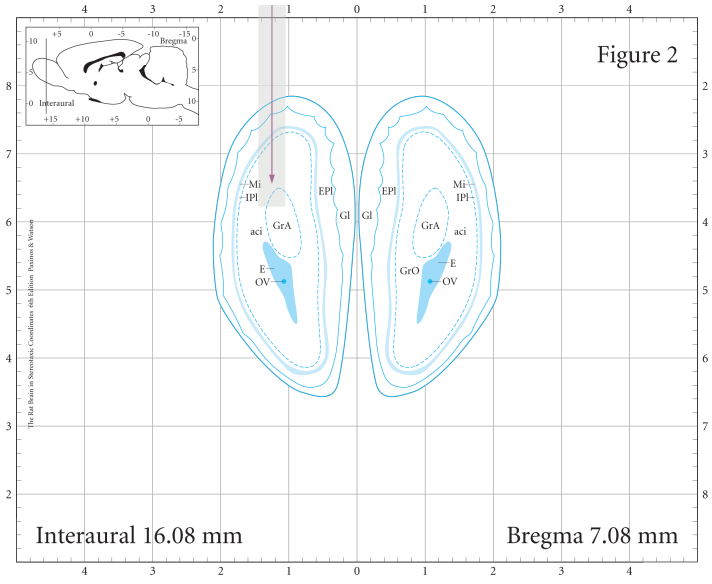

Figure B.3: Olfactory bulb (Glomerular layer)

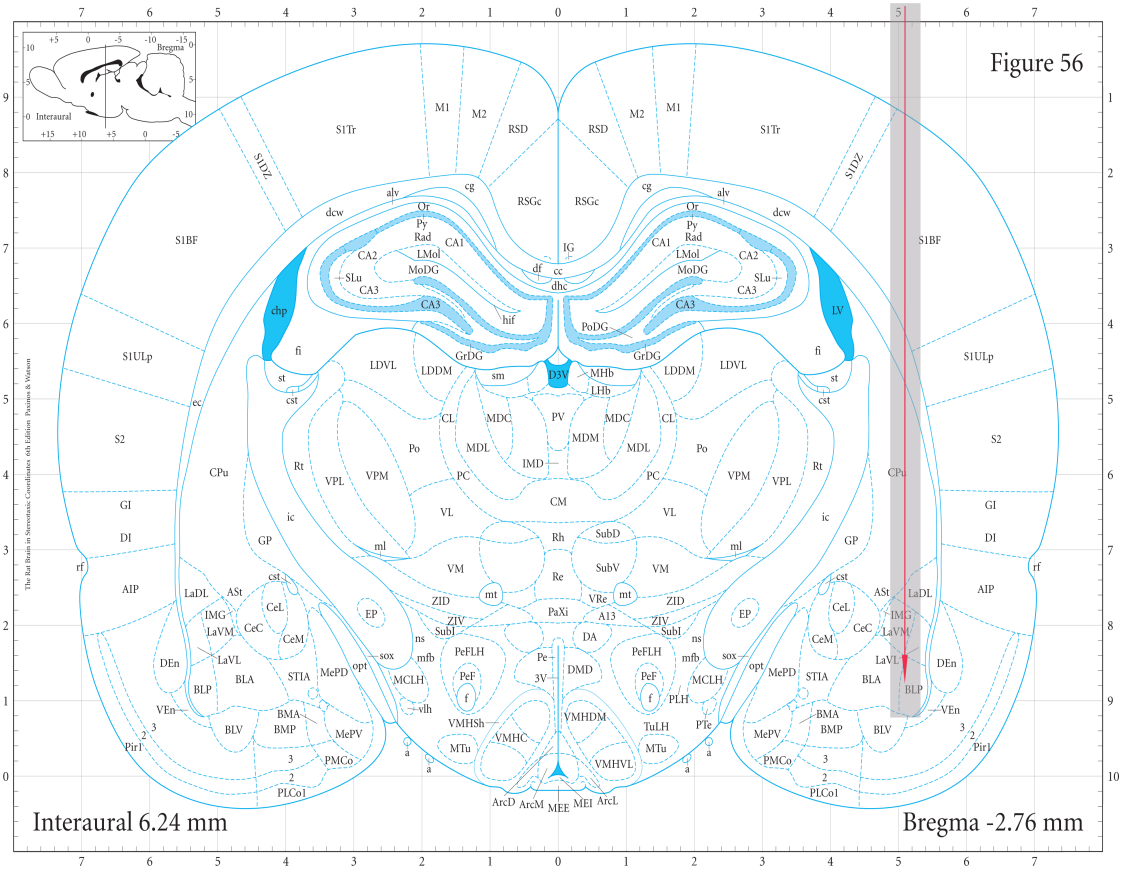

Figure B.4: Basolateral amygdala

Approximate electrode locations. Images reproduced from Paxinos and Watson (2007)

Appendix C

Supplementary Data

C.1 EPI & Anatomical Images

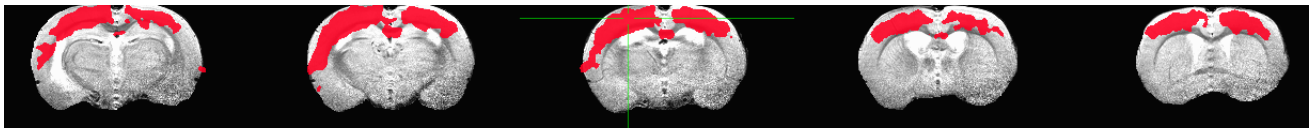

Figure C.1: **The spatial activation map overlaid onto the anatomical T2 image of a representative rat.** The spatial map was computed using the temporally filtered data using a seed (arbitrarily chosen, indicated by the green crosshairs) in the left neocortex, with the aid of InstaCorr tool included with the AFNI package. Right to left indicates anterior to posterior extent of the rat brain. Pearson's correlation coefficient, r = 0.86.

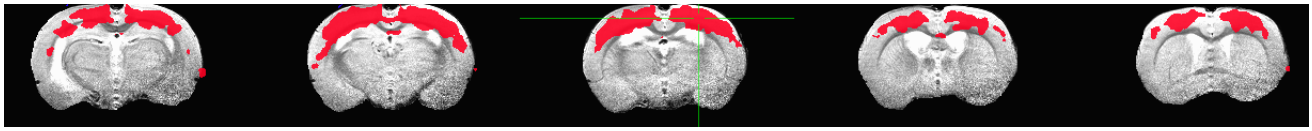

Figure C.2: **The spatial activation map overlaid onto the anatomical T2 image of a representative rat.** The spatial map was computed using the temporally filtered data using a seed (arbitrarily chosen, indicated by the green crosshairs) in the right neocortex, with the aid of InstaCorr tool included with the AFNI package. Right to left indicates anterior to posterior extent of the rat brain. Pearson's correlation coefficient, r = 0.86.

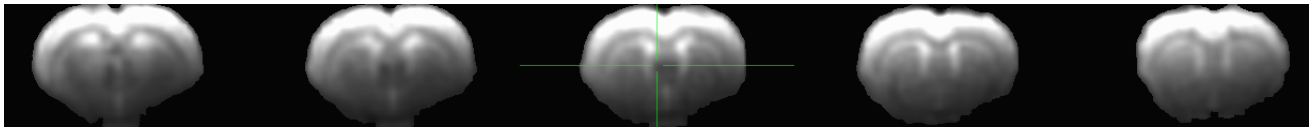

Figure C.3: **The EPI image of a representative rat** The EPI slices serves to indicate the presence of a signal gradient that is most likely responsible for weaker signal recorded from deeper brain structures using linear coil. Right to left indicates anterior to posterior extent of the rat brain.

C.2 EPI Spectrum

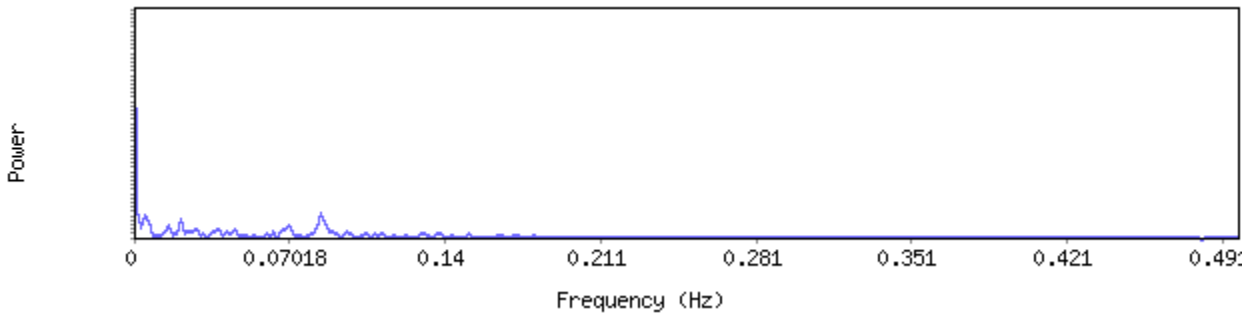

Figure C.4: **Unfiltered spectrum:** The EPI data with no spatial smoothing or preprocessing except skull stripping.

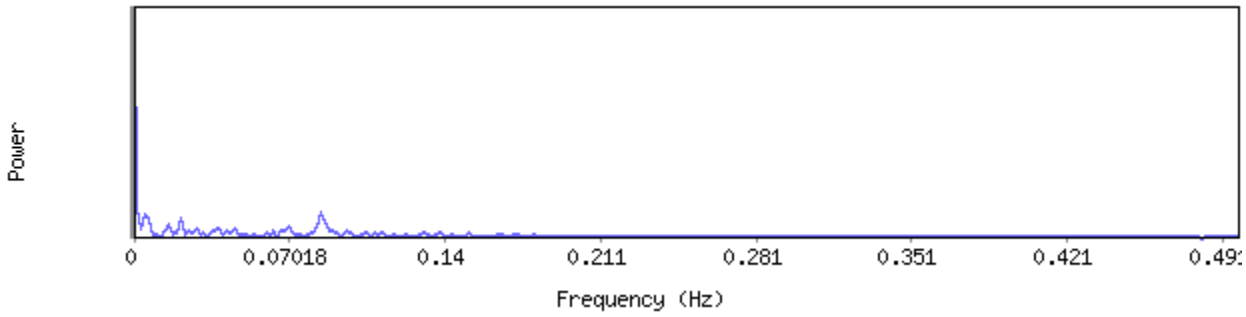

Figure C.5: **Unfiltered spectrum:** The power spectrum post-spatial smoothing, $FWHM_{xy}$ = 0.8×0.8 mm^2.

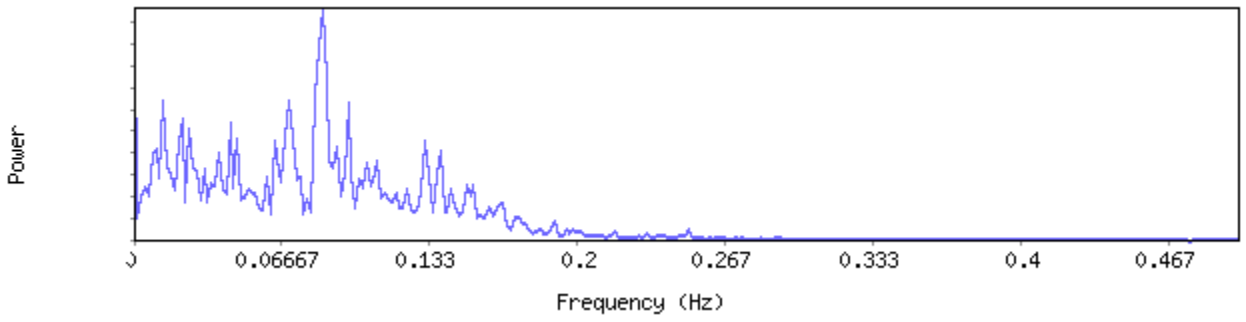

Figure C.6: **Bandpss filtered spectrum:** Temporal bandpass (0.01–0.1 Hz) filtering was achieved using an eighth-order Chebyshev Type-I filter. The dataset was spatially smoothed ($FWHM_{xy}$ = 0.8×0.8 mm^2) before subjecting the data to temporal filtering.
Relative scale: unfiltered power = ~100×bandpass power.

Appendix D

Documentation of Ethics Approval

2007-085-10::6:

AUP Number: 2007-085-10
AUP Title: fMRI and Neurophysiology During Seizure and Theta Rhythm

Yearly Renewal Date: 04/01/2014
The YEARLY RENEWAL to Animal Use Protocol (AUP) 2007-085-10 has been approved, and will be approved for one year following the above review date.

1. This AUP number must be indicated when ordering animals for this project.
2. Animals for other projects may not be ordered under this AUP number.
3. Purchases of animals other than through this system must be cleared through the ACVS office.
4. Health certificates will be required.

REQUIREMENTS/COMMENTS
Please ensure that individual(s) performing procedures on live animals, as described in this protocol, are familiar with the contents of this document.

The holder of this Animal Use Protocol is responsible to ensure that all associated safety components (biosafety, radiation safety, general laboratory safety) comply with institutional safety standards and have received all necessary approvals. Please consult directly with your institutional safety officers.

Submitted by: Kinchlea, Will D
on behalf of the Animal Use Subcommittee

The University of Western Ontario
Animal Use Subcommittee / University Council on Animal Care
Health Sciences Centre ▲ London, Ontario ▲ Canada N6A 5C1
PH: 519-661-2111 ext. 86770 ▲ http://www.uwo.ca/animal

Curriculum Vitæ

Name:	Ravnoor Gill
Post-Secondary Education and Degrees:	University of Western Ontario London, ON, Canada 2012—2014 Master of Science (Neuroscience)
	Panjab University Chandigarh, India 2008—2012 Bachelor of Engineering (Biotechnology)
Honours and Awards:	Western Graduate Research Scholarship (WGRS) 2012—2014
	Ministry of Human Resource & Development (MHRD) Graduate Aptitude Test in Engineering (GATE) Post-graduate Scholarship 2012—2014 [*Untenable outside India*]
Related Work Experience:	Teaching Assistant The University of Western Ontario 2012—2014